Optimizing carbon/carbon supercapacitors in aqueous and organic electrolytes

Qiang Gao

UNIVERSITÉ D'ORLÉANS

ÉCOLE DOCTORALE Energie, Matériaux, Sciences De la Terre et de l'Univers (EMSTU)

Centre de Recherche Sur la Matière Divisée

THÈSE présentée par:

Qiang Gao

Soutenue Publiquement
Le **08 Juillet** 2013 *à* **14 h 30**
Amphithéâtre Cabannes *d'Ecole* Polytechnique de l'Université d'Orléans

Pour obtenir le grade de : **Docteur de l'université d'Orléans**

Discipline: Chimie

Optimizing carbon/carbon supercapacitors in aqueous and organic electrolytes

THÈSE dirigée par:

François Béguin, Professeur, Université d'Orléans

RAPPORTEURS :

Thierry Brousse, Professeur, Université de Nantes

Jacek Machnikowski, Professeur, Wroclaw University of Technology, Poland

---

JURY :

Thierry Brousse, Professeur, Université de Nantes

Jacek Machnikowski, Professeur, Wroclaw University of Technology, Poland

François Béguin, Professeur, Université d'Orléans

Pascal Brault, Directeur de Recherche, CNRS-GREMI Orléans

Katia Guérin, Maître de conférences HDR, Université Blaise Pascal, Clermont Ferrand

Encarnación Raymundo-Piñero, Chargé de recherche, CNRS-CRMD Orléans

Acknowledgements

I am sincerely and heartily grateful for my PhD advisor, Prof. Dr. François Béguin, due to his excellent guidance and patience throughout my PhD work.

It is a great pleasure to thank Dr. Encarnación Raymundo-Piñero, who always patiently teaches me the knowledge in carbon materials & supercapacitors and corrects our publications.

I am also truly indebted and thankful for Dr. Laurent Demarconnay, Dr. Celine Decaux, Dr. Nicolas Batisse, Dr. Edourd Gilbert, Dr. Roman Mysyk, Dr. Yasin Eker, and Dr. Sandrine Delpeux for guiding my research for the past four years and helping me develop the skill or knowledge in electrochemistry, carbon materials, and experimental facilities, etc.

My stay in Orléans was financially supported by the ministry of education of PRC and China Scholarship Council. The program was China state-sponsored post-graduate study abroad program 2009, which provides me the precious opportunity to meet many great brains and visit many beautiful countries.

"In the end, maybe it's wiser to surrender before the miraculous scope of human generosity and to just keep saying thank you, forever and sincerely, for as long as we have voices."

- Elizabeth M. Gilbert

*Art is '**I**'; Science is '**We**'.*

-Claude Bernard

(12 July 1813 – 10 February 1878) French physiologist

Contents

Introduction Générale 1

General Introduction 5

Chapter I: *Bibliography* 10

1 Introduction 11

2 Principles and properties of supercapacitors 12

2.1 The electrical double-layer 12

2.2 Construction of a supercapacitor 14

2.3 Energy and power of supercapacitors 15

3 Electrolytes 15

3.1 Aqueous medium 16

3.2 Organic electrolytes 17

3.3 Ionic liquids 18

4 Carbons for electrical double-layer capacitors (EDLCs) 19

4.1 Effect of porous texture on the capacitive performance 20

4.2 Methods for adapting the pore size of carbons to the ion size 29

4.3 Models for EDL formation inside carbon pores 33

5 Pseudo-capacitive contributions 34

5.1 Pseudo-capacitance involving metal oxides and conducting polymers 35

5.2 Pseudo-capacitance from surface functional groups on carbons 36

5.2.1 Oxygen enriched carbons 36

5.2.2 Nitrogen enriched carbons 38

5.3 Pseudo-capacitance related to reversible hydrogen storage in carbons 40

5.4 Pseudocapacitance related to the use of redox-active electrolytes 42

6 Asymmetric supercapacitors 46

6.1 Hybrid/Asymmetric capacitor operating in aqueous electrolytes 47

6.2 Hybrid capacitors operating in organic electrolytes 49

7 Conclusions 50

Chapter II 52

Optimizing carbon/carbon supercapacitors by enhancing the voltage range in aqueous alkali sulfate electrolytes 52

Résumé 53

1 Introduction 55

2 Symmetric AC/AC capacitors in neutral aqueous alkali sulfates at different operating temperatures 56

2.1 Introduction 56

2.2 Physicochemical properties of the carbon material 56

2.3 Electrochemical performance of symmetric carbon/carbon capacitors in aqueous Li_2SO_4, Na_2SO_4 and K_2SO_4 electrolytes 57

3 Understanding the electrodes potential limits of symmetric carbon/carbon capacitors in lithium sulfate electrolyte 66

3.1 Introduction 66

3.2 Physicochemical characterization of modified carbon materials 67

3.3 Electrochemical performance of AC and AC/AC supercapacitors 68

3.4 Electrochemical performance of the oxidized AC carbon (ACH) and of ACH/ACH supercapacitors 72

4 Asymmetric carbon based supercapacitors in aqueous lithium sulfate 75

4.1 Introduction 75

4.2 Modification of the surface functionality of activated carbon 76

4.3 Electrochemical characterizations of the modified carbons 77

4.4 Symmetric carbon/carbon systems in 2 mol L^{-1} Li_2SO_4 79

4.5 Asymmetric carbon/carbon configurations in 2 mol L^{-1} Li_2SO_4 82

5 Symmetric carbon/carbon pouch cells in aqueous lithium sulfate electrolyte 84

5.1 Textural characteristics of the ACX and ACY carbons 85

5.2 Electrochemical characterizations of ACX and ACY-based symmetric capacitor 85

6 Conclusions 90

Chapter III 92

Optimizing carbons for supercapacitors in organic medium by a novel high pressure/low temperature activation protocole 92

Résumé 93

1 Introduction 94

2 Cyclic oxidation/thermal desorption as an effective process to tailor the pore size of EDLC carbons 95

2.1 Starting materials 95

2.2 Effect of the activation parameters on the physicochemical characteristics of carbons 96

2.3 Electrochemical characterization of the porous carbons in 1 mol L^{-1} $TEABF_4$/Acetonitrile electrolyte 102

3 Carbons for supercapacitors obtained in only one step of pressure induced oxidation at low temperature 106

3.1 Introduction 106

3.2 Porosity and surface chemistry characterizations 106

3.3 Electrochemical performance of the resulting carbons 110

4 Conclusions 114

General conclusion 115

Conclusions Générale 120

Experimental annex 125

1 Synthesis of porous carbon and surface modification 126

1.1 Modification of surface functionality for the applications in Li_2SO_4 electrolyte 126

1.2 Nanoporous carbons for organic electrolyte prepared by cyclic oxidation/thermal desorption 126

2 Physico-chemical characterizations of the porous carbons 127

2.1 Textural properties 127

2.2 Surface oxygenated functionality analysis 128

3 Electrochemical characterizations 128

3.1 Electrodes preparation 128

3.1.1 Pellet type electrodes 128

3.1.2 Coated electrodes 128

3.2 Electrochemical cell configurations 129

3.2.1 Three electrode cell 129

3.2.2 Two electrode cell 129
3.3 Electrochemical tests 130
Bibliographical References 131
Résumé 147
Abstract 148

Introduction Générale

Le changement climatique et la diminution des réserves en énergies fossiles obligent notre société à se tourner vers de nouvelles sources d'énergie durables et renouvelables. En conséquence, la production d'énergie alternative, via le solaire et l'éolien par exemple, connait un essai marqué alors que dans un même temps on peut noter la de généralisation de l'utilisation de véhicules à faible émission de CO_2, voire de véhicules électriques. En raison de la disponibilité restreinte ou aléatoire des sources d'énergie renouvelable et de la nécessité de concevoir des véhicules disposant de plusieurs heures d'autonomie, un problème majeur apparait: le stockage de l'énergie sous forme électrique tiennent une place.

Parmi tous les systèmes de stockage existants, les batteries et les supercondensateurs sont prépondérantes en raison de leurs propriétés respectives. Le fonctionnement d'un supercondensateur est très différent de celui d'une batterie électrochimique. En effet, ils ne fonctionnent pas sur la base de réactions chimiques et peuvent donc se charger ou se décharger très rapidement et délivrer des puissances plus élevées que les batteries et ce durant un million de cycles de charge-décharge**.** Cependant, la densité d'énergie stockée par les supercondensateurs reste inférieure à celle d'une batterie. Ainsi, les supercondensateurs sont utilisés pour diverses applications dans différents domaines tels que l'électronique domestique, l'automobile, l'ouverture d'urgence des portes de l'A380, le transport collectif urbain, la mobilité des missiles et aéronefs, etc.…

Généralement, on peut classer les supercondensateurs en deux types suivant la nature des électrodes : les supercondensateurs à double couche électrochimique (EDLC) et pseudocapacitifs. Actuellement, parmi les différents types de supercondensateurs, ceux dont les électrodes sont à base de carbones activés, appelés supercondensateurs carbone/carbone, sont les systèmes les plus aboutis. Les carbones activés sont des matériaux largement étudiés car ils possèdent de grandes surfaces spécifiques permettant d'obtenir de grandes capacités.

Actuellement, les travaux de recherche portant sur les supercondensateurs sont d'atteindre les densités d'énergie les plus élevées possible afin d'obtenir des composants, pour une application donnée, avec un volume et un poids minimal. Pour réaliser ces objectifs, il est indispensable d'augmenter la capacité spécifique de stockage de charges des carbones activés et/ou la tension de fonctionnement du système.

Le but de cette thèse est d'améliorer les performances (notamment en termes de la densité d'énergie stockée) des supercondensateurs de type carbone/carbone fonctionnant dans

un électrolyte aqueux neutre ou organique. Pour atteindre cet objectif, deux axes de travail ont été envisagés:

-L'augmentation des densités d'énergie massique du système opérant dans un électrolyte aqueux neutre.

L'étude d'électrolytes aqueux neutres a été menée puisque aux ci ont démonté une bonne stabilité sur une large gamme de potentiel, très supérieure à la fenêtre théorique de 1,23 V des milieux aqueux acide ou basique classiquement étudiés. Cette aptitude permet d'augmenter significativement la tension de cellule. L'objectif principal sera d'aboutir à un mécanisme réaliste permettant d'expliques la fenêtre de tension des condensateurs à double couche électrochimique.

-L'augmentation des densités d'énergie volumique des supercondensateurs fonctinonant en électrolyte organique.

Pour ce faire, l'étude d'un procédé de synthèse de carbones activés à base de la cellulose par l'activation cyclique a été menée. L'objectif principal sera d'améliorer la capacité volumique de stockage des supercondensateurs grâce à la synthèse de carbones denses. Pour améliorer la capacité de stockage des supercondensateurs**,** il faut encore déterminer précisément si l'augmentation de l'énergie stockée est due seulement à une grande surface ou si la taille des pores et la géométrie du carbone jouent également un rôle.

La première partie de cette thèse présentera une synthèse bibliographique exposant les concepts des régissantes, le fonctionnement de supercondensateurs carbone/carbone à double couche électrochimique, ainsi que les nombreux travaux qui ont été effectués afin de comprendre le rôle de la surface et de la porosité des carbones activés sur la formation de la double couche électrochimique. La littérature montre plus particulièrement que l'adéquation de la taille des pores du carbone avec la taille des ions de l'électrolyte joue un rôle prépondérant dans l'abstention de capacités spécifiques élevées. Ensuite, les travaux publiés sur les supercondensateurs pseudocapacitifs et asymétriques sont également rapportés.

La deuxième partie traite de la sélection des électrolytes grâce à des mesures électrochimiques. Nous nous sommes concentrés sur l'augmentation de la fenêtre de tension et sur les phénomènes permettant d'obtenir ces résultats dans des condensateurs à double couche électrochimique utilisant du sulfate de lithium comme électrolyte neutre aqueux. Dans la seconde partie de ce chapitre, nous présenterons l'augmentation de la tension de

fonctionnement obtenue dans le cadre de un supercondensateur asymétrique. Nous allons également développer un supercondensateur plus proche du système industriel utilisant des électrodes en carbone enduit sur une feuille d'acier inoxydable.

La troisième partie est consacrée à la préparation des carbones activés à base de cellulose comme précurseur via une méthode de synthèse permettant un contrôle de la taille des pores. La corrélation des propriétés de ces matériaux avec leur comportement électrochimique apporte des éléments de réponse à la compréhension des mécanismes de stockage. Nous avons obtenu des carbones denses et des électrodes, préparées par enduction de ces carbones sur feuille d'aluminium, de très haute densité.

Enfin, la conclusion générale résume les principaux résultats obtenus au cours de cette thèse.

General Introduction

Currently our planet faces huge energy challenges from the scarcity of fossil fuels and the simultaneous greenhouse effects. Burning of fossil fuels with large anthropogenic CO_2 emissions outpaces nature's recycling capability, resulting in significant environmental harm, such as global warming and oceans acidification. Thus, energy insecurity, rising prices of fossil fuels and climate changes threat remarkably our health and political stability. Consequently, we are observing an increase in renewable energy technologies from solar, wind as well as the advent of hybrid electric vehicles with low emissions. However, due to the intermittent character of renewable, reliable electrical energy storage systems are required for adapting these technologies to the demand in electricity.

Among the various realistic solutions, energy can in particular be stored electrochemically in accumulators (batteries) and supercapacitors. Although batteries currently present much higher energy density, their relatively low power density and poor cycle life hinder high power demanding applications such as regenerative braking and load leveling systems. By contrast, supercapacitors store larger amounts of energy than the traditional dielectric capacitors and provide energy far faster than batteries. Therefore, they are particularly adapted for applications requiring energy pulses in short periods of time, e.g., seconds or tens of seconds. Such exceptional properties arise from the nanometric scale capacitors formed by the polarized electrode material and a layer of attracted ions from the electrolyte on its surface. The thickness of the electrode-electrolyte interface is directly controlled by the size of ions.

Recently, supercapacitors have been proposed and widely marketed for various applications. Coupled for example with a battery/internal combustion engine in hybrid vehicles, supercapacitors improve the battery lifetime/fuel economy and the energy recovery efficiency in braking. They can also stabilize current when intermittent renewable energies are introduced in the energetic mix.

Although supercapacitors are now commercially available, they still require improvements, especially for enhancing their energy density and cut the cost at the same time. It requires a fundamental understanding of their properties and exact operating principles, in addition to improving electrode materials, electrolytes and integration in systems. All these topics led to a very strong motivation of academics and industry during the last decade.

The energy density of supercapacitors can be enhanced by increasing the voltage and/or the capacitance. For reaching these objectives, various strategies have been proposed in the

literature, involving the development of new materials, new geometries and new electrolytes. However, the performance and the cost of the supercapacitor device are the main parameters which guide the choices of industry. For these reasons, most of the supercapacitors presently available on the market are based on activated carbon (AC) electrodes and an organic electrolyte. The main advantages of activated carbon are related to its high versatility of structure/texture, low cost and highly developed surface area. More important, its high electrical conductivity allows the realization of high power systems without requiring designing complicated, and consequently expensive, electrode materials. Although generally unfriendly, due to the use of acetonitrile as solvent, the organic electrolytes are preferred by industry to the aqueous ones because of their high stability window, e.g., 2.7 – 2.8 V, allowing high energy density to be reached.

Although the symmetric AC/AC technology in organic electrolyte is now mature, it can be still improved by developing new porous carbons and/or electrolyte formulations. Beside, alternative solutions based on other kinds of electrolytes must be investigated in order to develop either more performing systems or cheaper ones. For these reasons, in the presented work, two directions have been followed for developing optimized symmetric AC/AC supercapacitors:

i) In order to enhance the gravimetric and volumetric capacitance in organic electrolyte, and consequently the energy density, the pore size of the carbon electrode materials has been finely tuned in order to adapt it to the size of electrolyte ions. We will show that highly micro-porous carbons, with highly controlled pore size distribution, average pore width and pore volume, can be produced through high pressure and low temperature induced oxidation of non-porous carbons. In particular, the density of electrodes realized with the resulting carbons can reach higher values than with conventional steam activated carbons. Therefore, we have paid a particular attention to optimizing the preparation parameters in order to achieve larger volumetric energy density through higher density electrodes.

ii) Recent works performed by the Energy/Environment Group in CRMD demonstrated that aqueous AC/AC supercapacitors based on neutral aqueous sodium sulfate (Na_2SO_4) solutions allow higher cell voltage (1.6 V) to be reached than the traditionally investigated aqueous electrolytes, e.g., H_2SO_4 or KOH, where the maximum voltage is generally around 0.7 – 0.8 V. Although the energy density of AC/AC systems in Na_2SO_4 is obviously lower

than in organic electrolyte, it makes sense to optimize and develop the concept, because these capacitors are by far much cheaper than the organic ones, as they do not require a high purity atmosphere for their construction and careful and long drying of the activated carbon electrodes. In this thesis, we have explored different possibilities for extending the operating voltage range either by using other alkali sulfate electrolytes or by modifying the surface functionality of the activated carbon electrodes.

Overall, the dissertation is divided into three chapters:

Chapter I is a literature review showing the state-of-art on carbon based supercapacitors. We describe the principles of electrical double-layer capacitors, and we present an overview on systems based on aqueous, organic and ionic liquids electrolytes. The performance of carbon materials in electrical double-layer capacitors and pseudocapacitors is summarized, highlighting especially the effect of porous texture on the capacitive performance. Hybrid and asymmetric carbon based supercapacitors in organic and aqueous media are introduced to show the profit that can be gained on the point of view of voltage. Finally, in order to orient the choice of our investigations, we conclude on the challenges which still need to be solved and on possible solutions.

Chapter II is dedicated to improving the energy density of symmetric carbon/carbon supercapacitors in aqueous medium by the use of neutral aqueous electrolytes. The electrochemical performance is investigated in lithium sulfate, sodium sulfate and potassium sulfate, at different operating temperatures. Since the best performer is lithium sulfate, this medium has been further selected to determine carefully the parameters affecting the ageing mechanism at high voltage. This allows us to providing solutions to extend the voltage range in lithium sulfate. Finally, we introduce the asymmetric carbon/carbon configuration as a solution to expand the voltage window.

Chapter III presents an attempt of improving the volumetric energy density of carbon/carbon supercapacitors in organic electrolyte by enhancing the density of electrodes through a novel production process of activated carbon. We demonstrate that the porous parameters of carbon (micropore volume, pore size distribution, average pore size) can be exactly tailored to the size of electrolyte ions by repeated high pressure oxidation of a non-porous carbon and thermal desorption of the surface functional groups. Then, we show that

the process can be simplified, e.g., it can be reduced to only one oxidation/thermal desorption cycle by adjusting the oxidation parameters, such as temperature, pressure and time.

Finally, the manuscript ends with a general conclusion and some perspectives of future works in the directions which we have investigated.

Chapter I: *Bibliography*

This chapter intends to present the state-of-the art on capacitors, and particularly the strategies to enhance the energy density. Since the literature which appeared within the last years is quite abundant, the review will be essentially focused on the topics intended to be developed in this thesis. After a short introduction on the general properties and electrolytes used in supercapacitors, the fundamental role played by carbons will be discussed in detail, taking particularly into account the effect of pore size on the electrical double-layer capacitance and the strategies to tailoring the pore size to the size of electrolyte ions. The sources of capacitance enhancement through pseudo-capacitive contributions arising from surface functionalities on carbons, electrochemical hydrogen storage and novel carbon/electrolyte interfaces will be presented. Finally it will be shown that hybrid and asymmetric constructions of supercapacitors help in enhancing the maximum voltage of supercapacitors and consequently their energy density.

1 Introduction

Supercapacitors (or electrochemical capacitors, or ultracapacitors), based on activated carbon electrodes, mainly store the charge in an electrical double-layer (EDL) formed at the electrode/electrolyte interface [1][2][3]. The primary advantages of supercapacitors involve high power density and almost unlimited cycle life, etc. Furthermore, they provide higher energy density than conventional capacitors while higher power density than batteries. To clearly compare their power and energy capabilities, Figure 1 summarizes power and energy relations in a Ragone plot for supercapacitors and batteries. It becomes obvious that supercapacitors are particularly adapted for applications which require energy pulses during short periods of time, e.g. hybrid vehicles, tramways, buses, cranes, forklifts, wind turbines, electricity load leveling in stationary and transportation systems, in opening emergency doors of aircrafts, etc.

The first patent of supercapacitors using porous carbon electrodes in aqueous medium dates back to 1957 by Becker assigned to General Electric [4]. The commercialization of a supercapacitor in aqueous electrolyte actually started in the 1970s by Nippon Electric Company (NEC) [5]. By the 1980s, many companies produced such devices such as Gold capacitor by Matsushita, Dynacap by Elna, PRI ultracapacitor by PRI designed for military applications such as laser weaponry and missile guidance systems, etc [6][7]. Since 2000, supercapacitors have effectively permeated in industrial applications mainly including

automobiles, tramways, buses, cranes, forklifts, wind turbines, electricity load leveling in stationary and transportation systems, etc [1].

The supercapacitor manufacturers mainly include Maxwell and Ioxus in USA, LS Mtron and NESS in South Korea, Nippon Chemi-Con, Meiden and JSR Micro in Japan, Batscap in France, ELIT and ESMA in Russia, Wima in Germany, Yunasko in Ukraine. The Japanese companies occupy a large market share [7][8]. It is reported that the supercapacitor industry will annually achieve a compound revenue growth of 10.9 % for the next decades, with $ 205.9 million in revenue generated by 2014 in a comparison with about $ 99.6 million in 2007 [8]. The continuous growth will open new markets, leading to a bright future for supercapacitors.

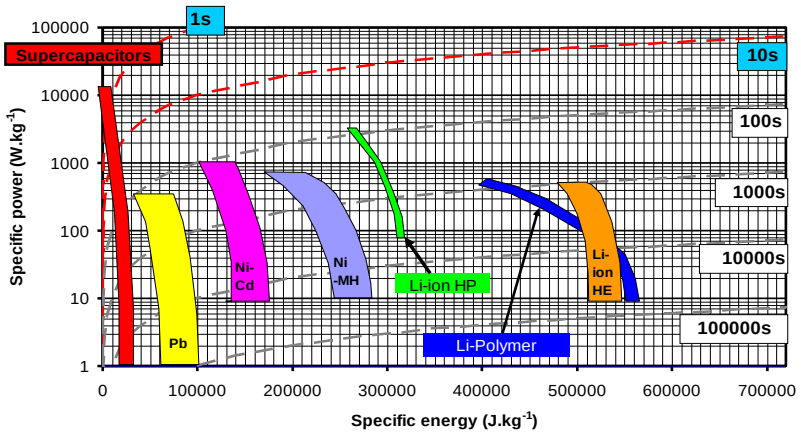

Figure 1 Ragone plot for electrochemical energy storage devices. Times shown are the time constants of the devices, obtained by dividing the energy density by the power [1].

2 Principles and properties of supercapacitors

2.1 The electrical double-layer

The electrical double-layer mechanism, which arises from the electrostatic attraction between the surface charges of activated carbon and ions of opposite charge, plays the major role in carbon/carbon supercapacitors. As described by Helmholtz in 1853, a charge separation takes place on polarization at the electrode-electrolyte interface with a double layer distance ***d*** (Figure 2a), leading to a capacitance ***C*** (equation 1):

$$C = \frac{\varepsilon_r \varepsilon_0 A}{d} \quad (1)$$

where $\boldsymbol{\varepsilon_r}$ and $\boldsymbol{\varepsilon_O}$ are the dielectric constants of the electrolyte and vacuum, respectively, and $\boldsymbol{A}$ is the specific surface area of electrode/electrolyte interface (accessible surface area).

The model was further refined by Gouy & Chapman proposing a diffuse layer (Figure 2b), which takes into account a continuous distribution of ions driven by thermal motion. On the other hand, the potential decreases exponentially away from the surface to the fluid bulk (Figure 2b). However, the Gouy & Chapman model overestimated the capacitance arising from charged ions close to the electrode surface. Later, Stern suggested a model combining the Helmholtz and Gouy-Chapman models, and introducing a compact layer with ions strongly adsorbed onto the electrode surface and a diffuse layer as defined in the Gouy & Chapman model (Figure 2c). As a result, the EDL capacitance (C_{dl}) of the electrode becomes a combination between the Helmholtz/compact double-layer capacitance (C_H) and the diffusion region capacitance (C_{diff}), and can be expressed as in equation (2):

$$\frac{1}{C_{\mathrm{dl}}} = \frac{1}{C_{\mathrm{H}}} + \frac{1}{C_{\mathrm{diff}}} \tag{2}$$

Generally, the double-layer capacitance is in a range of 5 to 20 µF cm^{-2} depending on the electrolyte and the electrode material [9].

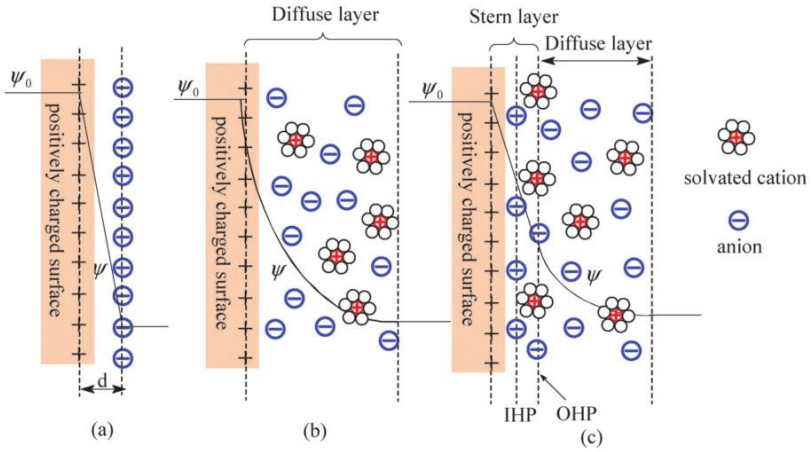

Figure 2 Scheme of the electrical double-layer: a) Helmholtz model, b) Gouy-Chapman model, and c) Stern model. IHP and OHP represent the inner Helmholtz plane and outer Helmholtz plane, respectively. *d* is the double-layer distance described by the Helmholtz model. φ_o and φ are the potentials at the electrode surface and the electrode/electrolyte interface, respectively [10].

2.2 Construction of a supercapacitor

The most common configuration for a supercapacitor is a symmetric system assembled with two identical activated carbon electrodes immersed in an electrolyte. In this case, during operation of the system, the dominant mechanism is the charge/discharge of the electrical double-layer, and the system is called an electrical double-layer capacitor (EDLC). The positive electrode attracts the anions while the cations are accumulated onto the negative electrode. The EDL capacitance results from the pure electrostatic attraction between ions and the charged surface of electrodes. The electrode, the heart of a supercapacitor, determines its capacitance and partially its resistance and self-discharge characteristics. The most used electrode materials can be categorized into carbon materials, metal oxides, and conducting polymers [8][11]. Beside the EDL behavior, pseudo-faradic effects related with reversible redox reactions may also contribute to the capacitance of the device, especially with metal oxides and conducting polymers.

The positive and negative electrodes of the AC/AC symmetric system are separated by a porous membrane called separator. Each electrode/electrolyte interface represents a capacitor and hence the simplified equivalent circuit of the complete device can be represented by two capacitors in series, as shown in Figure 3 [6][12], and the total capacitance (C) expressed by equation (3) [2] is essentially controlled by the electrode with the smallest capacitance:

$$\frac{1}{C} = \frac{1}{C_1} + \frac{1}{C_2} \tag{3}$$

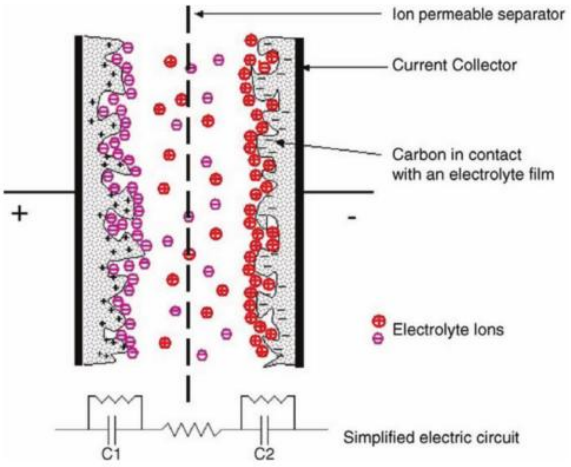

Figure 3 Representation of an electrical double-layer capacitor in its charged state [6].

2.3 Energy and power of supercapacitors

The maximum energy *E* (J) stored in a supercapacitor is given by equation (4) [2]:

$$E = \frac{1}{2}CU^2 \tag{4}$$

where *C* is the specific capacitance (F), *U* is the maximum cell voltage (V). The capacitance depends essentially on the electrode materials used. The voltage is limited by the stability potential window of the electrolyte. Generally, the maximum voltage is 0.6-0.8 V in aqueous electrolytes and 2.5-2.7 V in organic medium. A further expansion of the voltage range can be realized by using ionic liquids as it will be discussed later.

The maximum power (P) of a supercapacitor is calculated according to equation (5):

$$P = \frac{U^2}{4R_S} \tag{5}$$

where *U* is the maximum cell voltage (V), R_S the equivalent series resistance (ESR in Ω) and *P* the maximum power (W). The factors which mainly contribute to the overall series resistance of supercapacitors are the conductivity of the electrode material, the contact resistance between the electrode material and the current collector, the electrolyte resistance, the ionic diffusion resistance due to the movements in micropores and the ionic resistance caused by the separator. Thanks to the electrostatic charge storage mechanism, the series resistance does not include any charge transfer resistance contribution associated with electron exchange, as observed for redox reactions. Thus, the series resistance is lower than that of batteries at cell level, explaining the higher power density of supercapacitors compared to batteries. The ESR is reduced by adding a percolator which improves the conductivity of the electrode and by improving the electrical contact between the current collectors and the active materials [13][14][15].

3 Electrolytes

The electrolyte is typically composed of one or more solvents containing one or more salts. As shown in equation (4) and (5), higher operating voltage and lower resistance allow higher energy and power density to be reached. Therefore, the electrolytic system must exhibit: 1) a good conductance which determines the power output capability; 2) a good ionic adsorption which determines the specific double-layer capacitance; 3) the dielectric constant

which also determines the double-layer capacitance value and its dependence on electrode potential as well as the extent of ionization or ion pairing of the solute salt, which influences the conductance. Overall, the desirable properties of an electrolytic system for supercapacitors are: high ionic conductivity, wide voltage window, and high electrochemical and thermal stability, low viscosity, low toxicity, low cost, etc [8]. The currently used electrolytes are aqueous electrolytes (H_2SO_4 and KOH), organic electrolytes (propylene carbonate and acetonitrile based ones), and recently ionic liquids [16].

3.1 Aqueous medium

Until recently, the most commonly used aqueous electrolytes were 1 mol L^{-1} H_2SO_4 and 6 mol L^{-1} KOH [17]. Compared with non-aqueous electrolytes, the aqueous medium provides a much higher conductivity leading to higher power density. The conductivity (25 ^oC) of 6 mol L^{-1} KOH exceeds 600 mS cm^{-1} while it is only 20 mS cm^{-1} for tetraethylammonium tetrafluoroborate in propylene carbonate and ~10 mS cm^{-1} for typical room temperature ionic liquids [18]. On the other hand, low cost and easy manipulation could be further advantages for aqueous electrolytes. Unfortunately, the lower voltage of aqueous medium is restricted via the thermodynamic window of water at 1.23 V. When the voltage is higher than 0.8 V, the potential of one of the electrodes may be beyond the thermodynamic limit resulting in the water decomposition. It is much lower than in non-aqueous electrolytes (e.g., 2.7 V-2.8 V for the organic medium) resulting in much lower energy and power stored.

Interestingly, it has been demonstrated that neutral aqueous electrolytes such as alkali sulfates could achieve higher voltages with symmetric carbon/carbon capacitors than generally obtained in acidic or basic medium. In previous work from CRMD, a stability potential window around 2.0 V has been demonstrated with activated carbon in 0.5 mol L^{-1} Na_2SO_4. As a result, a practical voltage of 1.6 V has been attained during 10,000 reversible charge/discharge cycles in symmetric carbon/carbon systems [19]. The electrochemical analysis of seaweed carbons in 0.5 mol L^{-1} Na_2SO_4, demonstrated that the nature of the electrode material and the electrolyte pH influence both the capacitance values and the stability potential window; due to the presence of nitrogenated functionalities in these carbons, the potential window reached 2.4 V in 0.5 mol L^{-1} Na_2SO_4 [20]. Qu *et al.* [21] reported that the migration rate of hydrated ions in the bulk electrolyte and within the inner pores of activated carbon increase in the order of $Li^+ < Na^+ < K^+$, and that the rate

performance improves in the order $Li_2SO_4 < Na_2SO_4 < K_2SO_4$. The highest operating voltage of 2.2 V with an exceptional cycling stability has been demonstrated in Li_2SO_4; Fic *et al.* have suggested that the stronger hydration of Li^+ compared to Na^+ and K^+ ions is responsible for larger voltage in Li_2SO_4 solution[22]. Those findings have opened a new door for the aqueous medium. Although acidic and basic solutions has been reported mainly due to their high electrochemical activity, their corrosive properties severely hinder large-scale commercialization because of the high price of corrosion-resistant current collectors such as gold or platinum [23]. Therefore, neutral-pH aqueous electrolytes appear as a more promising choice from industrial point of view, according to the pragmatic rule "supercapacitors will see growth only when their costs fall" [23].

3.2 Organic electrolytes

Organic electrolytes allow higher operating voltages than aqueous electrolytes in supercapacitors, being preferred for reaching higher energy density according to equation (4). The practical operating voltage of organic electrolytes in symmetric carbon/carbon supercapacitors is about 2.7-2.8 V, which depends strongly on the impurities of the components, such as water and surface groups in carbons [24][25]. As a result, ten parts per million water dissolved in the organic medium decrease the voltage range by about 10 mV compared with the purified ones [26].

Conventional electrolytes contain a mixture of a solvent such as acetonitrile (ACN) or propylene carbonate (PC) and a salt such as tetraethyl ammonium tetrafluoroborate ($(C_2H_5)_4BF_4$). Tetraethyl ammonium salts have been widely utilized because of their good solubility in non-aqueous solvent and moderately good conductivity. Currently carbonates represented by PC are the most widely used solvent in Japan whilst ACN is more popular in USA and Europe. The low flash point of ACN (lower than 5 ^oC) might be an issue on safety concerns [27]. It is well-defined that PC- based electrolytes usually present lower conductivity than those based on ACN, resulting in relatively lower power output. The replacement of ACN with PC can only be achieved at the expense of the power density since the electrolyte conductivity drops by a factor of ~4 [28]. It is reported that the capacitance decrease with temperature decline is much more pronounced for PC than ACN based electrolytes [29][30]. Generally, manufacturers typically specify an operation temperature range from -40 ^oC to 70 ^oC for ACN and PC based supercapacitors. A maximum operating

temperature up to 100°C has been reported for PC based laboratory-scale supercapacitors [31] whereas the temperature is limited to 70 °C in the case of ACN due to its lower boiling point of 80°C [27].

Recently, Brandt *et al.* [32] claimed a maximum voltage expanded up to 3.75 V by using 0.7 mol L^{-1} Et_4NBF_4 in adiponitrile. The wide electrochemical stability of adiponitrile contributes to the higher potential range at which conventional organic solvents, e.g. ACN, normally suffer from the decomposition processes. However, the conductivity of such medium is much lower than for conventional solutions in acetonitrile. Consequently, the ohmic loss is relatively important and the real voltage window between the electrodes is not as high as claimed. Intensive cyclability tests should be realized in this medium in order to evaluate correctly its potentialities versus other organic electrolytes.

Although organic electrolytes are the most widely adopted solution by industry, one must take into account several of their disadvantages, including high cost, low conductivity resulting in power loss, low dielectric constant reducing the capacitance as well as safety concerns due to the flammability and toxicity of the organic solvent [10].

3.3 Ionic liquids

Ionic liquids (ILs) are room temperature molten salts, which are entirely composed of cations and anions [33]. ILs show promising properties for supercapacitor applications including a high thermal stability as high as 300 °C with near zero vapor pressure, non-flammability with very low toxicity, non-corrosive to supercapacitor components at elevated temperatures and high electrochemical stability over a wide voltage window from 2 to 6 V (typically about 4.5 V) [8][16]. Since ILs are solvent-free without solvation shell, they can thus offer a well-defined ion size, which on the fundamental point of view might help in better understanding the behavior of ions in the porosity of carbons. However, they still cannot satisfy the requirements for large-scale supercapacitor applications due to their high price and relatively low conductivity at room temperature. The typical ionic conductivity is in the range of ~14 mS cm^{-1} at room temperature [34]. Furthermore, maintaining the required high purity during the production requires complex processes.

Currently, the main ILs studied for supercapacitor electrolytes are imidazolium, pyrrolidinium, as well as asymmetric, aliphatic quaternary ammonium salts with anions such as tetrafluoroborate, trifluoromethanesulfonate, bis(trifluoromethanesulfonyl)imide,

bis(fluorosulfonyl)imide or hexafluorophosphate [8]. The resistivity of ILs depends strongly on temperature and requires a temperature of about 125 ^{o}C to have a comparable resistivity to the acetonitrile-based electrolyte [16]. Therefore, the use of ionic liquids as electrolytes might be interesting at high temperature where the resistance is acceptable and where they demonstrate much higher thermal stability than the classical organic electrolytes. However, a breakthrough has been shown at low temperature, using an eutectic electrolyte mixture (1:1 by weight) of N-methyl-N-propylpiperidinium bis(fluorosulfonyl)imide and N-butyl-N-methylpyrrolidinium bis(fluorosulfonyl)imide, where the working temperature range could be extended from -50 ^{o}C to 100 ^{o}C [27]. Although the carbon selected for this experiments exhibits a low density (related to its mesoporous character), this kind of mixture opens the door for expanding the operating range of ILs based supercapacitors under extreme climatic conditions.

4 Carbons for electrical double-layer capacitors (EDLCs)

At present, various carbon materials can be used as active materials for EDLC electrodes in academia and industry, owing to their high conductivity, high surface area, a rich variety of dimensionality, good corrosion resistance, controlled pore structure, processability and compatibility in composites, relatively low cost, etc [2][3][9][35][36]. A developed surface area and controlled distribution of pores for porous carbons, produced by well established chemical and physical activation methods, determine the electrode/electrolyte interface in supercapacitor applications. Figure 4 presents a porous network in an activated carbon granule, which includes micropores (lower than 2 nm width), mesopores (between 2 and 50 nm), and macropores (larger than 50 nm). Most of the adsorption process takes place in the range of micropores, whereas meso- and macropores play very important roles in transporting the adsorbate to the micropores [37].

Table 1 compares the properties of different carbon structures presented in the literature as supercapacitor electrode materials, including activated carbons [2][3], onion-like carbon [38], carbon nanotubes [39][40], graphene [41][42], and carbide-derived carbons [43]. Considering the essential criteria of low cost and high volumetric capacitance considered by industry, it is clear that activated carbon remains the material of choice for this application. Its slightly lower conductivity compared to other forms of carbons can be easily compensated by using a good percolator and by manufacturing high quality electrodes. In supercapacitor

industry, a metallic current collector, e.g., aluminum foil, is coated by a slurry containing the electrochemically active material (activated carbon) together with a binder (polyvinylidene fluoride-PVdF, polytetrafluoroethylene-PTFE, etc) and the conductive agents (carbon black, etc) playing as percolator between the AC grains [8].

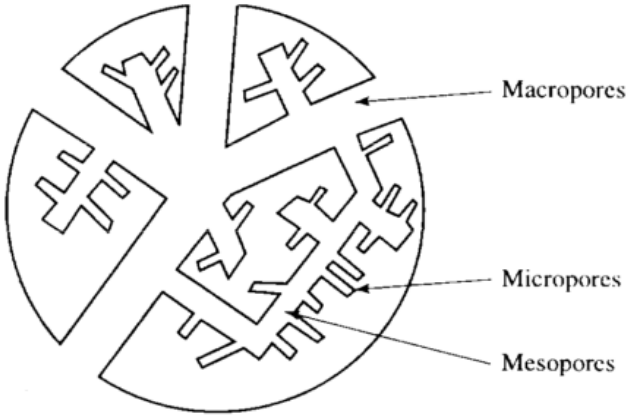

Figure 4 Schematic representation of an activated carbon granule [37].

Table 1 Different carbon electrode materials used in supercapacitors [44]

Material	Carbon onions	Carbon nanotubes	Graphene	Activated carbon	Carbide derived carbon	Templated carbon
Dimensionality	0-D	1-D	2-D	3-D	3-D	3-D
Conductivity	High	High	High	Low	Moderate	Low
Volumetric Capacitance	Low	Low	Moderate	High	High	Low
Cost	High	High	Moderate	Low	Moderate	High
Structure	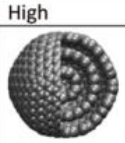	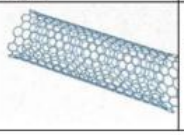	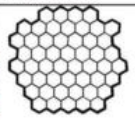	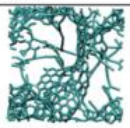	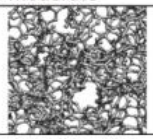	

4.1 Effect of porous texture on the capacitive performance

According to equation (1), the capacitance of carbon electrode materials is directly related to the surface area of the electrode/electrolyte interface. Numerous works have attempted to correlate the EDL capacitance with the BET or DFT specific surface area. It is generally accepted that the BET model, based on multilayer gas adsorption on the solid surface, gives an unreliable large surface area for micro-porous carbons [45]. For instance, below the pore size of 0.9 nm, the BET model underrates the realistic surface area while overrates it from 0.9 to 4 nm or even beyond such range [46]. Therefore, the Dubinin-

Radushkevich (DR) equation or the Density Functional Theory (DFT) model appears to be a more reliable estimation [46]. Nevertheless, whatever the specific surface area determined using either the BET or DFT model [45], the specific capacitance of carbon materials does not show a linear relationship with the total surface area. As shown in Figure 5, the specific capacitance tends to keep at a constant value when the specific surface area is higher than 1200 $m^2 g^{-1}$ [47][48].

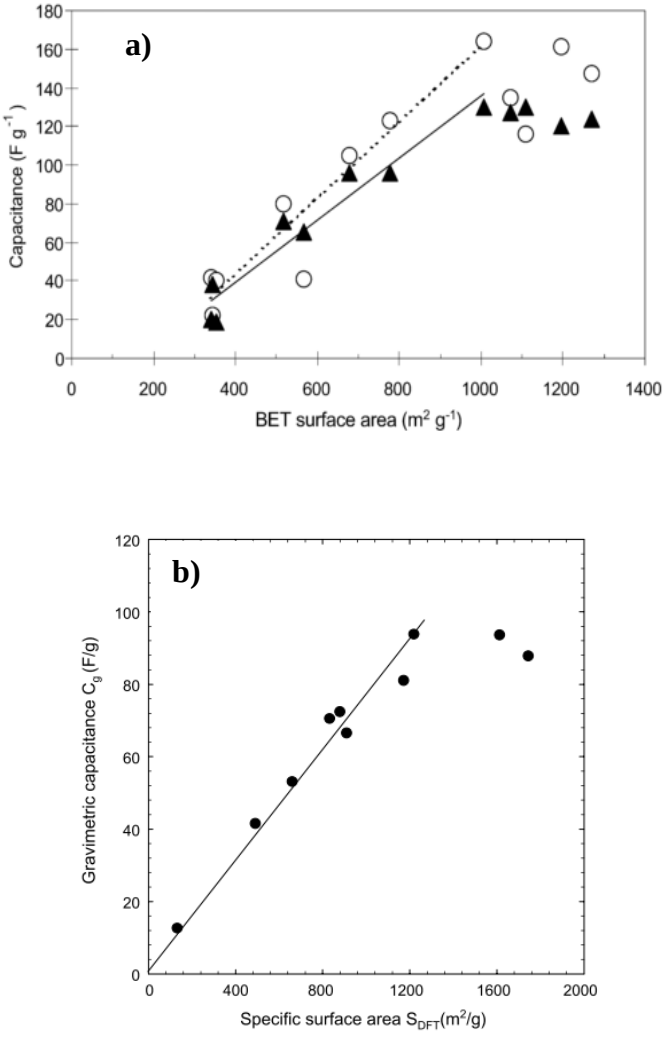

Figure 5 Specific capacitance of activated carbons (a) in 1 mol L^{-1} H_2SO_4 (O) and 6 mol L^{-1} KOH (▲) as a function of the BET specific surface area [48]; (b) in 1 mol L^{-1} $(C_2H_5)_4NBF_4$ in acetonitrile as a function of the DFT specific surface area [47].

Overall, the specific capacitance cannot be simply improved by developing the specific surface area. In fact, the development of surface area with whatever activation method is

usually accompanied by a widening of the pores, which might be responsible of modified interaction of ions with the pore walls. Thus, the pore size of carbon materials is another parameter to be taken into account in order to optimize the capacitive performance.

Aurbach *et al.* have explored the influence of relative pore size and ions size on the electrochemical behavior of carbons with different average pore widths into electrolytes which have different ion sizes [49][50][51]. Figure 6 presents three-electrode cyclic voltammograms (CVs) of carbon electrodes in aqueous 0.1 N $MgSO_4$, Li_2SO_4, and $MgCl_2$ solutions as electrolytes. When comparing the carbons with average pore width of 5.1 Å (C5.1) and 5.8 Å (C5.8) in aqueous 0.1 N $MgSO_4$, the current is negligible for the former while much larger current and better capacitive behavior are observed with the latter. It thus suggests that 5.1 Å is too narrow to adsorb the large Mg^{2+} and $SO4^{2-}$ ions. In the case of the aqueous Li_2SO_4 and $MgCl_2$ media, the corresponding triangular shaped CVs can be ascribed to the adsorption of the relatively small size ions into the pores and the absence of adsorption for the bivalent and large dimensions ions. Finally, when the pore size is smaller than the ion size, ion electro-adsorption cannot properly occur and an ion sieving effect is observed.

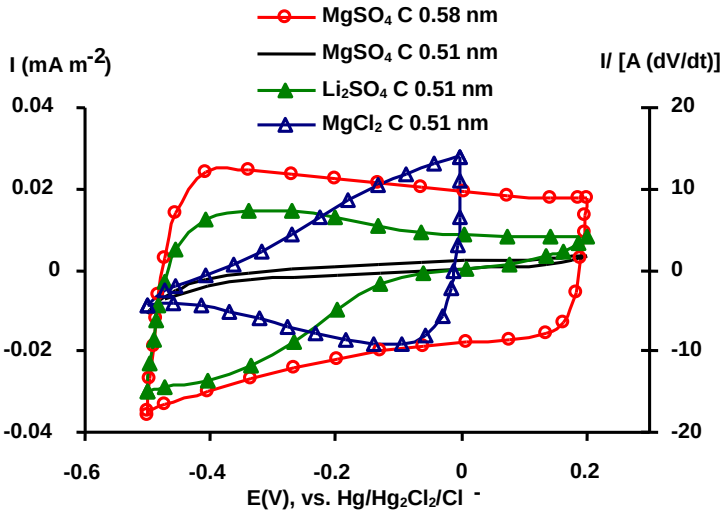

Figure 6 Cyclic voltammograms (CVs) of activated carbon electrodes with average pore size of 0.51 (C5.1) and 0.58 nm (C5.8) in 0.1 N $MgSO_4$, Li_2SO_4, and $MgCl_2$ solutions. The current is normalized per unit of BET specific surface area [50].

Studying the effect of the porous texture on capacitance for a series of templated carbons in organic (1 mol.L^{-1} Et_4NBF_4 in acetonitrile) and aqueous electrolytes, Vix-Guterl *et al.* have found a linear relationship between the specific capacitance and the ultramicropore volume obtained by CO_2 adsorption (0.7-0.8 nm pore size), showing that this size of pores is optimal for enhancing the adsorption of ions [52]. Considering additionally the diameters of solvated Et_4N^+ (1.30 nm) and BF_4^- (1.16 nm), and neat Et_4N^+ (0.68 nm) and BF_4^- (0.48 nm), this result suggested for the first time that ions are at least partly desolvated when stored in ultramicropores [53]. This finding was confirmed recently by a solid-state NMR study of electrolyte organization in charged nanoporous carbon electrodes using 1 mol.L^{-1} Et_4NBF_4 in acetonitrile [54]. Indeed, as shown in Figure 7, when increasing the voltage, the solvent concentration noticeably decreases in the negative electrode (the electrode where the Et_4N^+ ions, named TEA^+, are stored) until no acetonitrile (ACN) is detected when the supercapacitor operates at 2.7 V. While the solvent molecules are adsorbed in all carbon porosity in absence of polarization, they progressively leave the space available between the graphene layers in the micropores of the negative electrode and occupy the mesopores, which proves the desolvation of the Et_4N^+ cations. By contrast, the amount of solvent remains almost constant in the positive electrode (Figure 7). Actually, when entering the micropores, the bulky Et_4N^+ cations push away acetonitrile molecules from the negative electrode, while the smaller BF_4^- anions leave sufficient space to accommodate the solvent molecules in the positive electrode.

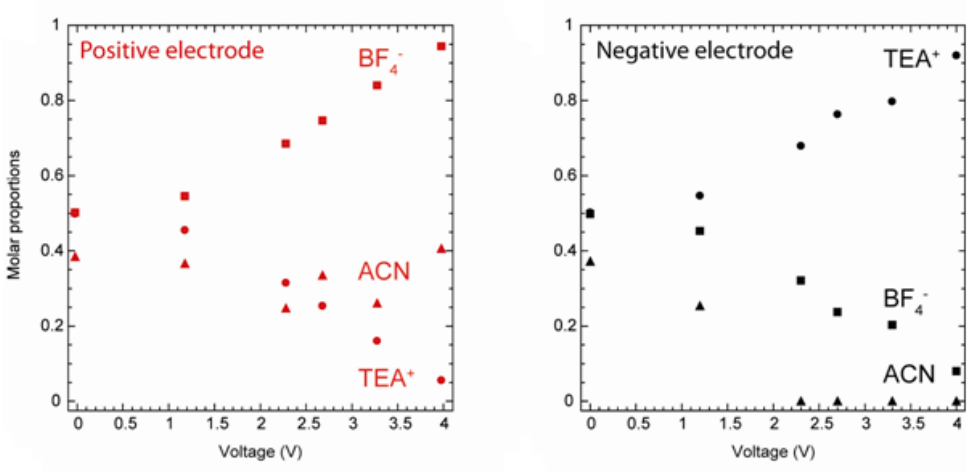

Figure 7 Molar proportions of TEA^+ ($n_{TEA}/n_{TEA}+n_{BF4}$) and BF_4^- ($n_{BF4}/n_{TEA}+n_{BF4}$), as well as relative amount of ACN vs total amount of electrolyte species ($n_{ACN}/n_{ACN}+n_{TEA}+n_{BF4}$) after polarization at 0V (i.e. 2.3V for 30 minutes followed by 30 minutes at 0V), 1.2V, 2.3V, 2.7V, 3.3V and 4.0V for 30 minutes in the positive and negative electrodes of a supercapacitor using 1 mol L^{-1} Et_4NBF_4 in acetonitrile electrolyte [54].

The existence of an optimal pore size is clear when representing the normalized capacitance (capacitance divided by the Dubinin Raduskevich pore volume - V_{DR}) versus the average pore size L_0 for a series of activated carbons. Figure 8 shows that the optimal pores filling arises when the pore size reaches approximately 0.7 nm in aqueous electrolyte (6 mol L^{-1} KOH, 1 mol L^{-1} H_2SO_4) and 0.8 nm in 1 mol L^{-1} tetraethylammonium tetrafluoroborate in acetonitrile [55]. The slightly larger optimal pore size in organic medium than that of aqueous solutions is reasonable considering generally the larger ion sizes in organic ones. On the other hand, one can qualitatively conclude that according to equation (1) large pores show worse interaction with ions than small pores [56].

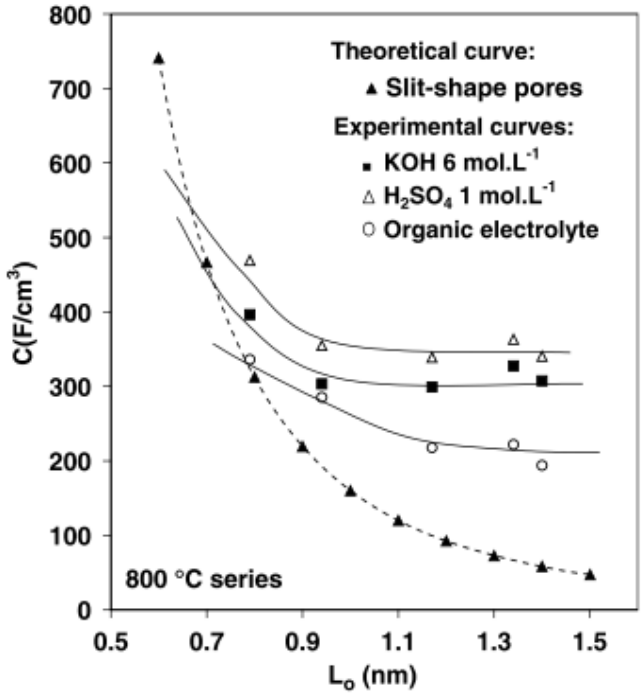

Figure 8 Relationship between the theoretical and experimental normalized capacitance (capacitance divided by V_{DR}) of a series of activated carbons and their average pore size in aqueous and organic electrolytes [55].

Chmiola *et al.* have pointed out that increasing the volume of micro-pores improved the specific capacitance while increasing the volume of pores larger than 2 nm by using ZrC and TiC derived CDCs in aqueous electrolyte had a detrimental effect on capacitance [57]. Expanded their investigations with a series of TiC-CDCs in organic electrolyte, they observed also an increase in normalized capacitance (capacitance divided by BET specific surface area) when the average pore size decreases from 1.10 to 0.68 nm [58]. Similarly, the

electrochemical investigations on the positive and negative electrodes reveal a sharp increase of EDL capacitance when the pore size varies from 0.8 nm to 0.7 nm, especially for the negative electrode (Figure 9). Since the respective diameters of the desolvated Et_4N^+ and BF_4^- ions obtained by computer simulation are 0.74 and 0.49 nm [52], respectively, such observations confirm that the optimal capacitance could be achieved when the pore size is very close to the size of the desolvated cation. The capacitance increase from 1.1 to 0.7 nm cannot simply be ascribed to purely electrostatic reasons. Herein, it is proposed that the energy relating with de-solvation upon charging and re-solvation upon discharging leads to a reversible charge-storage mechanism.

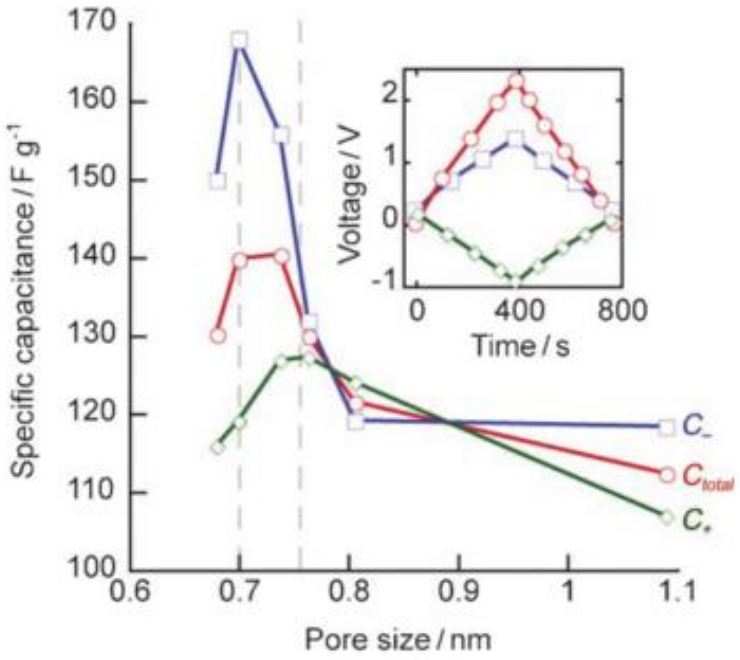

Figure 9 The specific capacitances calculated from a constant current discharge (inset, colors as for main plot) for the anion/positive electrode (C_-) and cation/negative electrode (C_+) show similar behavior until a critical average pore size of ~0.8 nm is reached. At pore sizes below this value, the capacitance values of positive and negative electrodes diverge [53].

Hence, the pore size maximizing the double-layer capacitance is very close to the size of the desolvated ions. This has been confirmed by Largeot *et al.* by using an ionic liquid (EMI-TFSI) as electrolyte with carbide derived carbons (TiC-CDCs) with average pore sizes close to the electrolytes ion size [59]. Particularly, ionic liquids were used as electrolytes because they offer well identified ion size as they do not need a solvent and do not have a solvation

shell. For the $TFSI^+$ EMI^- ionic liquid, the ion sizes were calculated as 0.79 nm and 0.76 nm in the longest dimension for the anion and cation, respectively. Figure 10 shows that the largest normalized capacitance corresponds to a pore size of around 0.7 nm. It confirms that there is no space available for more than one ion per pore and that the most efficient pores are those in which the pore size is perfectly adapted to the ion size. Therefore, it is necessary to keep a narrow pore size distribution and average pore size below 1 nm for carbon electrode materials. Finally, EDL theory taking into account solvation effects could demonstrate an improved understanding of the charge storage mechanisms in EDLCs [60].

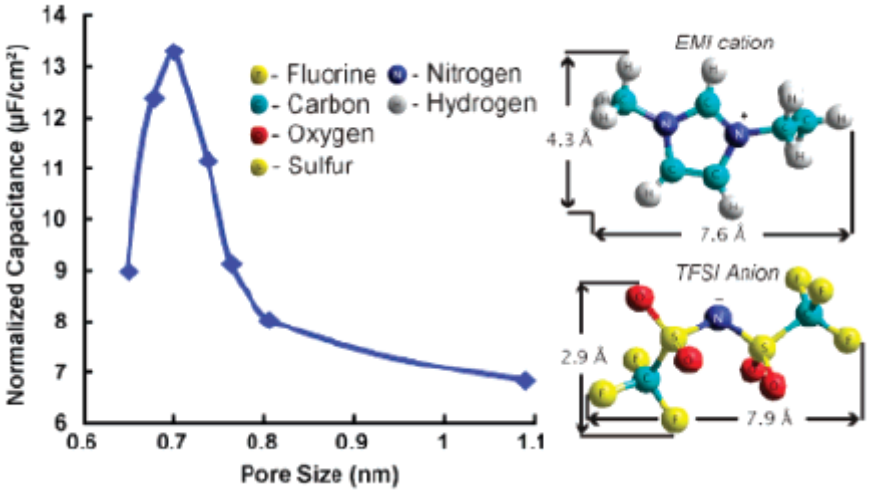

Figure 10 Normalized capacitance changes versus the pore size of TiC-CDC samples produced at different temperatures; the normalized capacitance is obtained by dividing the specific capacitance by the BET specific surface area. HyperChem models of the structure of EMI and TFSI ions show a size correlation [59].

Recently, Merlet *et al* [61] used molecular dynamics simulation to explain the mechanisms occurring during the charge of a supercapacitor with microporous carbon electrodes using an ionic liquid as electrolyte, i.e., 1-butyl-3-methylimidazolium hexafluorophosphate (BMI-PF_6). The EDLC simulation cell is shown in Figure 11, where the top panel is a snapshot extracted from a simulation, and the bottom panel illustrates the electrification of an electrode held at various potentials. The two key features taken into account were a realistic atomistic structure of the CDC carbon electrode and the polarization of the electrode atoms by the ionic charges. Such approach allows simulations of conducting electrodes of arbitrary geometry under constant applied potentials to be performed, i.e. in the same way as experiments are performed. Through this simulation, capacitance values of 87

and 125 F g^{-1} were obtained for CDC-1200 and CDC-950, respectively. As a consequence, capacitance value of 87 and 125 F g^{-1} were obtained for CDC-1200 and CDC-950, respectively. These values show a quantitative agreement with experimental data [59], and are far higher than the values reported in previous simulations for ionic liquids adsorbed in carbon nanotubes [62]; these simulations did not consider that the electrode is wetted by the ionic liquid even at null potential.

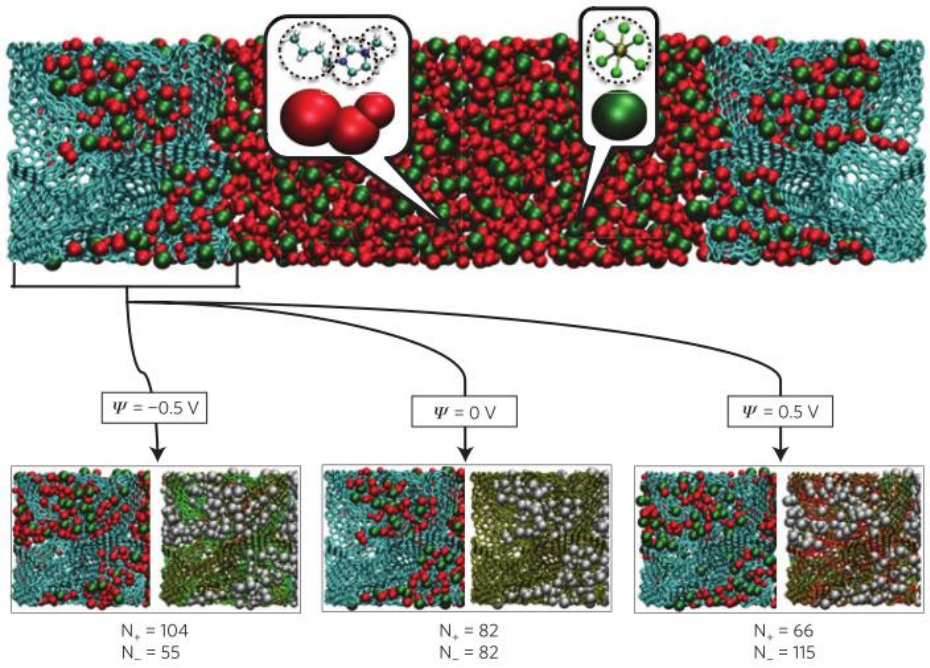

Figure 11 The EDLC simulation cell. Upper panel: the simulation cell consists of a BMI-PF_6 ionic liquid electrolyte surrounded by two porous electrodes (CDC-1200) held at constant electrical potentials (blue: C atoms, red: the three sites of BMI^+ and green: PF_6^- ions; a coarse-grained model is used to describe these ions). Lower panel: structure of the electrode for various voltages. For each value, the same snapshot is shown twice: the ionic distribution is shown on the left. The degree of charging of the electrode atoms is shown on the right, where the carbon atoms are colored according to the charge *q* they carry (green: $q<0$, red: $q>0$ and yellow: q_0). The charging mechanism involves the exchange of ions between the bulk and the electrode [61].

By comparing the electrochemical performance of a carbon with almost all the pores below 1 nm (PC, S_{DFT} = 1434 m^2 g^{-1}, Figure 12) and another one with a wider pore size distribution (VC, S_{DFT} = 2160 m^2 g^{-1}, Figure 12), Mysyk *et al.* have demonstrated that porosity may be saturated by NEt_4^+ cations before reaching the maximum possible voltage for the considered electrolyte, e.g., 2.7 – 2.8 V for NEt_4BF_4 in ACN [63]. Figure 13 shows the cyclic voltammograms of two-electrode cells built in ACN + 1.5 mol.L^{-1} NEt_4BF_4

electrolyte with the carbons PC and VC. The PC carbon exhibits a capacitive current decrease when the voltage increases beyond 1.5 V, whereas the VC carbon demonstrates a rectangular shaped voltammogram indicating a typical capacitive behavior.

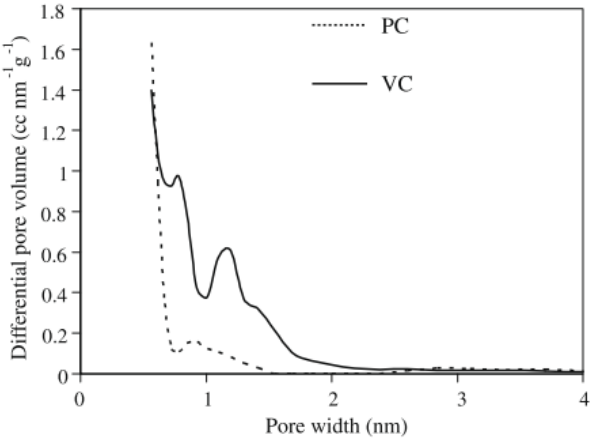

Figure 12 Pore size distribution of mesophase pitch (PC) and viscose (VC) derived nano-porous carbons [63].

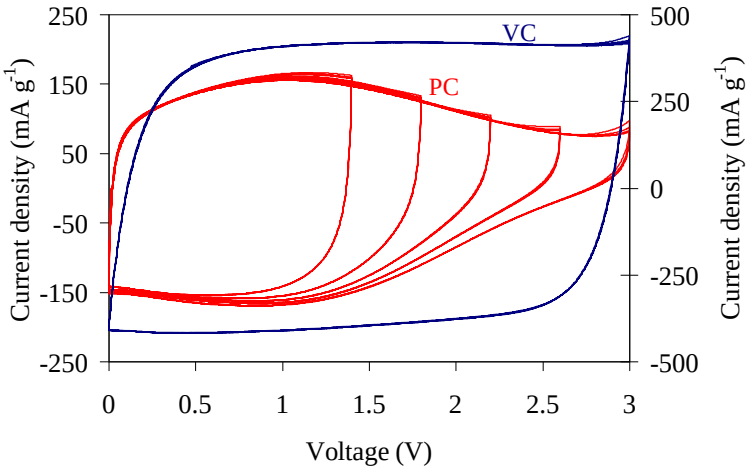

Figure 13 Cyclic voltammograms (CVs, 5 mV s^{-1}) for supercapacitors based on carbon PC (left-hand side Y-axis for current) and carbon VC (right-hand side Y-axis for current) [63].

Similar shape of voltammogram as for the PC carbon was observed by Conway *et al.* in diluted electrolyte solution or at high scan rate and was interpreted by an "electrolyte starvation" effect [64]. Generally, such effect depends on the electrolyte concentration, electrolyte volume and electrodes mass. In order to check whether the electrolyte starvation is the reason for the current decrease observed in Figure 13, voltammograms of carbon PC were further recorded using a 0.1 mol L^{-1} solution of NEt_4BF_4 in acetronitrile (Figure 14). Since

the result is the same as for the 1.5 mol L^{-1} solution, the concentration-dependent electrolyte starvation is not the cause for the current decay with carbon PC. Consequently, porosity saturation (accessible surface area) was further suggested to be responsible for the current decay observed in Figure 13 with PC based supercapacitors. The electrode active surface is completely covered by ions at a voltage lower than the electrolyte decomposition point [63][65]. As a consequence, this saturation phenomenon precludes the system to profit from high voltage and further limits the energy and power density.

In summary, a relatively high specific surface area together with a narrow pore size distribution is mandatory to achieve high capacitive performance. Highly micro-porous carbons with a moderately developed porosity/surface area, narrow pore size distribution and average pore size below 1 nm seem to be the practical and appropriate choice for supercapacitor applications.

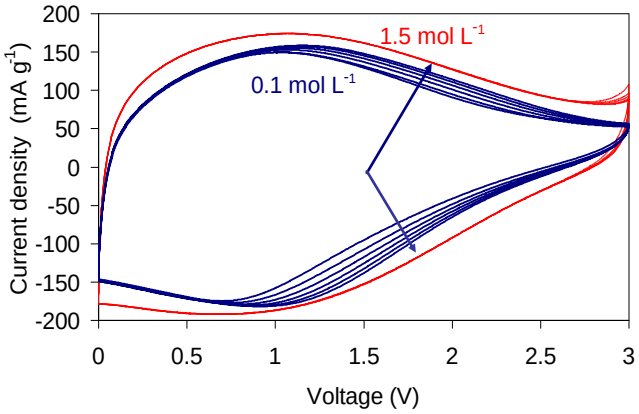

Figure 14 Cyclic voltammograms (CVs, 5 mV s^{-1}) for symmetric PC/PC capacitors in 0.1 and 1.5 mol L^{-1} tetraethylammonium tetrafluoroborate solutions [65].

4.2 Methods for adapting the pore size of carbons to the ion size

With the improved understanding about the effects of specific surface area, pore size and pore size distribution (PSD) on the capacitive properties of carbons, various methods have been proposed to reach pore size-controlled micro-porous carbons for EDLC applications.

Firstly, the protocol of using zeolite templates to deposit a carbon layer and further dissolve the zeolite is one of the most powerful methods to achieve PSD-controlled micro-porous carbons having an ordered structure [66][67][68][69]. The concept of this method shown in Figure 15 [66] followed pioneer works by Kyotani *et al.* using layered clay minerals

and then micro-porous inorganic frameworks with different structures as templates [70]. Subsequently, numerous works emerge in endless stream.

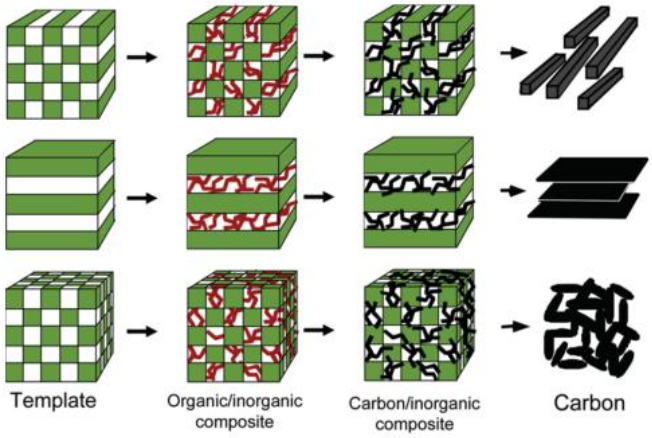

Figure 15 Concept of the template carbonization method using host materials with different nanospace dimensions [66].

Three-dimensional nano-porous carbons with interconnected pores of average size 1.2 nm have been developed through the zeolite template procedure. The carbons show both high gravimetric (140-190 F g^{-1}) and volumetric (75-83 F cm^{-3}) capacitance in 1 mol L^{-1} Et_4NBF_4/propylene carbonate solution [71]. As shown in Figure 16, ZTC-L presents exceptional capacitance retention even at ultrahigh current density of 20 A g^{-1} indicating high rate performance. Such performance has been attributed to the high conductivity, unique three-dimensional array and interconnected 1.2 nm micro-pores structure [56][71]. The conclusion extracted in the above mentioned study is that the pore size of 1.2 nm could be the optimal nano-pore size to balance high volumetric capacitance and high rate performance in the system.

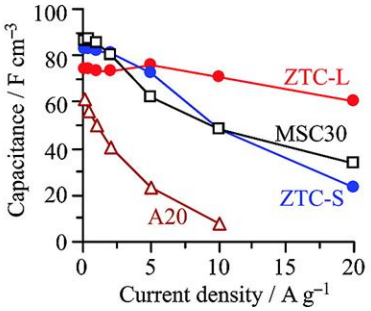

Figure 16 Volumetric capacitance vs current density of zeolite-templated carbons (ZTC) and two commercial activated carbons: A20 (Unitika, Ltd.) and MSC30 (Kansai Coke and Chemicals Co., Ltd). The volumetric capacitance was calculated by multiplying gravimetric capacitance and particle density [71].

Kajdos *et al.* reported an atomic-level micropore alignment control in carbons obtained over a robust zeolite lattice template [72]. They employed a low pressure chemical vapor deposition (CVD) method using acetylene as hydrocarbon precursor in order to retain the zeolite template shape and improve the carbon uniformity. As a result, the major pore size distribution is in the range of micro-pores smaller than 2 nm with low percentage of multi-walled structures. X-ray diffraction (XRD) revealed carbon walls regularly spaced at ~ 1.3 nm by increasing the synthesis time from 4 to 8 h. Electrochemical impedance spectroscopy at 1 mHz and cyclic voltammetry at an ultrafast scan rate of 500 mV s^{-1} shows comparable capacitance values of 200-300 F g^{-1} (Figure 17). It is thus proved that the rate of ion transport is greatly enhanced in porous carbons with aligned pore channels as proposed by Kyotani and co-workers [71]. As a consequence, pore alignment could significantly impact the power performance of supercapacitors. Such results also indicate that mesopores are not necessary required for delivering high power densities.

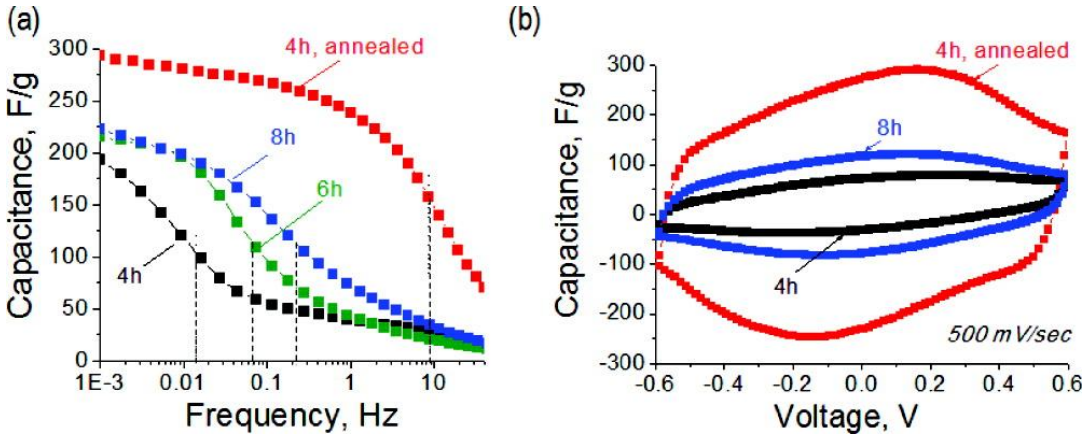

Figure 17 Effect of pore alignment in zeolite Y-templated carbons on the ion transport in EDLC by using 1 mol L^{-1} H_2SO_4 as electrolyte: (a) capacitance vs operating frequency; (b) cyclic voltammograms at 500 mV s^{-1} [72].

Although zeolite templated carbons have a narrow pore-size distribution, the fine-tuning of pore size is difficult because of the narrow porosity of the inorganic host. Overall, large amounts of materials cannot be prepared by this process and their cost is high. Another route which has been proposed to tailor the pore size of carbons is the selective etching of carbides, leading to the formation of carbide-derived carbons (CDCs) [43][73].

Metals and metalloids are eliminated from carbide precursors by high-temperature chlorination, leaving behind nano-porous carbons with 50 % to 80 % open pore volume. The average pore size can be tailored over a wide range by varying the chlorination temperature and the starting metal carbide [73][74][75]. Table 2 shows the example of TiC-derived carbons where the average pore size increases from 0.68 to 1.0 nm when the chlorination temperature varies from 500^{o}C to 900^{o}C **[**76]. An average value of 0.05 nm accuracy is claimed in the micro-pores range of 0.6-1.6 nm with an ability to reach a specific surface area up to 2800 m^2 g^{-1} [73][77].

Table 2 Porosity characteristics of TiC-CDC samples [76]

Chlorination temperature (^{o}C)	BET SSA (m^2 g^{-1})	Pore Volume (cm^3 g^{-1})	Average Pore width (nm)	Maximum Pore width [a] (nm)
500	1140	0.50	0.68	1.18
600	1269	0.60	0.74	1.23
700	1401	0.66	0.76	1.41
900	1625	0.81	1.0	2.50

[a] 85 % of pore volume is below this size.

The uniform pore size and controlled pore size distribution of CDCs allowed assessing the optimal pore-to-ion size relations for a variety of electrolytes [43]. SiC-CDC displays a specific capacitance larger than 200 F g^{-1} in aqueous electrolyte and 185 F g^{-1} in IL electrolyte [77]. A volumetric energy density of 10.8 Wh L^{-1} has been demonstrated for TiC-CDC based EDLCs when the cell operates at 2.7 V in organic medium [78]. For TiC-CDCs in organic electrolyte, the normalized capacitance (specific capacitance divided by the BET specific surface area) increases with decreasing the average pore width from 1.1 to 0.7 nm [58], and at average pore sizes below 0.8 nm, one can observe a sharp increase of double layer capacitance (see Figure 9) [53].

Apart from the concepts of ZTCs and CDCs, other attempts have been developed to prepare PSD-controlled and/or high performance micro-porous carbon for EDLCs. A carbon obtained by pyrolysis of polyvinylidene chloride was oxidized by nitric acid in order to create uniformly chemisorbed oxygen-containing groups, which were further removed by thermal treatment at 900 ^{o}C under nitrogen flow. The repetition of such oxidation/desorption

processes allowed an uniform pore size broadening, and an exceptional large EDL capacitance value of 340 F g^{-1} could be achieved in acidic medium [51].

In resume, for microporous carbons for EDLCs applications, adequate pore dimensions, pore architecture and pore size distribution are more important than a high specific surface area. Carbon materials with a large amount of micropores in the range 0.7-0.9 nm are the most desirable for an efficient ions electro-sorption; however, a reasonable amount of mesopores is necessary for quick transportation of ions to the active micropores [3].

4.3 Models for EDL formation inside carbon pores

The above presented data show clearly that the classical models of the double-layer, including a compact layer and a diffuse layer, do not apply when microporous carbons are used as electrode materials.

Models based on cylindrical mesopores and cylindrical micropores, both shown in figure 18, have been considered by Huang *et al.* [78,79]. In the mesopore regime (2 to 50 nm), solvated counter ions approach the pore wall and form an electrical double-cylinder capacitor (EDCC, Figure 18a) of capacitance given in equation (6):

$$C/A = \frac{\varepsilon_r \varepsilon_0}{b \ln [b/(b-d)]} \tag{6}$$

where $\boldsymbol{\varepsilon_r}$ is the electrolyte dielectric constant, $\boldsymbol{\varepsilon_o}$ is the vacuum permittivity, $\boldsymbol{A}$ is the accessible surface area of the electrolyte/electrode interface, $\boldsymbol{b}$ is the pore radius and $\boldsymbol{d}$ is the distance of approach of ions to the carbon surface. In the case of micropores (< 2 nm), desolvated or partially desolvated counter ions line-up to form an electrical wire-in-cylinder capacitor (EWCC, Figure 18b), which capacitance is given by equation (7):

$$C/A = \frac{\varepsilon_r \varepsilon_0}{b \ln (b/a_0)} \tag{7}$$

where a_o is the effective size of the desolvated ions and b the radius of the charged micropore. Macropores (>50 nm) are large enough so that pore curvature is no longer significant; the classical equation (1) can be applied. The increase in capacitance with decreasing pore size can be explained by the application of equations (6) and (7).

Overall, more theoretical and fundamental studies are still required to deeply explore the EDL charge storage mechanism in small pores, especially ultramicropores.

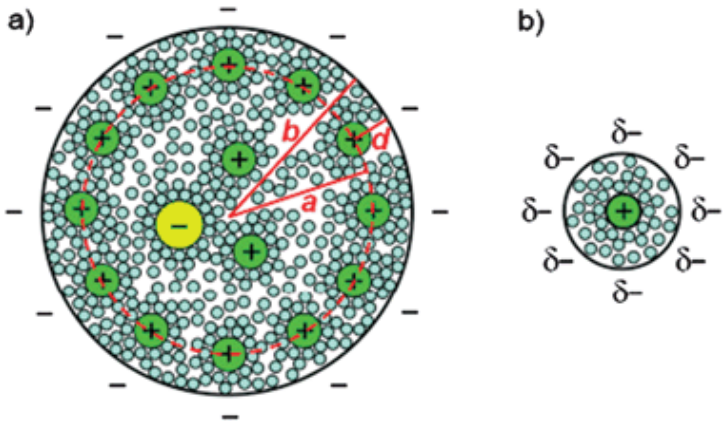

Figure 18 Schematic diagram (vertical axis) of a) a negatively charged mesopore with cations approaching the pore wall to form an electrical double-cylinder capacitor (EDCC) with radii b and a for the outer and inner cylinders, respectively, separated by a distance d; and b) a negatively charged micropore of radius b with cations of radius a_0 lining up to form an electrical wire-in-cylinder capacitor (EWCC) [80].

5 Pseudo-capacitive contributions

In addition to typical electrostatic interactions in the electrical double-layer, quick faradic redox reactions with electron transfer on the electrode/electrolyte interface may also contribute to the charge storage process and energy enhancement. Since the electrode potential (U) varies proportionally to the charge transferred (Q) as in capacitor, $dQ = C\,dU$, the process is referred to as pseudo-capacitance [81][82]. However, the typical faradic origin of these processes is associated with a slow kinetic of the heterogeneous reaction (limited mainly by the diffusion of the involved electrochemical species) and with a moderate cycle life (connected with changes of the material structure undergoing the oxidation or reduction process).

Metal oxides such as RuO_2 [83][84], MnO_2 [85][86], NiO [87][88], as well as electronically conducting polymers such as polyaniline and polypyrrole [89], have been extensively investigated in the last decades.

Pseudocapacitance in carbon materials has been revealed as an efficient way to increase their capacitance by adding this effect to the EDLC. In carbon materials, pseudocapacitance can have several origins: i) fast redox reactions involving oxygen- or nitrogen-containing surface functionalities and the electrolyte [90][91]; ii) reversible electrochemical hydrogen storage taking place when a negative polarization is applied to an activated carbon electrode

[92][93]; iii) redox-active electrolytes [94] at the carbon/electrolyte interface, such as iodide/iodine [95][96], vanadium/vanadyl [23], quinone/hydroquinone additive to aqueous electrolytes [97][98], bromide species [99][100], etc.

5.1 Pseudo-capacitance involving metal oxides and conducting polymers

Among metal oxides, RuO_2 has been the most studied due to its high theoretical specific capacitance (ca. 1400-2000 F g^{-1}) [101]). Such high values of capacitance are related to three distinct oxidation states accessible within a 1.2 V voltage window, and to a relatively high metallic conductivity (10^5 S cm^{-1}) [8][9]. However, a satisfying electrochemical activity of this compound is obtained only in protic medium. The corresponding mechanisms can be described as a rapid reversible electron transfer together with an electro-adsorption of protons on the particles surface, according to equation (8), where the Ru oxidation states can change from Ru (IV) to Ru (II):

$$RuO_2 + xH^+ + xe^- \leftrightarrow RuO_{2-x}(OH)_x \quad (8)$$

where $0 \leq x \leq 2$. In practice, high specific capacitance values, e.g. 1170 F g^{-1} [102] and 1340 F g^{-1} [103], have been reached with Ru-based systems. However, this material presents a relatively high cost and is environmentally harmful.

Therefore, the researchers have turned towards cheaper materials such as MnO_2, NiO, Fe_3O_4, and V_2O_5 [8]. Among them, manganese oxide has a high theoretical capacitance of 1200 F g^{-1}[85], while being cheap, naturally abundant and environment friendly. High specific capacitance values up to 1000 F g^{-1} have been claimed for this oxide in aqueous Li_2SO_4 electrolyte [104][105]. The capacitance is attributed to reversible redox transitions involving the exchange of protons and/or cations with the electrolyte, as well as the transitions between Mn (III)/Mn (II), Mn (IV)/ Mn (III), and Mn (VI)/Mn (IV) within the electrode potential window of the electrolyte. The overall mechanism can be expressed as in equation (9):

$$MnO_\alpha(OC)_\beta + \delta C^+ + \delta e^- \leftrightarrow MnO_{\alpha-\beta}(OC)_{\beta+\delta} \quad (9)$$

where $\mathbf{C}^+$ denotes the protons and alkali metal cations (Li^+, Na^+, K^+) in the electrolyte, $MnO_\alpha(OC)_\beta$ and $MnO_{\alpha-\delta}(OC)_{\beta+\delta}$ represent $MnO_2 \cdot H_2O$ in high and low oxidation states, respectively. For symmetric MnO_2 supercapacitors, the voltage is typically limited to less

than 1.0 V; the capacitance fades when the negative electrode is polarised below 0.0 V vs Ag/AgCl due to irreversible formation of inactive Mn (II) surface species [106]. Recently, the voltage could be extended up to 1.2 V with an exceptional stability over 10,000 cycles for a symmetric MnO_2 supercapacitor using Ti (IV)-containing aqueous KCl electrolyte [107]. Since MnO_2 does not exhibit reversible transitions below 0.0 V vs Ag/AgCl (aq), it is more suitable to apply it as positive electrode in a hybrid system which will be described in the next section.

Another good example of materials providing pseudocapacitance properties are various conducting polymers (polyaniline-PANI, polypyrrole-PPy, and derivatives of polythiophene-PTh) [89]. PANI has been the most studied because of its low cost, relatively easy preparation, high conductivity and stability. So far, the reported specific capacitance of pure PANI modified electrodes varies from 160 to 815 F g^{-1} [108]. Sivakkumar *et al.* synthesized PANI nanofibres by interfacial polymerization and reported a specific capacitance of 554 F g^{-1} and a poor charge/discharge cycling stability in a symmetric PANI/PANI cell using 1.0 mol L^{-1} H_2SO_4 [109]. Pure PTh [110] and PPy [111] exhibit specific capacitance values of 260 and 480 F g^{-1} in non-aqueous systems, respectively.

Actually, doping/dedoping of conducting polymers causes volumetric changes resulting in a poor cycling stability [11][112]. On the other hand, these materials present relatively low power performance because of the slow diffusion of ions within electrode bulk. Another disadvantage of conducting polymers is their narrow stability potential window. Therefore, current research efforts with conducting polymers for supercapacitor applications are directed towards hybrid systems [110][113].

5.2 Pseudo-capacitance from surface functional groups on carbons

The surface functionality of carbons is given by the presence of heteroatoms such as oxygen, nitrogen, phosphorus and sulfur, etc. Some surface functional groups can be electrochemically active and introduce the so-called pseudo-capacitance, which is related to the mass and/or charge transfer on these active sites.

5.2.1 Oxygen enriched carbons

Surface oxides are always present on the surface of carbons as a consequence of the preparation processes or as a “residue” from the carbon precursors. Figure 19 summarizes in a schematic way the current state of knowledge on surface oxygen-containing groups. The

main oxygenated functionalities include carboxyl-, lactone-, quinone-, pyrone-, and phenolic-type groups, etc [114].

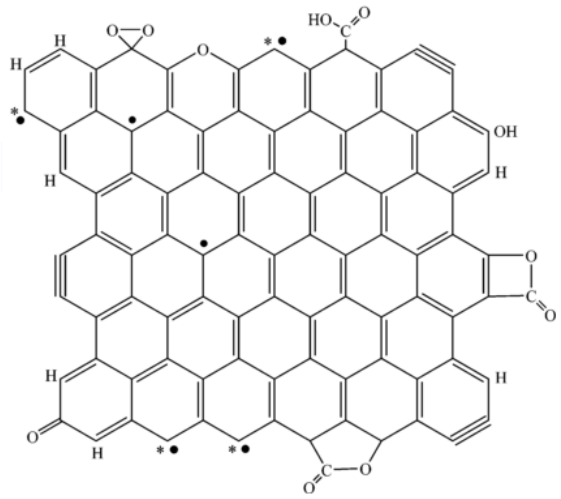

Figure 19 Schematic representation of the surface chemistry of a graphene layer, including carboxyl-, lactone-, quinone-, pyrone-, and phenolic-type oxygenated functionalities, etc [114].

The most documented case of pseudo-faradic reaction comes from hydroquinone/quinone groups as shown in the equation (10) [115]. For example, a correlation between capacitance and the amount of quinone groups has been reported by Okajima *et al.* on oxygen-plasma modified activated carbon fibers [116]. To date, other functionalities are reported to present, in a less extent than quinone, some pseudocapacitive effect such as pyrones [117].

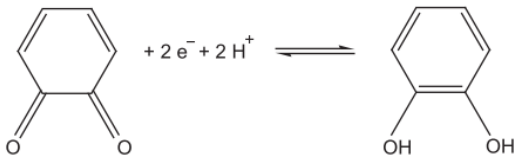

(10)

In this sense, some studies show the relationship between capacitance and the nature of surface functionalities. The latter can be determined by temperature-programmed desorption (TPD) analysis, as oxygenated functionalities on carbons are thermally decomposed into CO and CO_2. CO evolves at higher temperatures as a consequence of the decomposition of phenol, quinone, and ethers. On the other hand, the evolution of CO_2 takes place at lower temperatures corresponding to the decomposition of carboxylic groups or lactones [118]. As

shown in Figure 20, the specific capacitance presents a good correlation with the concentrations of CO-desorbed groups. Nevertheless, there is no linear relationship to the amount of oxygenated groups desorbing as CO_2 and to the total quantity of functional groups [119]. As a result, it is generally accepted that CO-type groups make positive contributions to the total capacitance, whereas CO_2-desorbing ones are proposed to retard the migration of electrolyte into carbon pores [119][120].

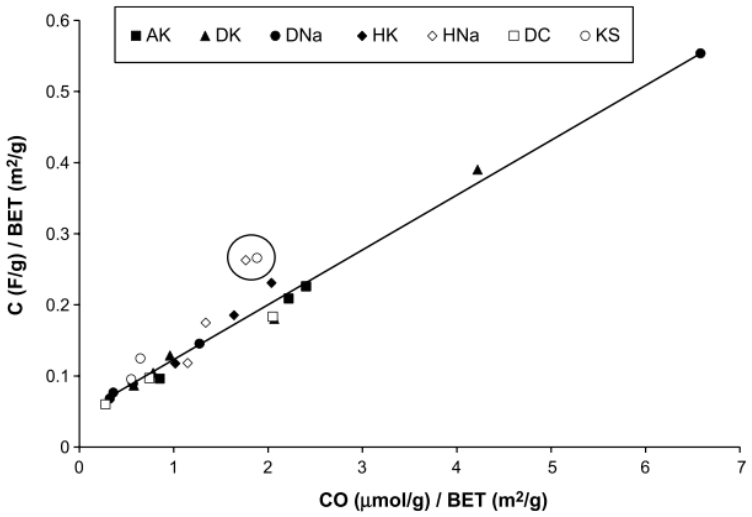

Figure 20 Relation between the capacitance of carbons and the evolved CO amount. Both values were divided by the BET specific surface area [119].

5.2.2 Nitrogen enriched carbons

Besides surface oxides, nitrogen-enriched carbons, such as N-doped porous carbons [121], N-doped carbon nanotubes [122] and N-doped graphene [123], are reported to present pseudo-capacitive properties during charging/discharging a supercapacitor. However, it is difficult to assess the pseudo-capacitance to nitrogen-containing groups, as oxygen-containing functionalities are always simultaneously present at the surface of carbons. Therefore, the pseudo-capacitance mechanisms in nitrogen-enriched carbons are still not well-established.

Nitrogen atoms (Figure 21) can be located at the edges of the graphene structures in the form of pyridinic (N-6), pyrrollic/pyridone (N-5), pyridine-N-oxide (N-X) or inside the graphene structure as quaternary (N-Q). Nitrogen can be introduced in the carbon material either by carbonizing a nitrogen rich precursor or by reaction of the carbon material with nitrogenated components. In particular, for introducing nitrogen, a wood-based activated

carbon can be modified with melamine and urea and further carbonized under an inert atmosphere [124]. The treatment significantly improves the specific capacitance from 253 to 330 F g^{-1}; the capacitance retention ratio is as high as 86 % when the current density is increased from 50 mA g^{-1} up to 1 A g^{-1} while only 15 % of the capacitance can be retained with the pristine carbon in the same conditions. Furthermore, the normalized capacitance per volume of micropores shows a good correlation with the content of quaternary nitrogen (N-Q) and pyridine-N-oxide (N-X), while the pyridinic (N-6) and pyrrolic/pyridone (N-5) nitrogen contribute positively to the pseudo-capacitance. Those findings have been further confirmed in a subsequent work from the same group by using coconut shell-based activated carbons [125].

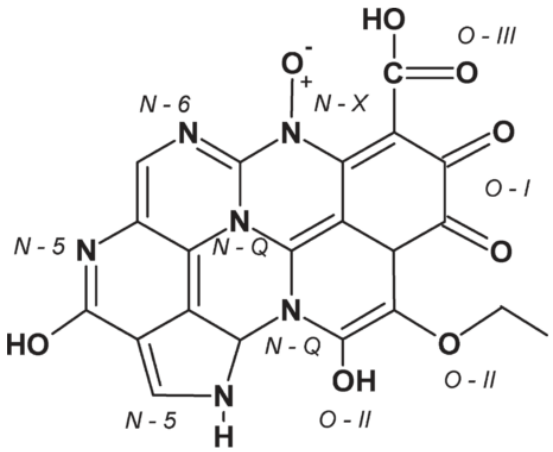

Figure 21 Scheme of nitrogen- and oxygen-containing surface groups on carbons [125].

In the case of nitrogen containing compounds as carbon precursors, it has been shown that a series of activated carbons with the same textural characteristics and containing nitrogen from 1 to 7 wt.% can be prepared from polyvinyl-pyridine and polyacrylonitrile blends. The capacitance of such materials in symmetric two-electrode capacitors in 1 mol L^{-1} aqueous H_2SO_4 and 1 mol L^{-1} $TEABF_4$/acetonitrile electrolytes shows a good correlation with the nitrogen content [91]. Good cycling stability proves that the redox reactions involving nitrogen are completely reversible during cycling. From these results, the pseudo-capacitance in acidic electrolytes originating from nitrogenated functional groups has been attributed to types of redox reactions as (11), (12) and (13) [91][115].

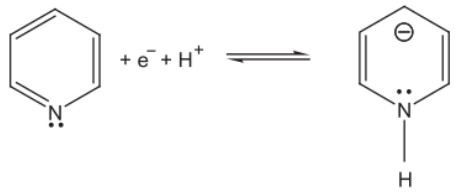

(11)

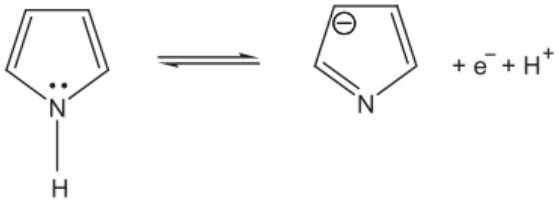

(12)

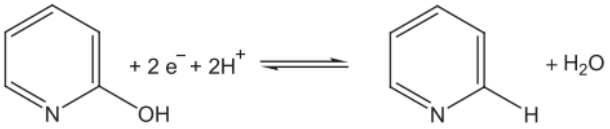

(13)

5.3 Pseudo-capacitance related to reversible hydrogen storage in carbons

The capacitance of carbon electrodes can be enhanced by pseudo-capacitive effects related to electrochemical reversible hydrogen storage. Porous carbon can store hydrogen up to ca. 2 wt% by cathodic electrochemical reduction of water under ambient pressure and temperature conditions [92]. Together with the further reversible anodic oxidation of the electrosorbed hydrogen, it leads to a potential pseudo-capacitive contribution in addition to the EDL capacitance of carbon materials.

In alkaline medium, for example, water is reduced according to the Volmer reaction (14):

$$H_2O + e^- \rightarrow H + OH^- \quad (14)$$

and the formed atomic/nascent hydrogen is adsorbed on the surface of nanopores (15):

$$\langle C \rangle + xH \rightarrow \langle CH_x \rangle \quad (15)$$

where <C> represents the carbon host and $<CH_x>$ hydrogen adsorbed in the later.

As shown in figure 22 [125], the overall charge/discharge phenomenon is summarized by equation (16):

$$\langle C \rangle + xH_2O + xe^- \leftrightarrow \langle CH_x \rangle + xOH^- \quad (16)$$

where ‹CH_x› represents the hydrogen inserted into the nanoporous carbon during charging and oxidized during discharging.

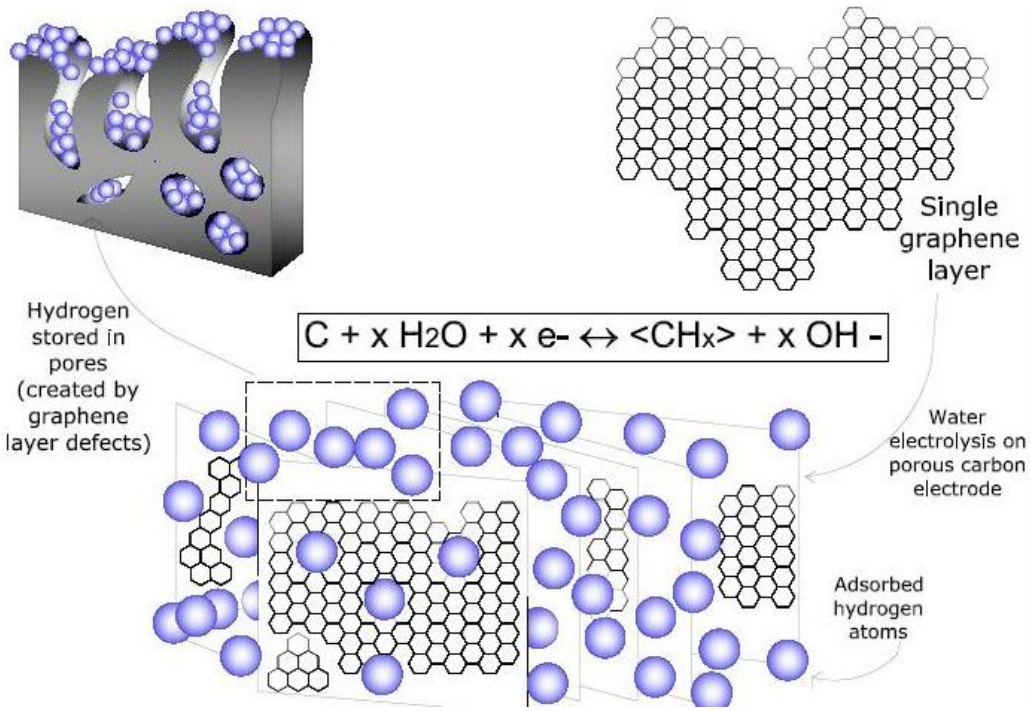

Figure 22 Scheme of electrochemical hydrogen storage in carbon materials [126].

Cyclic voltammetry has been employed to analyze the electrochemical hydrogen storage process on activated carbons. Based on the above mentioned mechanisms, one can distinguish three regions in the cathodic part of the voltammograms of figure 23: i) when the potential of the carbon electrode is above the thermodynamic value corresponding to water reduction, i.e. -0.908 V vs. Hg/HgO in 3 mol L^{-1} KOH, the shape of the voltammograms is almost rectangular, typically for charging the electrical double-layer; ii) when the potential cut-off is below -0.908 V vs. Hg/HgO, the negative current increases proving water reduction and hydrogen storage according to equations (14 and 15); iii) below -1.5 V vs. Hg/HgO, hydrogen is recombined into molecular di-hydrogen [92]. During the anodic scan, the overall redox reaction run in opposite direction and a peak corresponding to the electro-oxidation of sorbed hydrogen is observed. The important polarization between the cathodic and anodic processes indicates that hydrogen electrochemically stored is trapped more strongly than for a classical physisorption.

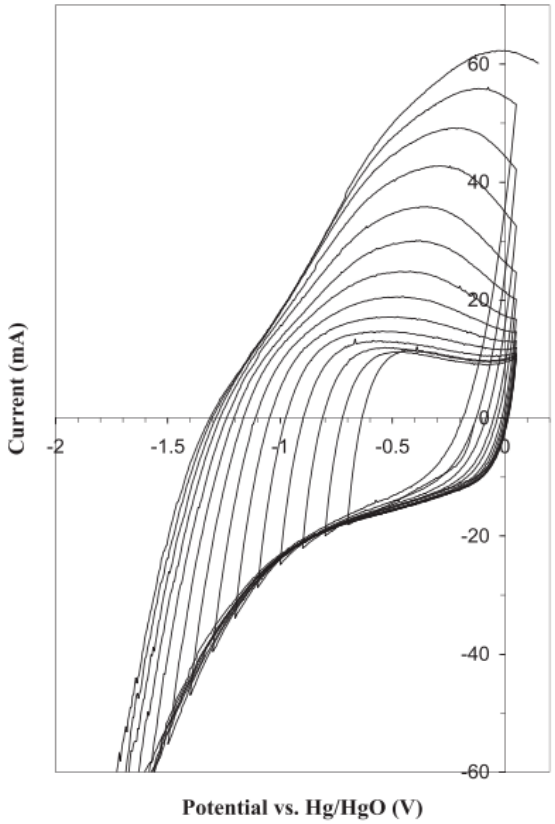

Figure 23 Cyclic voltammograms (5 mV s^{-1}) of an activated carbon electrode in 3 mol L^{-1} KOH where the various loops are obtained with a gradual shift to negative values of potential [92].

Hydrogen chemisorption has been confirmed by Temperature Programmed Desorption (TPD) analysis using template based carbons [93]. The activation energy of 110 KJ mol^{-1} for di-hydrogen desorption indicates a weak chemical character of the bond. For comparison, oxygen-containing groups weakly chemisorbed on carbon materials are desorbed in the form of CO and CO_2 at the same temperature with activation energy of 126 KJ mol^{-1} [127].

In summary, hydrogen electrosorption is a reversible phenomenon which takes place during the negative polarization of carbon materials giving an additional capacitance. For the supercapacitor application, it will be shown later that the over-potential of di-hydrogen evolution may positively affect the operating voltage.

5.4 Pseudocapacitance related to the use of redox-active electrolytes

The previously mentioned pseudo-capacitive processes are closely related with the electrode material. Recently, a new trend in pseudocapacitance, where the electrolyte stays at the origin of an additional charge accumulated, has been reported. Novel pseudo-capacitive

contributions from the carbon/iodine interface were obtained by using aqueous KI electrolyte in carbon based supercapacitors [95]. The electrochemical activity of this electrolyte involves equations (17) to (20).

$$2I^{-1} \leftrightarrow I_2 + 2e^- \quad (17)$$

$$3I^{-1} \leftrightarrow I_3^{-1} + 2e^- \quad (18)$$

$$2I_3^{-1} \leftrightarrow 3I_2 + 2e^- \quad (19)$$

$$I_2 + 6H_2O \leftrightarrow 2IO_3^{-1} + 12H^+ + 10e^- \quad (20)$$

Cyclic voltammetry (Figure 24) was applied to evaluate the capacitance of the carbon electrode and revealed an intriguing dependence on the type of alkali counter-ion [96]. It suggests that the porosity significantly contributes in the active transport of ions to/from the electrode/electrolyte interface. The capacitance of the electrode increases with the van der Waals radius of the alkali ion as follows: 300 F g^{-1} for LiI, 492 F g^{-1} for NaI, 1078 F g^{-1} for KI and reaching 2272 F g^{-1} for RbI. However, for the caesium ion, which has the biggest radius, the capacitance decreases to 373 F g^{-1}. This curious phenomenon is in perfect accordance with the ion-solvent and solvent-solvent interactions measured in the form of potential energy as well as cation mobility values and diffusion coefficients tendencies. For instance, the water diffusion coefficient values are the most similar in RbI solution, which suggests that the mobility of Rb^+ and I^- ions is not disturbed by any additional interaction and they can easily penetrate the porous structure of the carbon electrode. Moreover, the iodide anions have the smallest value of ion-water potential, what might suggest that they are rather active in water solution and preferably desolvated. It means that, beside the faradic reactions, they can be adsorbed in the micropores, giving a typical electrostatic response.

However, aqueous alkali iodides demonstrate striking capacitance values only for the positive electrode and in narrow potential range; the specific capacitance of a two electrode system in these media did not exceed 280 F g^{-1} at 1 A g^{-1}. Therefore, the vanadium/vanadyl redox couple was further employed to work as electrolyte for negative electrode. A high-energy ecocapacitor has been developed by using 1 mol L^{-1} KI as electrolyte for the positive electrode and 1 mol L^{-1} $VOSO_4$ as electrolyte for the negative electrode, both electrolytes being separated by a Nafion membrane in order to prevent from their mixing [23]. The

reported values are about 1200 F g^{-1} and 670 F g^{-1} for the positive and negative electrodes, respectively.

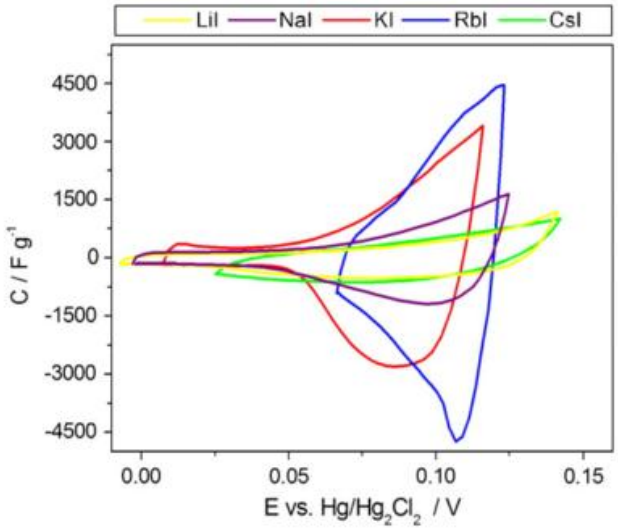

Figure 24 Cyclic voltammograms (5 m V s^{-1}) of a positive carbon electrode for different alkali iodide solutions [96].

The relatively high capacitance values of the negative electrode (1 mol L^{-1} $VOSO_4$ as electrolyte) could be explained considering the multi-electron reactions (21) to (25).

$$VOH^{2+} + H^+ + e^- \leftrightarrow V^{2+} + H_2O \quad (21)$$

$$[H_2V_{10}O_{28}]^{4-} + 54H^+ + 30e^- \leftrightarrow 10V^{2+} + 28H_2O \quad (22)$$

$$[H_2V_{10}O_{28}]^{4-} + 44H^+ + 20e^- \leftrightarrow 10VOH^{2+} + 18H_2O \quad (23)$$

$$HV_2O_7^{3-} + 9H^+ + 6e^- \leftrightarrow 2VO + 5H_2O \quad (24)$$

$$HV_2O_7^{3-} + 13H^+ + 10e^- \leftrightarrow 2V + 7H_2O \quad (25)$$

The carbon surface plays an important role in the faradic response of this system because the redox vanadyl transformation occurs with the contribution of the carbon functionality. The VO^{2+} ions can be transported from the bulk of the electrolyte to the electrode/electrolyte interface where a proton-exchange from the oxygenated functional groups takes place, leading to bonding of vanadyl groups onto the electrode surface. Additionally, electrons can be transferred from VO^{2+} to the electrode along the -$COOVO^+$ bond with VO_2^+ formation, and then VO_2^+ can diffuse to the electrolyte bulk. This process is presented in Figure 25.

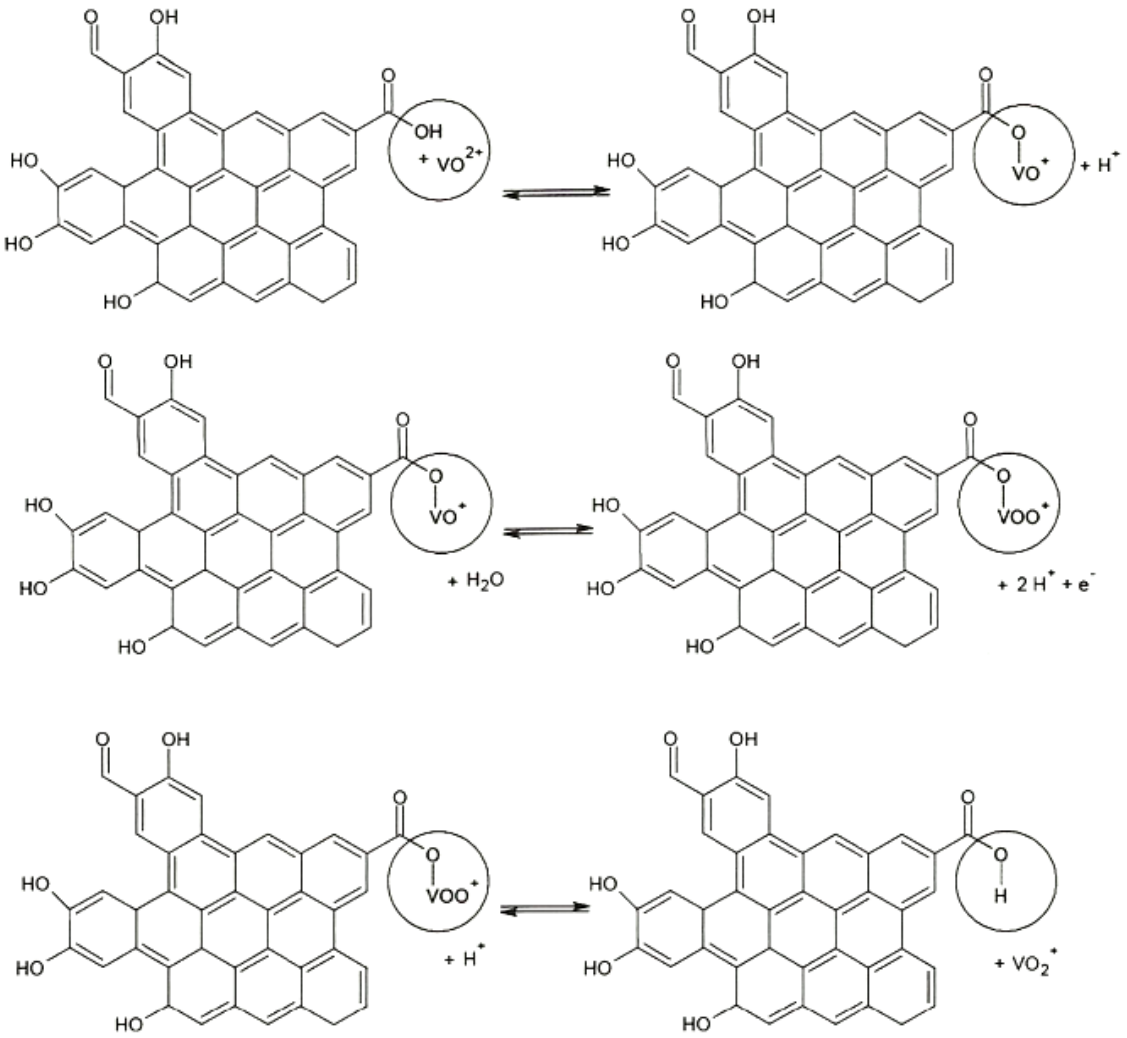

Figure 25 Various surface redox reactions with vanadium species [23].

Apart from the redox-active electrolytes, redox additive to the electrolytes could be another route to enhance the capacitance. Roldán *et al.* reported an increase in capacitance of carbon based supercapacitors by incorporating the quinone/hydroquinone redox couple into 1 mol L^{-1} H_2SO_4 solution [97][98]. The addition of hydroquinone to aqueous H_2SO_4 transforms the positive electrode in a battery-like one because of the development of the quinone/hydroquinone redox reactions on the carbon surface. The negative electrode remains of the supercapacitor type one, while electrochemical storage hydrogen may take place when lowering its potential. The overall system behaves like a symmetric-hybrid supercapacitor due to the distinct energy storage mechanisms of both electrodes. A tremendous capacitance value of 5017 F g^{-1} was recorded by cyclic voltammetry at 1 mV s^{-1} for the positive electrode,

probably due to the development of quinoid redox reactions on the activated carbon surface. Meanwhile, the capacitance of the negative electrode also increases significantly, from 290 to 477 F g^{-1}, when compared to the value obtained for the electrode operating in the electrolyte without hydroquinone. Accordingly, the energy density shows a noticeable improvement from 10.1 to 30.6 Wh kg^{-1}.

More recently, Senthilkumar *et al.* reported the capacitance/energy improvement of symmetric carbon/carbon capacitors by adding 0.08 mol L^{-1} KI into 1 mol L^{-1} H_2SO_4, and compared with 1 mol L^{-1} H_2SO_4 + 0.08 mol L^{-1} KBr and 1 mol L^{-1} Na_2SO_4 + 0.08 mol L^{-1} KI solutions [99]. Interestingly, nearly two-fold increase in capacitance and energy density were realized with exceptional cycling stability over 4,000 cycles by adding KI into H_2SO_4. Especially, the similar pseudo-capacitive contributions to iodine-based redox couple of the Br^-/Br_3^- pair were demonstrated, though the improvement is less pronounced than iodine-based pairs.

Apart from the aqueous medium, the electrochemical activity of bromide species has been described in non-aqueous ionic liquid electrolyte by dissolving 1 mol L^{-1} 1-ethyl-3-methylimidazolium bromide in 1-ethyl-3-methylimidazolium tetrafluoroborate. Yamazaki *et al.* proposed a novel supercapacitor fabricated with activated carbon fiber electrodes and the above mentioned redox active ionic liquid electrolyte [100]. Although such a charge-storage concept should usually be useless due to inevitable, undesirable reactions, e.g. shuttle reaction or migration of active redox species between the electrodes, much-enhanced capacitance with an excellent reversibility and energy density limited by diffusion process is obtained. Moreover, the coulombic efficiency of such type of cell is quite high, approaching 100%. The redox species such as Br_2 or Br_3^- being the source of reversible charge do not diffuse from the positive electrode into the electrolyte, which might suggest some kind of insertion phenomena, still not confirmed. Finally, an exceptional cycling stability has been demonstrated with a capacitance retention ratio of 98 % after charge/discharge 10,000 cycles.

6 Asymmetric supercapacitors

The performance of supercapacitors depends not only on the electrode materials but also on the cell configuration [12][128]. Symmetric capacitors use the same material with the identical design and mass loading for the positive and negative electrodes. Asymmetric capacitors incorporate capacitive electrodes of different nature and/or mass, while hybrid

systems relate to a distinct charge storage mechanism for the positive and negative electrodes, one being capacitor-like and the other of the battery type [129][130]. Improvements in energy density can be realized with asymmetric or hybrid systems mainly because of extending the operating voltage [131][132]. The first approaches to asymmetric/hybrid systems were developed depending on the electrolyte used: i) pseudo-capacitive material/porous carbon combinations in aqueous electrolyte, and ii) activated carbon/Li-intercalation compound combinations in organic electrolytes.

6.1 Hybrid/Asymmetric capacitor operating in aqueous electrolytes

For the systems operating in aqueous electrolytes, carbon materials are combined with pseudo-capacitive materials as metal oxides or electronically conducting polymers. The most popular system uses manganese oxide as positive electrode and activated carbon as negative one. Manganese oxide is one of the most commonly utilized pseudo-capacitive metal oxides because of its low-cost [131] [133] [134]. It presents a high reversibility in the positive range of potentials while porous carbons can reversibly perform down to very low potentials because of their ability to store hydrogen. The combination of these two materials allows a theoretical cell voltage of 2.2 V. However, at this voltage, gas evolution results in a constant energy fade, i.e., up to 45 % after 10,000 cycles in 0.65 mol L^{-1} K_2SO_4 [135]. By contrast, more than 195,000 cycles were achieved with remarkable capacitance retention ratio of 87.5 % when the cell operation is limited at 2.0 V [133].

Conducting polymers have a very narrow stability window which precludes their use in symmetric configurations [112]. Therefore, polypyrrole and polyaniline have been extensively studied as active electrode materials combined in a hybrid configuration with activated carbon as negative electrode [112][136], but the cell voltage is not as advantageous as for the MnO_2/carbon system.

Taking into account that carbons are low cost materials with a high electrical conductivity, the most promising asymmetric systems in aqueous electrolytes are carbon/carbon configurations. For example, a new concept of high performance asymmetric supercapacitor has been developed in 1 mol L^{-1} H_2SO_4 aqueous electrolyte, taking profit of the different pseudo-capacitive phenomena for both electrodes [132]. In the positive potential range, the pseudofaradaic reactions involving oxygenated functionalities can give an additional capacitance, whereas on the negative side the pseudofaradaic reactions involving

hydrogen storage provoke an increase of the capacitance together with a large over-potential which enhances the stability potential window of carbon. By taking profit of these pseudofaradaic processes, it is possible to optimize the system either by balancing the mass of the electrodes with the same carbon or by using different carbons for the two electrodes.

Figure 26 presents the cyclic voltammograms (2 mV s^{-1}) obtained in three-electrode cells in aqueous 1 mol L^{-1} H_2SO_4 for two different carbons, Aox (oxidized by nitric acid) and Box (oxidized by hydrogen peroxide). Aox operates at higher potential values than Box which can be in turn polarized down to very low potentials. In both cases, the pseudo-capacitive contributions are noticeably reflected by redox humps. Theoretically, combining Aox and Box at positive and negative electrodes should allow a stability voltage window of 1.8 V, after appropriate mass balancing.

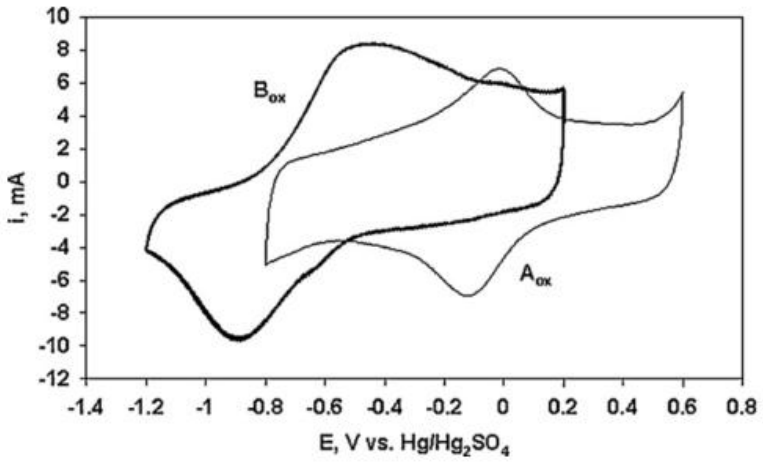

Figure 26 Three-electrode cyclic voltammograms of the activated carbons Aox and Box in 1 mol L^{-1} H_2SO_4[132].

In practice, operating voltages up to 1.6 V could be achieved during 10,000 charge/discharge cycles in the asymmetric Aox/Box capacitor with a capacitance as high as 321 F g^{-1}. This value was much larger than those obtained with the symmetric Aox/Aox and Box/Box configurations, e.g. 137 and 230 F g^{-1}, respectively. Therefore, energy density as high as 30 Wh kg^{-1} could be reached being one order of magnitude larger than that of symmetric carbon/carbon capacitors in aqueous electrolytes. Such values are comparable to the ones obtained for EDLCs in organic electrolytes while avoiding the disadvantages of these electrolytes.

6.2 Hybrid capacitors operating in organic electrolytes

Pioneering work on systems operating in organic electrolytes has been realized by Amatucci *et al.*; a positive activated carbon electrode was paired to a lithium-intercalation negative electrode, e.g., $Li_4Ti_5O_{12}$ [137]. This configuration could operate between 1.4 V and 2.8 V during charge-discharge 450,000 cycles, delivering 10-15 Wh kg^{-1} at 1000-2000 W kg^{-1}. During the last years, other studies have demonstrated the possibilities to design more performing system as it is shown in the section below.

In organic electrolytes, better performance was obtained for the LIC system using graphite as Li-intercalation material for the negative electrode and a porous carbon for the positive one. Those systems were developed as commercial devices in the early 2000's, mostly by Japanese industries such as ACT, JM Energy Corp., Asahi Kasei FDK Energy and TAIYO YUDEN Co., Ltd [138]. The advantages of LIC are a high voltage even greater than 4 V and commercially available electrode materials. The only issue is lithium pre-loading of the negative electrode, e.g. graphite [139][140][141]. The Li pre-doping methodology plays a crucial role in the stability of the negative electrode. While most of the systems use a sacrificial lithium electrode, which might lead to thermal runaway and firing of the system, it has been shown that pre-loading of graphite by using the Li-ions from the electrolyte could be an alternative strategy [139][140].Another approach for improving the performance of the system is to optimize the material used as negative electrode. By comparison with graphite, it has been demonstrated that hard carbon is a more suitable choice as negative electrode in terms of power and reliability performance [142].

In 2009, Naoi *et al.* proposed a "nanohybrid capacitor" (NHC) and utilized an ultrafast negative electrode based on nano-crystalline $Li_4Ti_5O_{12}$ (LTO) hyper-dispersed and grafted within a nano-carbon matrix as negative electrode combined with an activated carbon positive electrode (Figure 27) [138]. The objective aims at tackling the poor power characteristics and electronic conductivity of the conventional $Li_4Ti_5O_{12}$ [129]. LTO operates at a potential of 1.55 V (vs. Li/Li^+) within the electrolyte stability potential range. NHC achieves as high energy density as Li-ion capacitors with higher stability, safety and productivity. Furthermore, the system does not require pre-doping with lithium ions while extending the operating temperature range down to -40 ^oC instead of -10 ^oC for the LIC capacitor. In particular, NHC provides higher energy than conventional EDLCs not only in

the low power density region (0.1-1 kW L^{-1}) but also in the high power density region (1-6 kW L^{-1}) [129].

As a consequence, the appearance of LIC and NHC capacitors opens a new age for enhancing the energy density of supercapacitors in organic electrolytes.

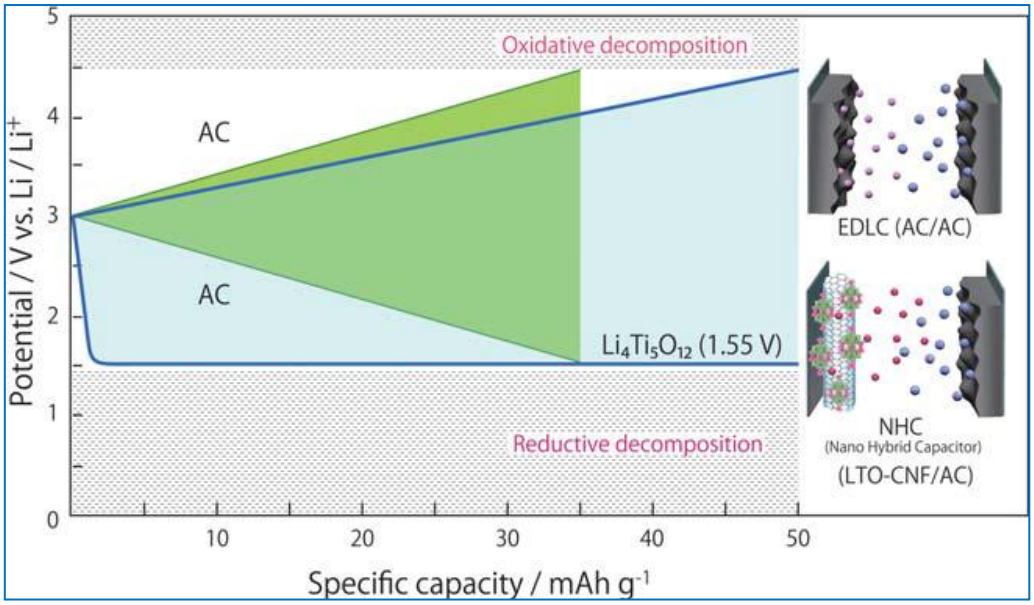

Figure 27 Nano-hybrid capacitor using an ultrafast $Li_4Ti_5O_{12}$ (LTO)/CNF nano-composite as negative electrode and activated carbon (AC) as positive electrode.

7 Conclusions

Increasing the operating voltage, while keeping a high reliability of capacitors, is the best strategy to enhance the energy density owing to the U^2 term in equation (4). Since the voltage range is restricted by the stability potential window of the electrolyte, most commercial supercapacitors use organic electrolytes because of their voltage range up to 2.7-2.8 V compared to 0.7-0.8 V for conventional aqueous electrolytes. However, considering the drawbacks of organic electrolytes (section 3.2), neutral aqueous electrolytes, e.g, alkali sulfates, able to achieve a voltage around 2.0 V in AC/AC systems, seem to be a more promising choice for commercial utilizations in the long term, especially for the development of low cost systems intended for stationary applications. Furthermore, aqueous electrolytic solutions containing redox active species (halides, vanadium, quinones), have been found in presence of activated carbon by far more promising than metal oxides and conducting

polymers to enhance the capacitance values. In sum, plenty of room is available to develop high-voltage, low cost and high-capacitance systems using environment-friendly aqueous media based on neutral salts.

Besides, the most recent advances related with carbon materials for supercapacitors highlight an improved understanding of the ion confinement in nanopores. Especially, it is now proved that capacitance is enhanced in subnanometric pores and that the ions penetrate in these pores at least partially desolvated. Taking additionally into account that a high volumetric energy density is a key requirement of industry, dense and low cost carbon materials characterized by a narrow PSD, and porosity adapted to the specific electrolyte used, have to be developed. When it comes to the cost factor, one-step synthesis of dense carbon materials would be quite beneficial.

Overall, the combination of the right electrolyte with the proper carbon electrode material can successfully enhance the energy density. We will focus this PhD thesis on increasing the energy density and cutting the cost of carbon/carbon supercapacitors: i) by extending the voltage range in neutral-pH aqueous alkali sulfates; ii) by enhancing the volumetric capacitance in organic medium with cyclic activation methods in order to achieve high density carbon electrodes.

Chapter II

Optimizing carbon/carbon supercapacitors by enhancing the voltage range in aqueous alkali sulfate electrolytes

Résumé

La densité d'énergie d'un supercondensateur est proportionnelle au carré de la tension de fonctionnement du système. La tension de fonctionnement dépend de la fenêtre de stabilité de l'électrolyte. Le principal inconvénient des électrolytes aqueux est la faible fenêtre de stabilité électrochimique de l'eau qui est de 1.23 V. De plus, en milieu aqueux acide ou basique, la tension maximale obtenue est généralement de 0.7-0.8 V. Récemment, une tension de 1.6 V a pu être réalisée dans un condensateur carbone/carbone symétrique utilisant un milieu aqueux contenant 0.5 mol L^{-1} de Na_2SO_4 comme électrolyte. Cet électrolyte neutre (pH = 6.4) présente l'avantage d'être beaucoup moins corrosif que des électrolytes acide ou basique. Donc, il est nécessaire d'explorer systématiquement d'autres sulfates alcalins comme électrolyte pour les condensateurs carbone/carbone. La stabilité en cyclage, la variation de la résistance et la capacité spécifiques de stockage des supercondensateurs ont été évalués à basse température. Les plus grandes puissances et densités d'énergie ont été obtenues en utilisant un électrolyte aqueux K_2SO_4 en raison de la plus petite taille des cations et de la conductivité ionique plus élevée dans ce milieu à température ambiante. A basse température (-10 ^oC), les performances de supercondensateurs symétriques à base de Li_2SO_4 sont les meilleures. La stabilité exceptionnelle jusqu'à une tension de 1.8 V a été mise en évidence, avec un taux de rétention de la capacité atteignant 92 % après 10, 000 cycles de charge/décharge dans Li_2SO_4 á 2 mol L^{-1}.

L'analyse par thermodésportion programmée des électrodes après un cyclage longue durée d'un condensateur prouve que la tension maximale est limitée essentiellement par une électro-oxydation irréversible du carbone activé de l'électrode positive. Si le potentiel de l'électrode positive va au-delà d'une valeur donnée pendant le fonctionnement du système, une électro-oxydation trop importante du carbone entraîne une augmentation néfaste du potentiel maximal de fonctionnement de l'électrode et à une augmentation de la résistance du système conduisant à une diminution de la capacité. Ces phénomènes peuvent être limités en procédant à une oxydation chimique contrôlée de la surface du carbone activé par le peroxyde d'hydrogène. En conséquence, le potentiel maximum de l'électrode reste stable pendant le fonctionnement de la cellule jusqu'à une tension atteignant alors 1.9 V et le système peut être chargé/déchargé pendant 10, 000 cycles avec une perte très modérée de la capacité et une faible augmentation de la résistance.

Pour améliorer les performances et surtout la densité d'énergie stockée par les supercondensateurs, il est possible de développer des supercondensateurs asymétriques dont les électrodes sont constituées de matériaux différents (utilisation d'oxydes métalliques par exemple), ce qui permet d'augmenter la tension de fonctionnement. Dans un électrolyte aqueux neutre tel Li_2SO_4, la tension pourrait être améliorée jusqu'à 2.0 V en réalisant une configuration asymétrique avec un rapport massique entre les électrodes de 1.2 (R=m+/m-).

Sur la base des conclusions ci-dessus mentionnées dans ce chapitre, nous avons également développé un supercondensateur plus proche du système industriel, avec des électrodes réalisées par l'enduction de carbones activés sur des collecteurs en acier inoxydable, de type pouch-cell fonctionnant dans un électrolyte Li_2SO_4 á 2 mol L^{-1}. La tension maximum de l'électrode reste stable pendant le fonctionnement de la cellule jusqu'à une tension atteignant alors 2.1 V.

1 Introduction

Lately, it has been observed that the H_2 over-potential on a carbon electrode is higher in neutral aqueous electrolytes than in aqueous KOH or H_2SO_4; a stability potential window of 2.0 – 2.4 V could be observed in aqueous 0.5 mol L^{-1} Na_2SO_4 [19][20]. Consequently, a practical voltage of 1.6 V during 10,000 charge/discharge cycles has been obtained with a symmetric carbon/carbon capacitor in aqueous Na_2SO_4 [19]. Even higher voltage of 2.2 V has been recently claimed when using aqueous 1 mol L^{-1} Li_2SO_4 [22]. Such high voltage was attributed to the high hydration energy and to the low concentrations in protons and hydroxyl groups (due to the neutral pH) which do not favor di-hydrogen or di-oxygen evolution. Overall, the use of alkali sulfates as electrolytes eliminates partly the effects of corrosion, and it gives an opportunity to realize high energy density supercapacitors being environmental friendly, cost effective and safe. However, further research should be carried out in these media in order to realize supercapacitors with optimized performance.

This chapter will show the possibilities explored for enhancing the voltage of AC/AC supercapacitors operating in neutral aqueous alkali sulfate electrolyte and it will be divided into four sections:

- The first section is devoted to screening the electrochemical performance of symmetric AC/AC supercapacitors in aqueous Li_2SO_4, Na_2SO_4, and K_2SO_4 at different temperatures. The results will show that 2 mol L^{-1} Li_2SO_4 is the best electrolyte for an optimal performance in the widest temperature range.
- The second section attempts do better understand the parameters influencing the voltage range of AC/AC capacitors in aqueous lithium sulfate. It will be demonstrated that the electro-oxidation of the positive electrode limits the operating voltage and that a controlled chemical oxidation of carbon before operation can improve the performance of the supercapacitor.
- The third section will show that an asymmetric AC/AC configuration in lithium sulfate electrolyte could be further utilized to enhance the voltage range and consequently the energy density of the supercapacitor.
- Finally, the fourth section will present a successful up-scaling of the AC/AC capacitor operating in aqueous Li_2SO_4 to a system close to the industrial ones.

2 Symmetric AC/AC capacitors in neutral aqueous alkali sulfates at different operating temperatures

2.1 Introduction

Low temperature operation of supercapacitors is mandatory for specific applications such as for example cold-starting of trucks and cars. Although aqueous electrolytes display a higher electrical conductivity than organic ones, their relatively high freezing point might limit the operating temperature range of supercapacitors in this media. Therefore, this section focuses on investigating systematically different alkali sulfates (Li_2SO_4, Na_2SO_4, and K_2SO_4) as electrolytes in symmetric carbon/carbon capacitors at different operating temperatures. For this purpose, electrochemical impedance spectroscopy (EIS) has been in particular employed to analyze the ion diffusion behaviors in the electrolytes at temperatures ranging between -10°C and 20°C.

2.2 Physicochemical properties of the carbon material

For the present study, a highly micro-porous carbon (AC, Meadwestvaco, USA) with a specific surface area of 2224 m^2/g has been chosen as electrode active material. The comparable values of ultramicropore and micropore volumes (Table 3) indicate that the micropores of this carbon are essentially in the region of 0.7-0.8 nm. Moreover, it has a reasonable amount of mesopores which are very useful for enhanced charge propagation [3]. The XPS analysis (Table 3) reveals a relatively low oxygen amount of 2.4 at %, essentially in the form of ether groups.

Table 3 Porous texture of the as-received carbon from Meadwestvaco

Sample	$S_{BET}(N_2)$ $m^2\ g^{-1}$	$V_{ultramicro}$ [a] $cm^3\ g^{-1}$	V_{micro} [b] $cm^3\ g^{-1}$	V_{meso} [c] $cm^3\ g^{-1}$
AC	2224	0.83	0.83	0.45

(a) DR equation applied to the CO_2 adsorption data; (b) DR equation applied to the N_2 adsorption data; (c) NLDFT method applied to the N_2 adsorption data

Table 4 Surface functionality of the Meadwestvaco carbon from the C1s XPS data

Sample	C-OR/at% 286.3±0.2eV	C=O/at% 287.5±0.2eV	-O-C=O/at% 289.0±0.2eV	O/at%
AC	1.22	0.09	0.54	2.4

2.3 Electrochemical performance of symmetric carbon/carbon capacitors in aqueous Li_2SO_4, Na_2SO_4 and K_2SO_4 electrolytes

Three-electrode cyclic voltammograms (CVs, Figure 28) were recorded at a scan rate of 2 mV s^{-1} with a gradual decrease of negative potential cut-off, i.e., towards di-hydrogen evolution (The theoretical values are -0.325, -0.378, and -0.382 V vs. NHE for 0.5 mol L^{-1} Li_2SO_4, Na_2SO_4, and K_2SO_4). The maximum positive potential has been set at a value slightly lower than the theoretical one allowing water oxidation.

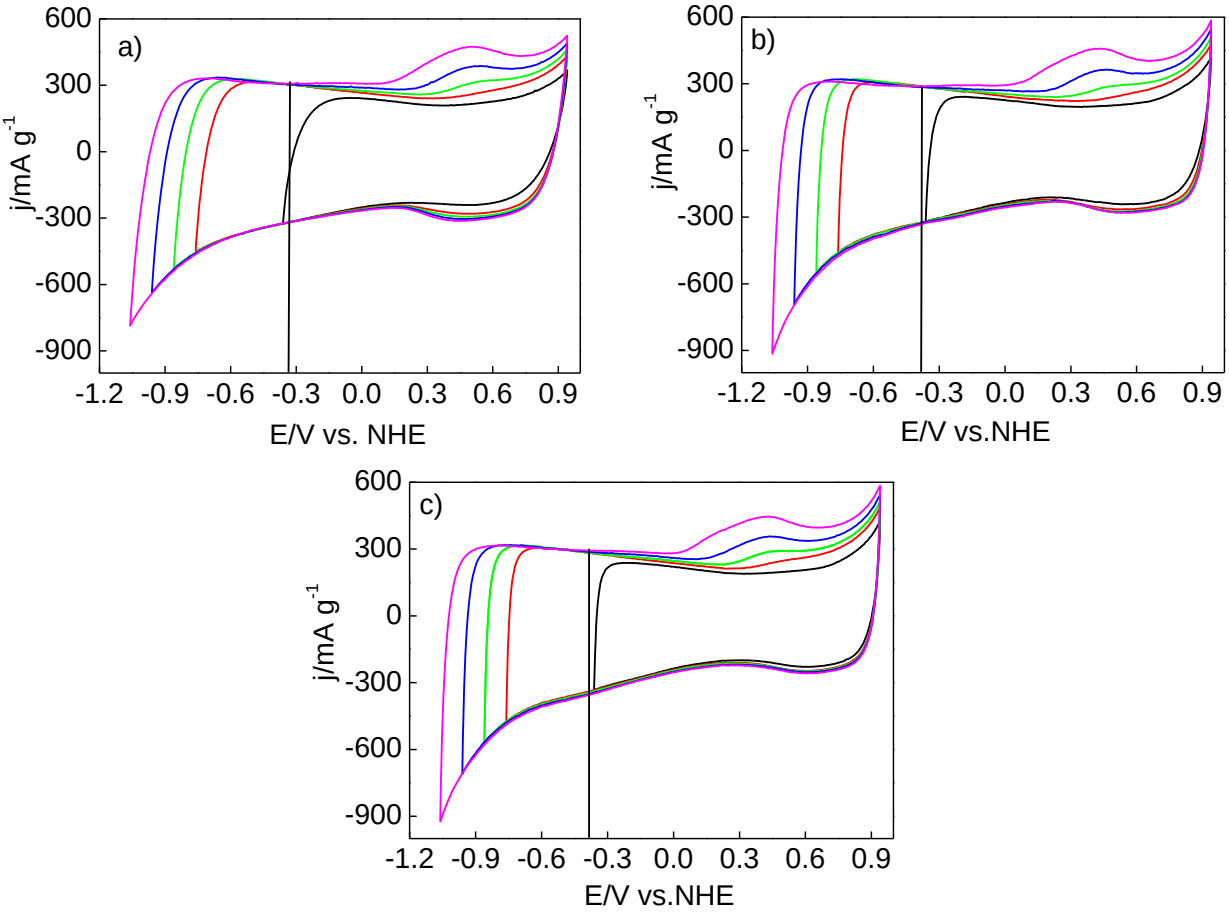

Figure 28 Three-electrode cyclic voltammograms (CVs, 2 mV s^{-1}) of AC in (a) 0.5 mol L^{-1} Li_2SO_4, (b) 0.5 mol L^{-1} Na_2SO_4, and (c) 0.5 mol L^{-1} K_2SO_4. The successive loops are obtained by stepwise shifting the negative potential limit to more negative values. The vertical lines correspond to the thermodynamic potential for water reduction.

The voltammograms look quite similar in all three electrolytic solutions. If the negative potential cut-off is higher than the value for water reduction, a rectangular shaped

voltammogram, typical of the double-layer charging, is obtained. When it becomes lower than the theoretical reduction potential values, water is reduced, and the double-layer formation takes place together with a pseudo-capacitive contribution related to the electrochemical reversible sorption of nascent hydrogen inside the pores of activated carbon [92][93]. A noticeable hump appears around 0.4-0.5 V vs. NHE during the anodic sweep, owing to the electro-oxidation process of the stored hydrogen [143]. Pseudo-capacitance due to reversible hydrogen storage might contribute effectively to the total capacitance in addition to the EDL capacitance. The negative current increases sharply from potentials below -1.0 V vs. NHE, indicating H_2 gas evolution and the plausible limit for negative polarization. Finally, we can estimate that the stability potential window of the AC carbon in the three electrolytes is around 2.0 V, confirming the previous results obtained with the same carbon material in 0.5 mol L^{-1} Na_2SO_4[19][20]. In summary, the stability potential window in aqueous alkali sulfates based electrolytes is larger than that in acidic or basic ones.

The specific capacitance calculated from galvanostatic (200 mA g^{-1}) discharge is 98, 109, and 129 F g^{-1} for 0.5 mol L^{-1} Li_2SO_4, Na_2SO_4, and K_2SO_4 based symmetric AC/AC capacitors, respectively. Such results indicate that the capacitance increases when the size of the hydrated cation decreases, i.e., Li+ (3.81 Å) > Na+ (3.59 Å) > K+ (3.34 Å) (Table 5).

The AC/AC capacitors in 0.5 mol L^{-1} Li_2SO_4, Na_2SO_4, and K_2SO_4 electrolytes have been investigated by electrochemical impedance spectroscopy (EIS). The Nyquist plots are presented in figure 29 where the inset displays an expanded view in the high frequency region. Generally, a supercapacitor behaves like a pure resistor at high frequencies and a capacitor at relatively low frequencies. The intersection on the real axis of the Nyquist plot in the high frequency region represents the bulk resistance of the electrolyte [31], which varies inversely with the conductivity of the solution. The conductivity values of the three electrolytes measured at room temperature (20 ^oC) are listed in table 5; as expected the conductivity decreases when the size of the hydrated cation increases, i.e. in the order K_2SO_4> Na_2SO_4> Li_2SO_4. The inset of Figure 29 confirms that the intersection values along the real axis are inversely proportional to the electrolyte conductivity. The equivalent distributed resistance (EDR), obtained from the linear projection of the almost vertical portion of the Nyquist plot to the real axis (Figure 29), represents the ions diffusion through carbon pores. The EDR varies inversely with the hydrated cation radius of three electrolytes (Table 5) [21][144].

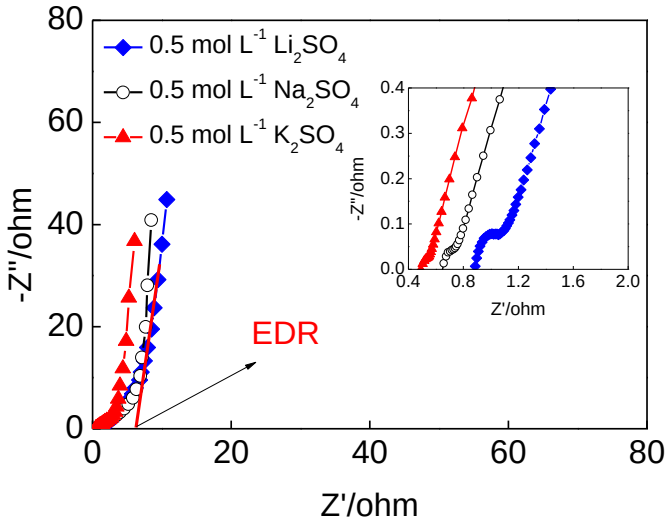

Figure 29 Nyquist plots of the symmetric AC/AC capacitors in 0.5 mol L^{-1} Li_2SO_4, 0.5 mol L^{-1} Na_2SO_4 and 0.5 mol L^{-1} K_2SO_4.

Table 5 Equivalent distributed resistance (EDR) obtained from the Nyquist plots, hydrated cations radius and conductivity at room temperature of the 0.5 mol L^{-1} alkali sulfate electrolytes.

Salt	EDR (Ω)	Hydrated cation radius (Å)	Conductivity (mS cm^{-1})
Li_2SO_4	6.58	3.82	45
Na_2SO_4	4.84	3.58	54.2
K_2SO_4	1.80	3.31	74.6

Because of the differences in resistance found for the three electrolytes, the power of the systems will be different. Ragone plots, which describe the relation between power density and energy density, have been further employed to highlight the effects of electrolytes on the system performance. Since a practical voltage of 1.6 V has been previously demonstrated in 0.5 mol L^{-1} Na_2SO_4 [19], the Ragone plots were realized at this voltage for symmetric AC/AC capacitors in the three electrolytes. The energy and power extractable at 10 s discharge time (see straight line in Figure 30) are the largest in 0.5 mol L^{-1} K_2SO_4. It confirms that the main contribution to the overall resistance of the system is the EDR (Figure 29) [144]. On the point of view of energy density, K_2SO_4 provides the largest one because of the highest specific capacitance in this medium. In conclusion, K_2SO_4 seems to be the best neutral aqueous electrolyte in terms of energy and power density.

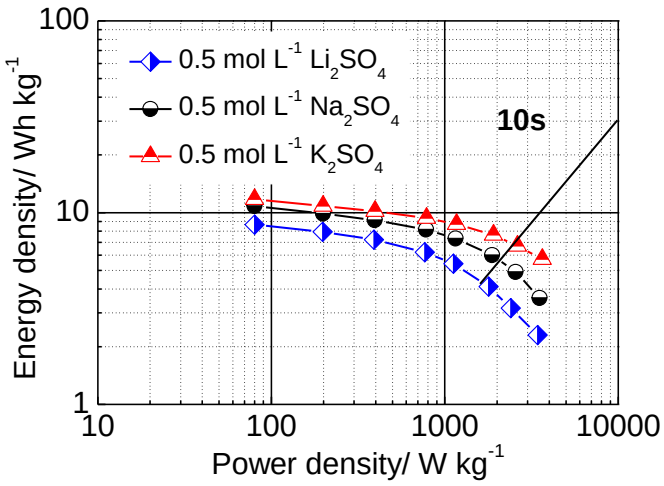

Figure 30 Ragone plots of symmetric AC/AC capacitors working at 1.6 V applying current densities from 0.2 to 10 A g^{-1}. Electrolytes: 0.5 mol L^{-1} Li_2SO_4, 0.5 mol L^{-1} Na_2SO_4 and 0.5 mol L^{-1} K_2SO_4.

As it has been previously discussed, low temperature performance of supercapacitors plays a significant role in some specific applications. Therefore, electrochemical impedance spectroscopy has been conducted at -10 °C in the three electrolytes, and the Nyquist plots are shown in Figure 31. In the three media, the characteristics of the Nyquist plots are resistor-like; the ESR extracted at 10 kHz reaches 4025, 4295, and 72 Ω in 0.5 mol L^{-1} K_2SO_4, Na_2SO_4 and Li_2SO_4, respectively. The larger resistance values in K_2SO_4 and Na_2SO_4 media are related with the low solubility of these salts at this temperature (Table 6) [145][146]; the initial concentration of 0.5 mol.L^{-1} is higher than their solubility, therefore they precipitate when the temperature is lowered to -10°C. Contrarily this limit does not exist with Li_2SO_4 which solubility is even higher at -10°C. The inset of an AC/AC capacitor in 2 mol.L^{-1} Li_2SO_4 shows excellent characteristics at -10°C, with an ESR of 1.5 Ω, due to the solubility increase with the decrease of temperature. In other words, the 2 mol.L^{-1} Li_2SO_4 solution allows the freezing point of the electrolyte to be depressed, while keeping good supercapacitor performance.

Table 6 Solubility of alkali sulfates in water at 0 °C and 25 °C [145][146].

Salt	Solubility mol L^{-1} (0 °C)	Solubility mol L^{-1} (25 °C)
Li_2SO_4	3	2.7
Na_2SO_4	0.34	1.97
K_2SO_4	0.4	0.69

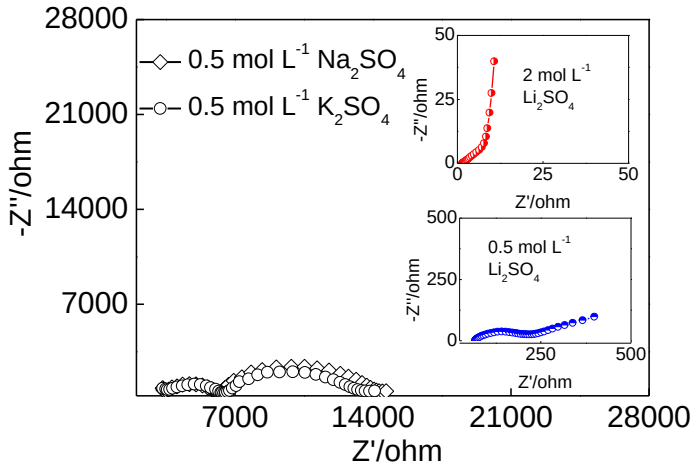

Figure 31 Nyquist plots of symmetric carbon/carbon capacitors in alkali sulfates at -10 °C.

Since 2 mol L^{-1} Li_2SO_4 seems to be a promising aqueous electrolyte for being integrated into a prototype device, we have more extensively investigated the electrochemical performance of the AC/AC capacitor in this electrolyte. Figure 32 shows the three-electrode cyclic voltammograms (CVs, 2 mV s^{-1}) of AC obtained with a gradual shift of potential cut-off to negative values (the theoretical value of di-hydrogen evolution at 20 °C in 2 mol L^{-1} Li_2SO_4 is -0.35 V vs. NHE). The general aspect of the CVs is comparable to those which have been obtained when using 0.5 mol L^{-1} Li_2SO_4 (Figure 28a). The stability potential window of the AC carbon is around 2.0 V, identical to the value found for the 0.5 mol L^{-1} one (Figure 28b). The only remarkable difference with the 0.5 mol L^{-1} Li_2SO_4 solution is a better defined anodic hump at around 0.5 V vs NHE which seems to indicate more hydrogen stored when the concentration is increased.

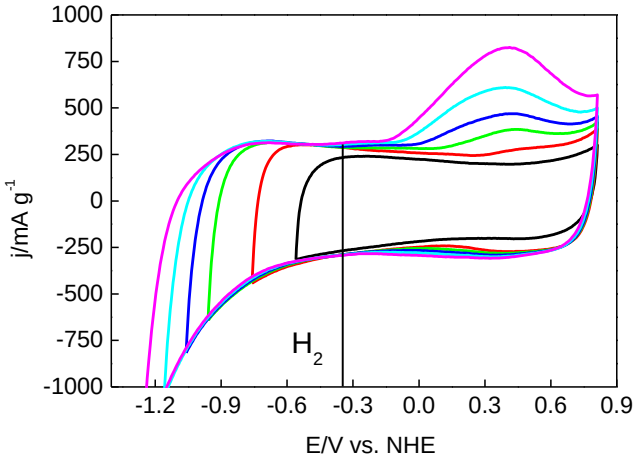

Figure 32 Three-electrode cyclic voltammograms (CVs, 2 mV s^{-1}) of AC in 2 mol L^{-1} Li_2SO_4. The loops are

obtained by stepwise shifting the negative potential limit to more negative values. The vertical line at -0.35 V vs NHE corresponds to the thermodynamic potential for water reduction.

The galvanostatic charge/discharge characteristics of the symmetric AC/AC capacitor in 2 mol L^{-1} Li_2SO_4 (Figure 33) demonstrate a pure capacitive behavior, with straight lines, up to 1.2 V. For cell voltages higher than 1.2 V, there is a distortion of the linearity associated to pseudo-capacitive effects related with the above mentioned hydrogen storage mechanism. This observation is in good agreement with the finding in Figure 32, i.e., the total capacitance combines the EDL capacitance and pseudo-capacitance.

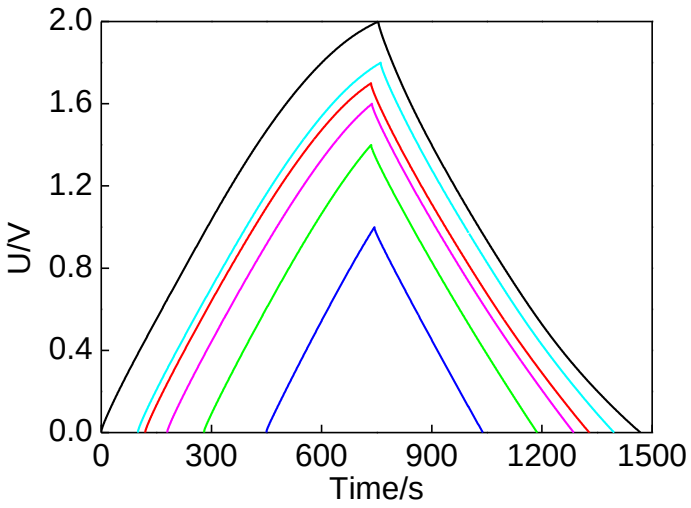

Figure 33 Galvanostatic (200 mA g^{-1}) charge-discharge characteristics of a symmetric AC/AC supercapacitor in 2 mol L^{-1} Li_2SO_4.

The cycling stability of the AC/AC system in 2 mol L^{-1} Li_2SO_4 has been evaluated at 20 ^oC and -10 ^oC by galvanostatic (1 A g^{-1}) charge/discharge cycling during 10, 000 cycles (Figure 34). At room temperature, the system shows a relatively good stability at 1.8 V; the capacitance slightly decreases during the initial 1,000 cycles and then it keeps almost constant until 10,000 cycles. However, if the cell voltage is increased up to 1.9 V, a pronounced capacitance decay of 30 % occurs after 10,000 cycles. If the temperature is decreased down to -10 ^oC, the initial capacitance if around 20 $F.g^{-1}$ smaller than at room temperature, but after 10,000 cycles at 1.8 V, only 8% of the initial capacitance is lost. It can be therefore concluded that the 2 mol L^{-1} Li_2SO_4 electrolyte allows a long cycle operation at temperatures ranging between 20 ^oC and -10 ^oC up to 1.8 V.

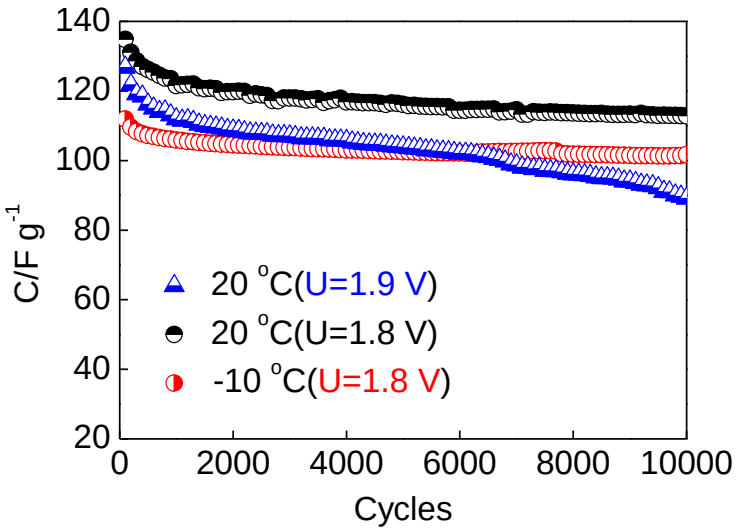

Figure 34 Evolution of the discharge capacitance of symmetric AC/AC capacitors in 2 mol L^{-1} Li_2SO_4 during galvanostatic charge-discharge cycling (1A g^{-1}) at 20°C and -10°C.

As the capacitance is smaller at 20°C and -10°C (see Figure 34), further tests have been done in order to understand such differences. In this sense, Figure 35 compares the cyclic voltammograms (CVs, 2 mV s^{-1}) obtained in three-electrode cells at 20°C and -10°C. The water reduction peak during the cathodic scan and its anodic counter-part are more important at 20°C than at -10°C, suggesting that more hydrogen was sorbed into the carbon porosity at higher temperature. This fact fits well with the chemical character of the carbon-hydrogen bond; in other words, the temperature increase impacts positively in decreasing the kinetic barrier for the hydrogen adsorption/desorption process [93]. As seen on figure 35, with the increase of temperature from -10°C to 20°C, the oxidation potential decreases from ca. 0.6 to 0.45 V vs NHE. Consequently, the over-potential for hydrogen electro-oxidation is lower at room temperature than at -10°C. This decrease of over-potential is related to a lower ohmic drop because of the higher conductivity of the solution at 20°C [93][147]. In conclusion, more hydrogen was reversibly sorbed into the carbon electrode at higher temperature, and is also extracted at lower potential; it becomes obvious that the pseudo-capacitive contribution related with the stored hydrogen is then larger at 20°C than at -10°C.

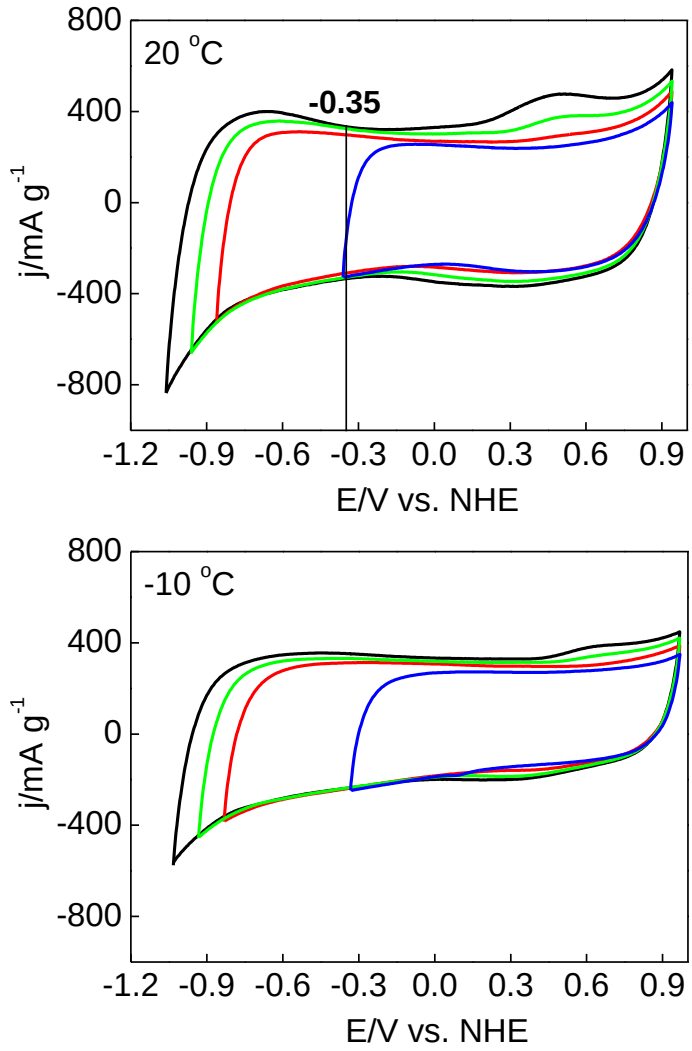

Figure 35 Three-electrode cyclic voltammograms (CVs, 2 mV s^{-1}) of AC in 2 mol L^{-1} Li_2SO_4 at 20°C and -10°C. The loops are obtained by stepwise shifting the potential to more negative values. The vertical line corresponds to the thermodynamic potential for water reduction.

The above described phenomena are also visible in the cyclic voltammograms of symmetric AC/AC capacitors at 20°C and -10°C (Figure 36). When the maximum voltage is lower than 1.2 V, a pure capacitive behavior, with typically rectangular shaped CVs, is obtained. The lesser defined rectangular shape at -10°C than at 20°C indicates a higher resistive character of the cell at -10°C due to the higher viscosity and lower conductivity of the lithium sulfate solution at this temperature [22][147]. As a result, the specific capacitance at 1.2 V reaches 126 and 105 F g^{-1} when operating at 20°C and -10°C, respectively. When increasing the voltage above 1.2 V, one can see at 20°C a well-defined current leap together

with an increase of the current during the negative scan between 0.4 and 0 V (Figure 36). These two features, more distinguishable at 20°C than at -10°C, are obviously related with hydrogen storage in the negative electrode (see Figure 35), being stored when the voltage is higher than 1.2 V and desorbed at voltage lower than 0.4 V. Consequently, due this pseudo-capacitive contribution, the specific capacitance at 1.6 V respectively achieves 137 and 116 F g^{-1} at 20°C and -10°C.

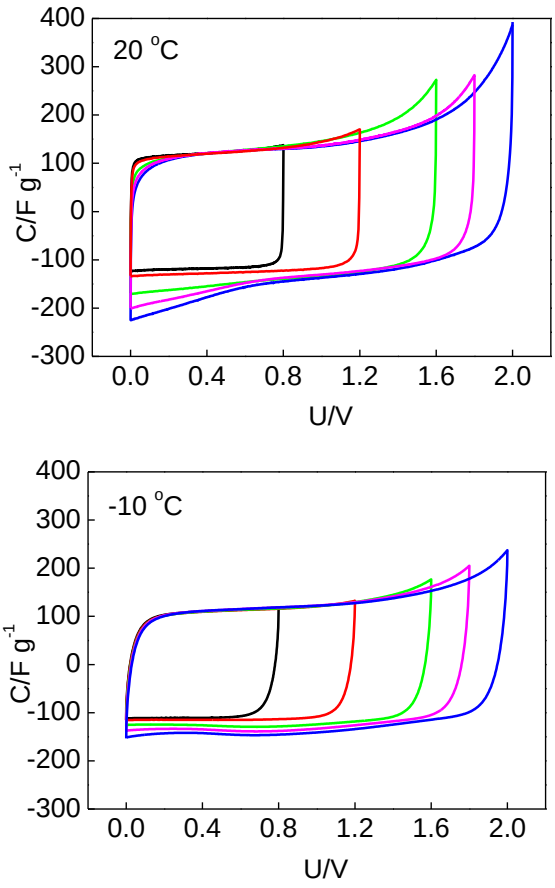

Figure 36 Cyclic voltammograms (2 mV s^{-1}) of symmetric AC/AC capacitors in 2 mol L^{-1} Li_2SO_4 at 20°C and -10°C.

The differences in electrochemical behavior between 20°C and -10°C when the cell voltage is below 1.2 V, i.e when there is only a capacitive contribution, can be further clarified by electrochemical impedance spectroscopy (Figure 37). The ESR values at 10 kHz are 0.61 and 1.50 Ω ar 20°C and -10°C, respectively. The EDR values, relating with the diffusion of ions inside the pores of carbon, are 3.3 and 7.7 Ω at 20°C and -10°C, respectively. The decrease of ESR and EDR when the temperature decreases to -10°C is easily explained

by the decrease of conductivity and increase of viscosity of the solution.. Actually, the lower kinetic energy at lower temperature reduces the free spaces between $Li+/SO_4^{2-}$ ions and the water molecules [31]. At low temperature, the ions are more strongly hydrated and their dehydration in order to penetrate in the narrow micropores is more difficult than at room temperature. All these factors contribute to a decrease of EDL capacitance from 20°C to -10°C.

Hence, among the three alkali sulfates investigated, lithium sulfate is the most interesting one because it remains highly soluble at relatively low temperature, allowing AC/AC capacitors to operate with good electrochemical performance at -10 °C when using a 2 mol L^{-1} solution.

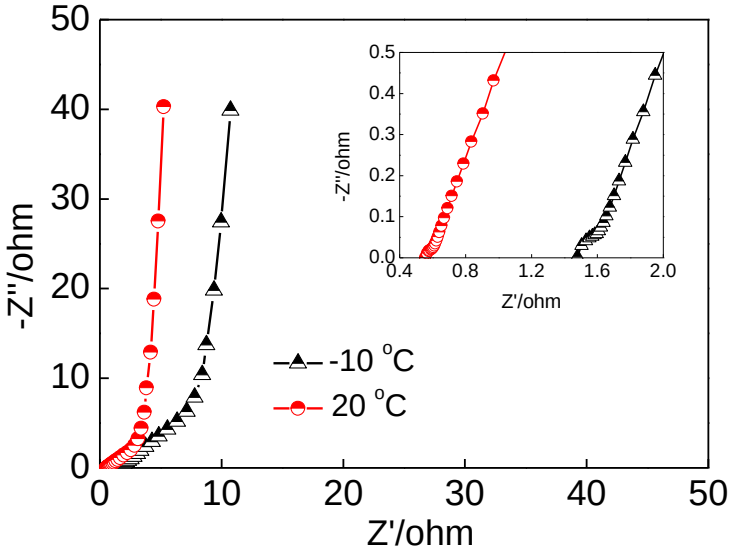

Figure 37 Nyquist plots of symmetric AC/AC capacitors in 2 mol L^{-1} Li_2SO_4 at 20°C and -10°C.

3 Understanding the electrodes potential limits of symmetric carbon/carbon capacitors in lithium sulfate electrolyte

3.1 Introduction

In the previous section, we have shown that 2 mol L^{-1} lithium sulfate is the most promising neutral aqueous electrolyte, because the systems can operate down to -10°C at a cell voltage as high as 1.8 V. Even if this voltage is interesting, considering that the system is operating in an aqueous electrolyte, such value is still lower than the maximum stability

potential range of the carbon electrode in that electrolyte (as it was estimated from Figure 32). That means that the system does not take full profit of the stability potential window. Therefore, it is necessary to understand the potential limitations of the carbon electrodes when operating in this electrolyte.

This section will particularly consider the behavior of the carbon electrodes close to the potential limits for clarifying the reasons of the limitations. For doing that, a reference electrode has been included in a symmetric AC/AC cell, in order to measure separately the potential and capacitance evolution of both electrodes during long term cycling. The surface functionality of the carbon electrodes is also analyzed after long-term operation of the cell at different values of maximum voltage. After coupling the results of both kinds of analysis, it will be possible to clarify the role of the positive and negative electrodes and the influence of surface groups in such systems during long-term cycling. Especially, it will be shown that after deactivation of the surface active sites by controlled chemical oxidation with hydrogen peroxide (H_2O_2), the positive carbon electrode can be protected from the destructive electro-oxidation during cell operation at high voltage.

3.2 Physicochemical characterization of modified carbon materials

The carbon AC has been mildly oxidized using H_2O_2 (ACH) and the physicochemical characteristics of the two materials have been compared. As expected, the porous texture is unchanged after surface modification of AC (Table 7): the specific surface area and pore volumes of the two materials are identical. Comparing ACH with AC, the TPD analysis (Table 8) shows an increase of surface functionalities evolving as CO and CO_2. More CO-type groups (phenol, quinone and carbonyl groups) were formed than CO_2-type groups (carboxylic groups) on ACH.

Table 7 Porous texture of as-received AC and of the modified carbon ACH

Carbon	$S_{BET}(N_2)$ $m^2\ g^{-1}$	$V_{ultramicro}$ [a] $cm^3\ g^{-1}$	V_{micro} [b] $cm^3\ g^{-1}$	V_{meso} [c] $cm^3\ g^{-1}$
AC	2224	0.83	0.83	0.45
ACH	2214	0.90	0.80	0.48

(a) DR equation applied to the CO_2 adsorption data; (b) DR equation applied to the N_2 adsorption data; (c) NLDFT method applied to the N_2 adsorption data

Table 8 Cumulated CO_2 and CO amounts and O evaluated from the TPD analysis of as-received AC and modified carbon ACH

Carbon	CO_2 evolution/μmol g^{-1}	CO evolution/μmol g^{-1}	Total O/wt%
AC	159	461	1.5
ACH	805	1946	6.6

The table 9 summarizes the results obtained from the deconvolution of the C1s XPS peak. After the mild oxidation of AC to give ACH, the surface functionality is enriched from 0.54 to 1.21 at% of carboxylic groups (–O-C=O, B.E. = 289.0 ± 0.2 eV), from 0.09 to 0.65 at% of keto and quinone groups (C=O, B.E. = 287.5 ± 0.2 eV) and 1.22 to 1.84 at% of phenol and ether groups (C=O, B.E. = 286.3 ± 0.2 eV) [148]. In good agreement with TPD analysis, it is noticeable that the content of C-O or C=O groups leading to CO evolution, is higher than the amount of –O-C=O groups.

Table 9 Amount of surface groups on the AC and ACH carbons determined from the C1s X-ray photoelectron spectra

Carbon	C-OR/at% 286.3±0.2eV	C=O/at% 287.5±0.2eV	-O-C=O/at% 289.0±0.2eV	O/at%
AC	1.22	0.09	0.54	2.4
ACH	1.84	0.65	1.21	4.8

3.3 Electrochemical performance of AC and AC/AC supercapacitors

As it has been pointed out before, the stability potential window of 2.0 V for the AC carbon is not completely used in a symmetric AC/AC capacitor, as the maximum cell voltage is 1.8 V (Figure 34). In order to understand the reason, the real working potential range of each electrode, during charge/discharge of the two-electrode cell, has been separately measured by adding a Hg/Hg_2SO_4 reference electrode. Figure 38 presents the maximum potential (E+) reached by the positive electrode and the minimum potential (E-) reached by the negative one, for a given maximum voltage applied to the supercapacitor. The E_{0V} values represent the electrode potential when the voltage is set to 0 V between two successive cycles at different maximum voltages. For maximum voltages of 1.8 and 1.9 V, the positive electrode potentials reach 0.99 and 1.06 V vs. NHE, respectively. Such values are beyond the

thermodynamic potential for di-oxygen evolution, e.g., 0.88 V. Furthermore, the negative potentials reach -0.81 and -0.84 V vs. NHE for voltages of 1.8 and 1.9 V, respectively. These potential values are lower than the thermodynamic limit for water reduction (-0.35 V vs. NHE in aqueous 2 mol L^{-1} Li_2SO_4) but they are still much higher than the practical negative potential limit of ca. -1 V vs. NHE estimated in Figure 32 (identically described by Figure 28). Hence, the maximum voltage of the system seems to be limited by the positive electrode, though the potential of the former may slightly exceed the thermodynamic limit without detrimental effect on the system cycle life.

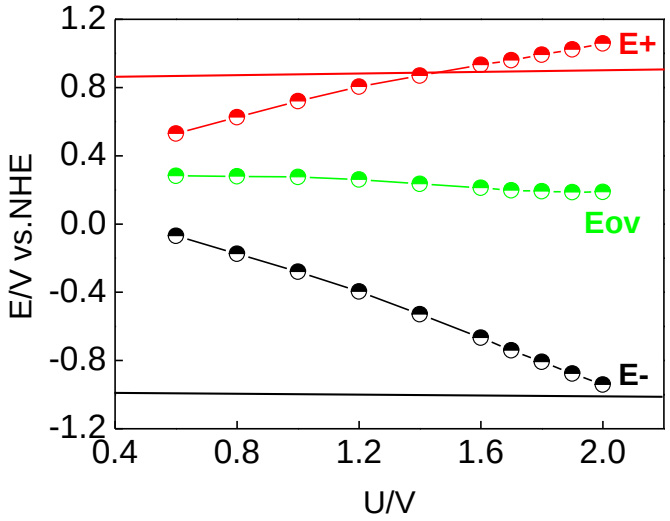

Figure 38 Potential limits of positive (E+) and negative (E-) electrodes during the galvanostatic (200 mA g^{-1}) cycling of a symmetric AC/AC supercapacitor up to different values of maximum voltage. The E_{0V} values correspond to the electrodes potential when the working voltage is shifted to 0 V before each change of maximum voltage. The lower horizontal line represents the negative potential limit related with a noticeable H_2 evolution estimated in three-electrode cell. The upper horizontal one corresponds to the thermodynamic limit for water oxidation. Electrolyte: 2 mol L^{-1} Li_2SO_4.

In order to detect possible changes of electrodes surface functionality during cell operation, the carbon materials from negative and positive electrodes have been analyzed by TPD after charging/discharging the system during 5,000 cycles at maximum voltages of 1.6 V, 1.8 V, and 1.9 V. Figure 39 displays the amount of CO_2 and CO evolved from the fresh electrodes and the cycled ones. CO_2 evolves at relatively low temperature (around 300°C) and can be attributed to the decomposition of carboxylic type acidic functionalities. CO evolves at higher temperatures, around 700°C, and is originated from the decomposition of basic

functionalities such as quinone, phenols [149]. At the negative electrode (Figure 39a), the amount of surface functionalities does not change significantly even at high cell voltages. By contrast, for the positive electrode, Figure 39b shows a clear electro-oxidation of AC at 1.6 V. Compared to the fresh electrode, the amount of acidic (evolving as CO_2) and basic (evolving as CO) [150] surface functionalities increases from 2-fold to 4-fold and 1.5-fold to 2-fold, respectively, when the maximum voltage increases from 1.6 V to 1.8 V. This change of functionality may explain the slight capacitance decay during the first thousands cycles, but it does not further affect the performance of the AC/AC capacitor during long term cycling up to 1.8 V.

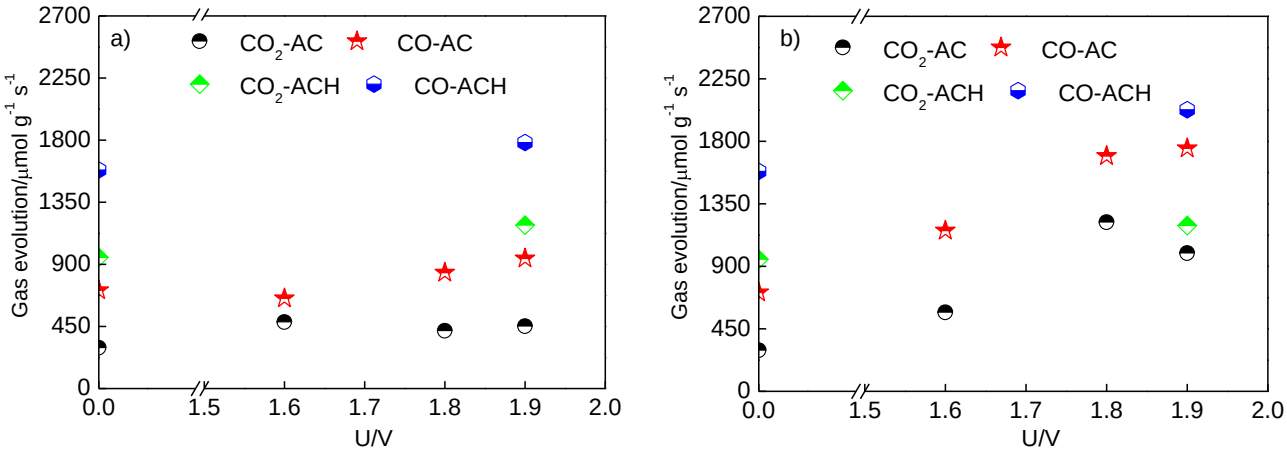

Figure 39 Evolved CO_2 and CO amounts measured by TPD on the fresh AC or ACH electrodes (values at 0 V) and on (a) negative and (b) positive electrodes of a symmetric capacitor after 5,000 charge/discharge cycles at different values of maximum voltage. Electrolyte: 2 mol L^{-1} Li_2SO_4.

Considering the higher potential reached by the positive electrode at a maximum voltage of 1.9 V after few cycles (see Figure 38), one could expect a more serious surface electro-oxidation of carbons after long-term cycling [151]. In fact, Figure 39b shows that after 5,000 cycles the amount of CO_2-type groups is smaller than at 1.8 V, whereas the CO-type groups only slightly increase. This behavior fits well with the mechanism suggested for the electrochemical oxidation of carbon at potentials higher than the value for water oxidation [152]. At high over-potentials, the acidic groups generated by electro-oxidation can be further oxidized leading to CO_2 evolution. As a consequence, the capacitance decay observed in Figure 34 for 1.9 V may be originated from: i) a mass loss of the positive electrode; ii) a reduction of electrode integrity and contact with the current collector due to gases evolution.

The latter is certainly related with the continuous resistance increase observed when the cell operates at 1.9 V (Figure 40a), whereas at lower voltage (1.8 V), the resistance remains almost constant. The progressive increase of maximum potential for the positive electrode (E+) recorded during the operation of the cell at 1.9V (Figure 40) provokes a more extensive electro-oxidation of carbon and, as exposed above, the evolution of CO_2 and a continuous decrease of capacitance during cycling. By contrast, when the voltage is such that capacitance is almost stabilized after few thousands cycles, e.g., at 1.6 and 1.8 V, the maximum potential of the positive electrode slightly decreases during the first thousand cycles and further remains unchanged during the next thousands cycles (Figure 40b).

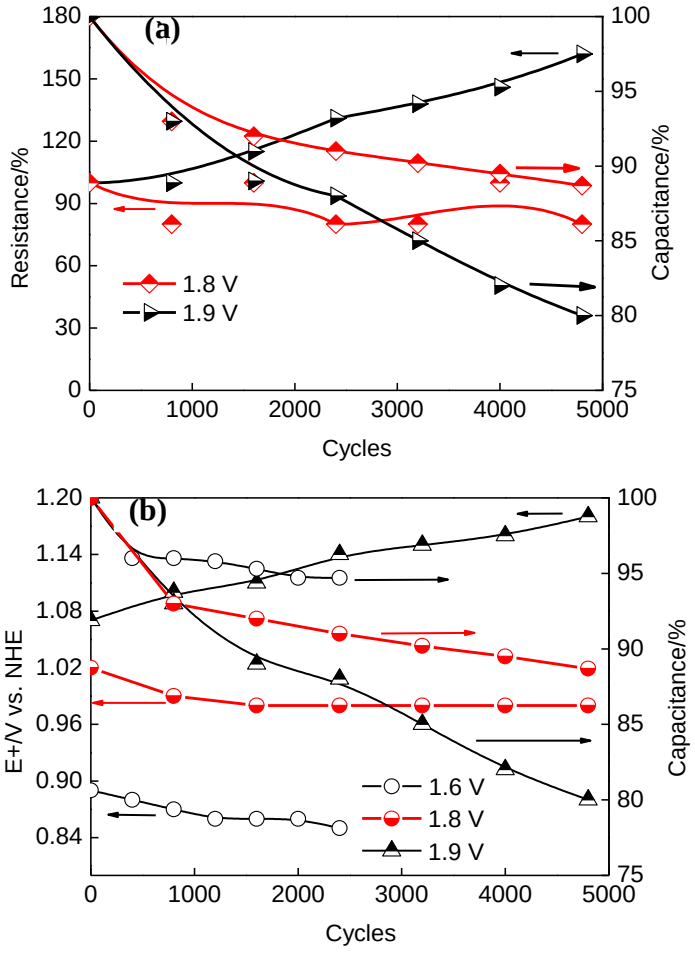

Figure 40 Capacitance retention ratio (C_n/C_1*100, where C_n is the capacitance at n^{th} cycle and C_1 at 1^{st} cycle) and (a) resistance variation ratio (R_n/R_1*100, where R_n is the resistance at n^{th} cycle and R_1 at 1^{st} cycle) or (b) maximum potential (E+) of the positive electrode vs. NHE during galvanostatic (200 mA g^{-1}) cycling of a symmetric AC/AC supercapacitor. Electrolyte: 2 mol L^{-1} Li_2SO_4.

From the foregoing, it is now clearly established that the capacitance decay occurring during cycling above a limit voltage is correlated with an increase of maximum potential of the positive electrode and its destructive electro-oxidation.

3.4 Electrochemical performance of the oxidized AC carbon (ACH) and of ACH/ACH supercapacitors

The uncontrolled electrochemical oxidation of the positive electrode gives an explanation for obtaining a cell voltage smaller than the stability potential window of the AC electrode. In order to explore the possibility of protecting the AC surface from a further serious electro-oxidation process, the latter has been chemically oxidized in a controlled manner by H_2O_2 giving the carbon ACH. The physico-chemical properties of the carbon ACH have been presented in section 3.2.

From the electrochemical point of view, the three-electrode cyclic voltammograms of ACH (Figure 41) and AC (Figure 32) are very comparable. Similarly, the galvanostatic charge/discharge profiles of ACH/ACH (Figure 42) and AC/AC (Figure 33) capacitors are quite similar, demonstrating that the values of specific capacitance are not much affected by the presence of oxygenated surface functionalities in aqueous 2 mol L^{-1} Li_2SO_4, as it is also the case in aqueous Na_2SO_4[20].

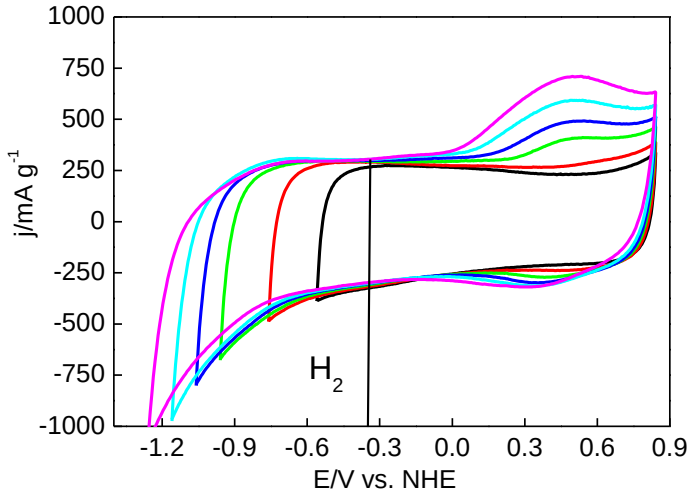

Figure 41 Three-electrode cyclic voltammograms (CVs, 2 mV s^{-1}) of ACH in 2 mol L^{-1} Li_2SO_4. The loops are obtained by stepwise shifting the negative potential limit to more negative values. The vertical line at -0.35 V vs NHE corresponds to the thermodynamic potential for water reduction.

However, Figure 43 shows that the maximum potential values for the ACH positive electrode, at whatever cell voltage, are higher than for the AC based supercapacitor (compare with Figure 38). Despite these higher values of maximum E+, the symmetric ACH/ACH capacitor can be reversibly cycled at 1.9 V instead of 1.8 V for the symmetric AC/AC one (see Figure 44).

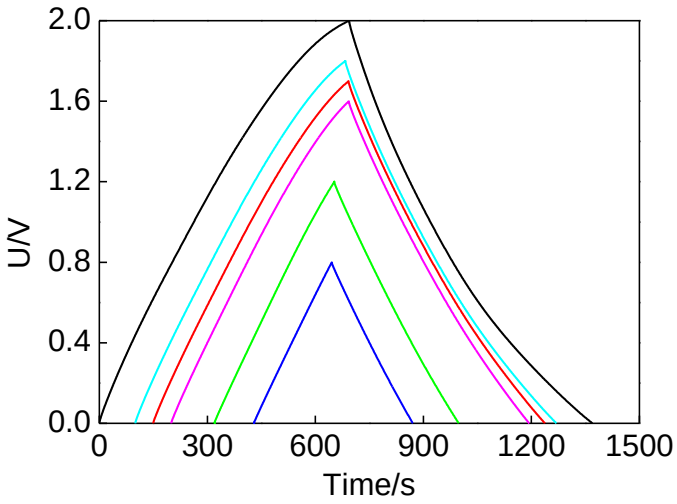

Figure 42 Galvanostatic charge-discharge characteristics (200 mA g^{-1}) of a symmetric ACH/ACH supercapacitor in 2 mol L^{-1} Li_2SO_4.

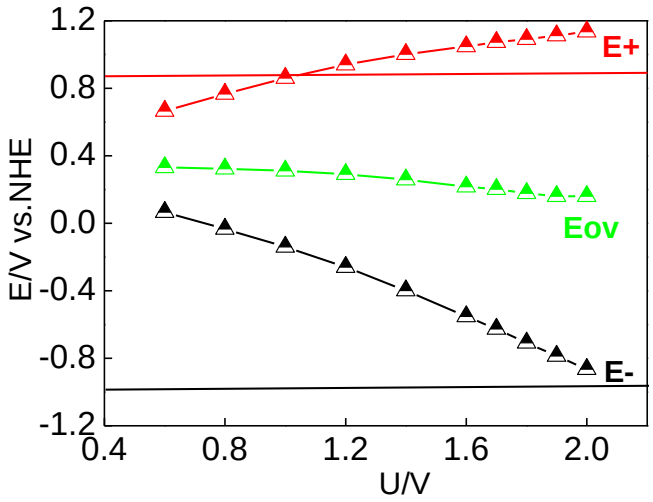

Figure 43 Potential limits of positive (E+) and negative (E-) electrodes during the galvanostatic (200 mA g^{-1}) cycling of a symmetric ACH/ACH supercapacitor up to different values of maximum voltage. The E_{0V} values correspond to the electrodes potential when the working voltage is shifted to 0 V before each change of maximum voltage. The lower horizontal line represents the negative potential limit related with a noticeable H_2

evolution estimated in three-electrode cell. The upper horizontal one corresponds to the thermodynamic limit for water oxidation. Electrolyte: 2 mol L^{-1} Li_2SO_4.

Actually, after 5,000 charges/discharges of the ACH/ACH capacitor at 1.9 V, the amount of CO_2-type and CO-type functionalities generated on the surface of the negative (Figure 39a) and positive (Figure 39b) electrodes does not exceed 1.3 times the amount found on the fresh electrode. At the same voltage, the electro-oxidation of the positive electrode is noticeably less important than for the AC electrodes (see Figure 39b). This result confirms that, after chemical oxidation, there are less active sites available for electro-oxidation than in the pristine AC [153]. Furthermore, Figure 45 shows that the maximum potential of the positive electrode slightly decreases during the first 1,000 cycles and remains almost constant up to 5,000 cycles. At 1.9 V maximum voltage, the maximum value of E+ for the ACH/ACH capacitor stabilizes at 1.08 V between 1,000 and 5,000 cycles (Figure 45), while it reaches 1.18 V for the AC/AC capacitor after 5,000 cycles (see Figure 40b). During galvanostatic cycling of the ACH/ACH supercapacitor up to 1.9 V, there is a very moderate loss of capacitance and the series resistance is constant (see inset in Figure 45). It is therefore anticipated that the controlled chemical oxidation of AC by H_2O_2 "neutralizes" most of the available active sites, allowing the system to be protected from deleterious electro-oxidation up to a voltage of 1.9 V.

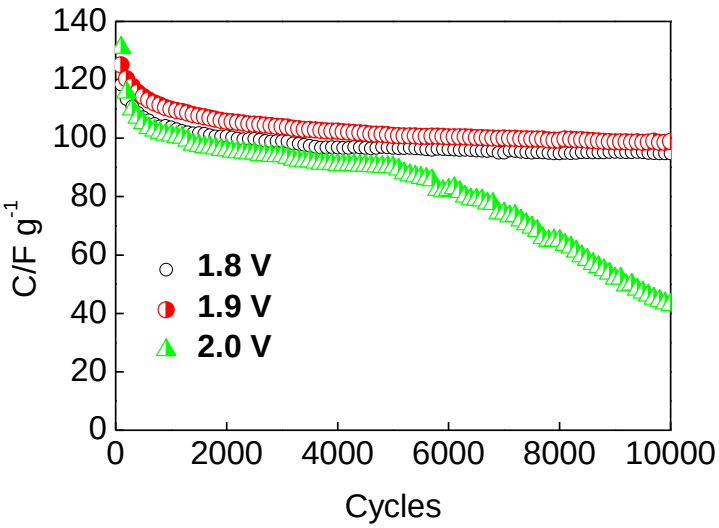

Figure 44 Evolution of the discharge capacitance during the galvanostatic (1 A g^{-1}) cycling of symmetric ACH/ACH supercapacitors in 2 mol L^{-1} Li_2SO_4.

In summary, the maximum voltage of symmetric carbon/carbon capacitors in 2 mol L^{-1} Li_2SO_4 is essentially limited by the positive electrode. When the maximum potential of this electrode (E^+) is too high, it provokes an irreversible electro-oxidation on the active sites of carbon and the evolution of CO_2. Due to this partial destruction of the positive electrode, the resistance increases continuously during cycling and the capacitance decreases. After controlled chemical oxidation of the AC carbon with hydrogen peroxide, the maximum potential of the positive electrode is pushed towars slightly lower values. Therefore, it might be anticipated that the high voltage value claimed by Fic *et al.* in reference [22] might be as well related to the existence of a specific surface functionality on the carbon electrodes used by these authors.

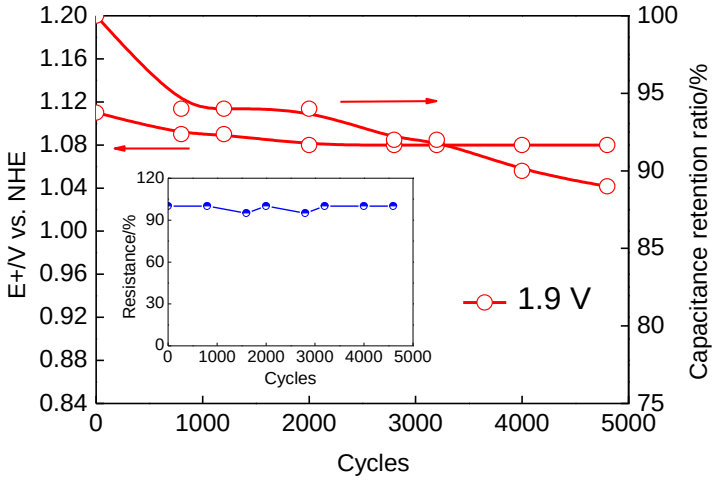

Figure 45 Capacitance retention ratio (C_n/C_1*100, where C_n is the capacitance at n^{th} cycle and C_1 at 1^{st} cycle) or maximum potential (E+) of the positive electrode vs. NHE during galvanostatic (200 mA g^{-1}) cycling of a symmetric ACH/ACH supercapacitor. Electrolyte: 2 mol L^{-1} Li_2SO_4. Inset: resistance variation ratio (R_n/R_1*100, where R_n is the resistance at n^{th} cycle and R_1 at 1^{st} cycle).

4 Asymmetric carbon based supercapacitors in aqueous lithium sulfate

4.1 Introduction

In order to extend the cell voltage and the energy density of supercapacitors operating in aqueous lithium sulfate, in this section, we propose the use of an asymmetric configuration, as already suggested for H_2SO_4 [132]. The general concept is to operate within the optimal working potential windows of positive and negative electrodes in order to increase the overall

voltage of the system. This can be realized either by balancing the mass of the electrodes or by using different optimized carbons for the positive and negative electrodes [132].

4.2 Modification of the surface functionality of activated carbon

Since we have demonstrated an effect of surface functionality on the electrochemical performance in section 3, for this part of the study, the carbon AC was modified by chemical oxidation in nitric acid or hydrogen peroxide solutions followed or not by a thermal treatment at different temperatures under nitrogen. The nomenclature used for the modified AC is ACN for the nitric acid oxidized one and ACN400, ACN500 for the ACN further heat treated at 400 ^{o}C and 500 ^{o}C, respectively. On the other hand, ACH400 was obtained by heat treating the ACH carbon (AC oxidized with H_2O_2 presented in section 3) at 400 ^{o}C.

As shown in Table 10, after modification by nitric acid and further thermal treatments, the modified carbons ACN, ACN400, and ACN500 remain highly micro-porous while a slight decrease of the specific surface area compared to AC is observed. This decrease could be due to the blockage of pore entrance by the surface groups [154][155]. The thermal treatments at 400 and 500°C provoke the desorption of surface groups and regenerate almost completely the surface area and/or volume of ultramicropores. Similarly, ACH400 presents slight higher BET specific surface area and larger volumes of micropores and ultramicropores than those of ACH. In the case of ACN400 and ACN500, the $V_{ultramicro}$ value is even larger than for AC, indicating that some ultramicropores have been formed or opened after the oxidation/thermal treatment [51]. Overall however, one can conclude that the porous texture of AC is not extensively altered by these treatments.

Table 10 Porous texture of the as-received AC and surface-modified carbons

Carbon	$S_{BET}(N_2)$	$V_{ultramicro}$ [a]	V_{micro} [b]	V_{meso} [c]
	$m^2 g^{-1}$	$cm^3 g^{-1}$	$cm^3 g^{-1}$	$cm^3 g^{-1}$
AC	2224	0.83	0.83	0.45
ACN	2056	0.71	0.72	0.45
ACN400	2082	0.87	0.73	0.46
ACN500	2125	0.89	0.75	0.41
ACH	2214	0.90	0.80	0.48
ACH400	2363	0.95	0.85	0.41

(a) DR equation applied to the CO_2 adsorption data; (b) DR equation applied to the N_2 adsorption data; (c)

NLDFT method applied to the N_2 adsorption data

The XPS analysis (Table 11) reveals differences in surface oxygen containing functionalities depending on the treatment. The total oxygen content is 10.9, 7.3, 6.7, and 3.7 at % for ACN, ACN400, ACN500, and ACH400, which is considerably higher than that of AC, i.e., 2.4 at%. During the thermal treatments, the C=O and –O-C=O groups are partly removed, while the C-OR type surface groups (phenol and ether groups) remain on the surface. Especially, the ether groups in-built in the carbon framework require much higher temperatures to be decomposed.

Table 11 Surface functionality of the modified carbons from the XPS C1s spectra

Sample	**C-OR/at%**	**C=O/at%**	**-O-C=O/at%**	**O/at%**
	286.3±0.2eV	**287.5±0.2eV**	**289.0±0.2eV**	
AC	1.22	0.09	0.54	2.4
ACN	3.39	1.79	2.48	10.9
ACN400	3.07	0.75	1.62	7.3
ACN500	3.06	0.74	1.28	6.7
ACH	1.84	0.65	1.21	4.8
ACH400	2.12	0.28	0.64	3.7

4.3 Electrochemical characterizations of the modified carbons

Figure 46 presents the three-electrode cyclic voltammograms (CVs, 2 mV s^{-1}) of the various carbons obtained with gradual decrease of negative potential cut-off. The first cycle has been performed in the narrow potential range from -0.36 V to 0.84 V vs. NHE in which only the EDL formation takes place. Considering the voltammogram of ACN in this range, one remarks a narrowing at high potential which could be attributed to a saturation of porosity [63]. However this interpretation seems to be unlikely for two reasons: i) as noticed before the pore volume is only slightly reduced, meaning that porosity saturation should not occur for such a limited potential increase; ii) the gravimetric capacitance in the considered potential range is 152, 135, and 110 F g^{-1} for ACN, ACN400, and ACN500, respectively, meaning that ACN operates better than any of the other materials, including the carbon AC. This better capacitance behavior of ACN (and to lesser extent of ACN400) might be attributed to a better wettability of the material or to pseudo-faradic contributions due in both

cases to the rich surface functionality (Table 11). These results confirm that the pseudo-capacitance related to oxygenated groups can be also found in neutral aqueous electrolytes [20]. Apart the pseudo-capacitive contribution of surface functionality, differences can be also observed in the polarization between the hydrogen reduction and oxidation peaks in the various material. In particular the oxidation peak is located at around 0.6 vs NHE for ACN, ACN400 and ACN500 and at 0.45 V vs NHE for ACH and ACH400.

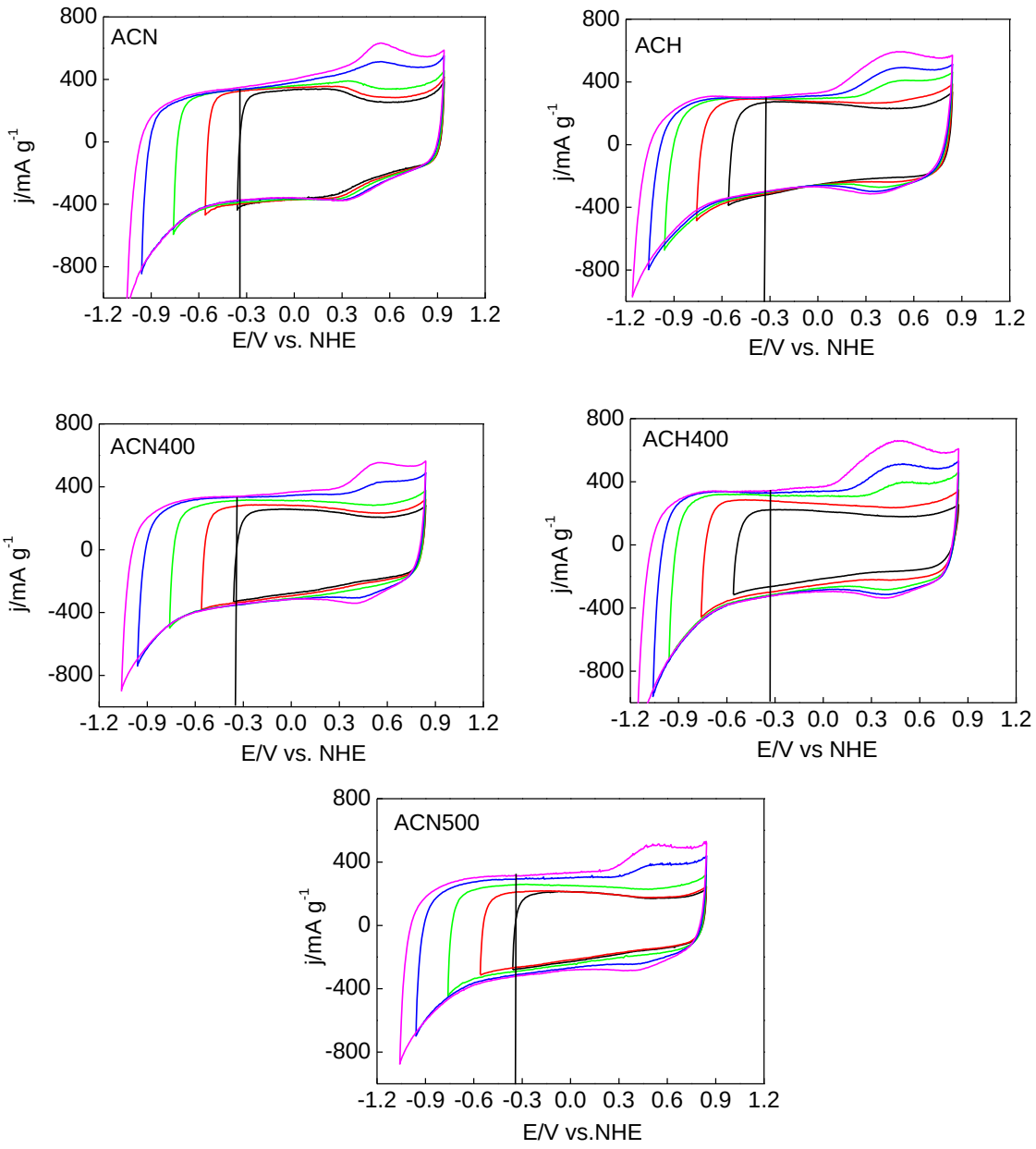

Figure 46 Three-electrode cyclic voltammograms (CVs, 2 mV s^{-1}) of the oxidized carbons in aqueous 2.0 mol L^{-1} Li_2SO_4 electrolyte. The loops are obtained by stepwise shifting the negative potential cut-off. The vertical line corresponds to the thermodynamic potential for water reduction.

4.4 Symmetric carbon/carbon systems in 2 mol L^{-1} Li_2SO_4

In order to check the performance of the different carbon materials as electrodes for supercapacitors, symmetric two-electrode cells were realized. Figure 47 presents the cyclic voltammograms (CVs, 2 mV s^{-1}) of the modified carbons (ACN, ACN400, ACN500, ACH, and ACH400) based symmetric systems together with the AC pristine one.

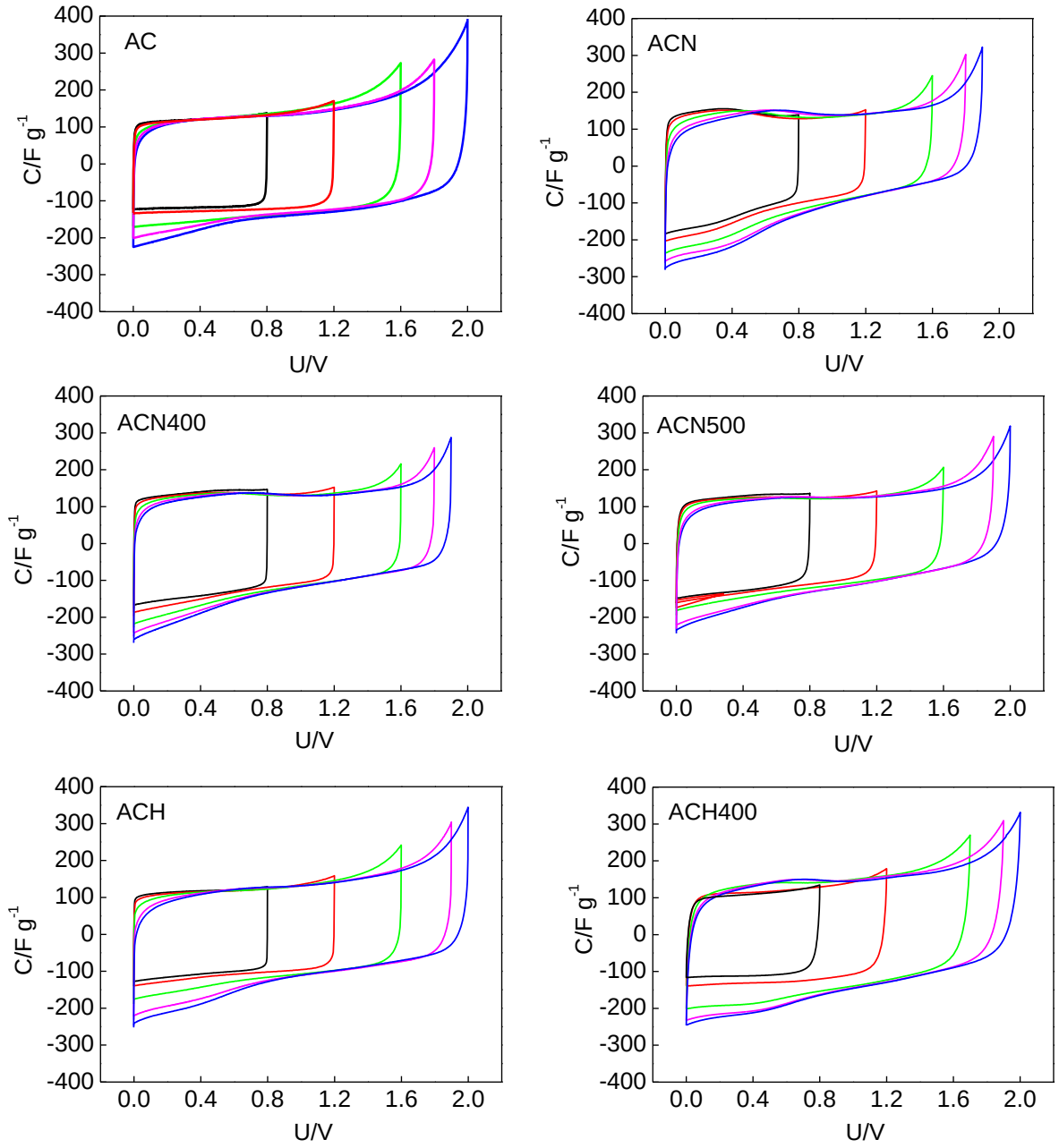

Figure 47 Cyclic voltammograms (CVs, 2 mV s^{-1}) of symmetric two-electrode capacitors recorded with pristine AC and the modified carbons in aqueous 2 mol L^{-1} Li_2SO_4.

Apart from ACN, all the other carbons show a typical EDL behavior up to 1.2 V. The hump present between 0-0.4 V for the ACN based system is directly related with the pseudo-capacitive contribution from surface functional groups as already shown in figure 46. The specific capacitance gravimetric values calculated from galvanostatic charge/discharge (200 mA g^{-1}) up to 0.8 V on symmetric cells are 116, 141, 139, 122, 113, and 101 F g^{-1} for AC, ACN, ACN400, ACN500, ACH, and ACH400 based supercapacitor, respectively. Such result reveals that the pseudo-capacitive contribution also increase with the content of surface groups in neutral aqueous electrolytes [20], being in good agreement with the results obtained in three electrode cells (Figure 46).

In all cases, a current leap involving the electrochemical hydrogen storage mechanism appears above 1.2 V and its counter-part from 0.4 to 0 V on the negative scan. The specific capacitance determined from galvanostatic charge/discharge (200 mA g^{-1}) at 1.8 V is 141, 139, 134, 124, 130, and 141 F g^{-1} for the AC, ACN, ACN400, ACN500, ACH, and ACH400 based supercapacitors, respectively. It is remarkable that, by increasing the cell voltage from 0.8 to 1.8 V, the capacitance increases only for the capacitors built with AC, ACH and ACH400 based electrodes, which have the smallest amount of oxygen functionalities [156]. Considering the remark about the hydrogen oxidation peak position in the paragraph 4.3, it is clear that for AC, ACH and ACH400 hydrogen is oxidized within the operating potential range of the negative electrode, giving a pseudo-capacitive contribution. By contrast, in case of ACN, ACN400 and ACN500, the hydrogen desorption potential is too high (0.6 V vs NHE) and cannot contribute to the capacitance of the negative electrode.

In order to determine the maximum operating voltage when using the modified carbons as electrodes in a symmetric configuration, galvanostatic (1 A g^{-1}) charge-discharge cycling at different operating voltages has been performed (Figure 48). Previous studies performed in aqueous H_2SO_4 electrolytes have shown that the presence of numerous oxygenated groups on carbons generates capacitance loss, leakage current and self-discharge during the operation of a supercapacitor [157]. Those detrimental effects have been attributed to the gradual reduction of surface functionalities in an irreversible way during the charge/discharge of the supercapacitor [158]. Figure 48 shows that the systems using the nitric acid treated carbon (ACN and ACN500) are not able to operate at cell voltages higher than 1.6 V. At the maximum cell voltage of 1.8 V previously determined for the AC based system, the capacitance loss during cycling is considerably high. Therefore, the introduction of a

noticeable amount of surface oxides by oxidizing AC with nitric acid solutions has a deleterious effect on the operating voltage.

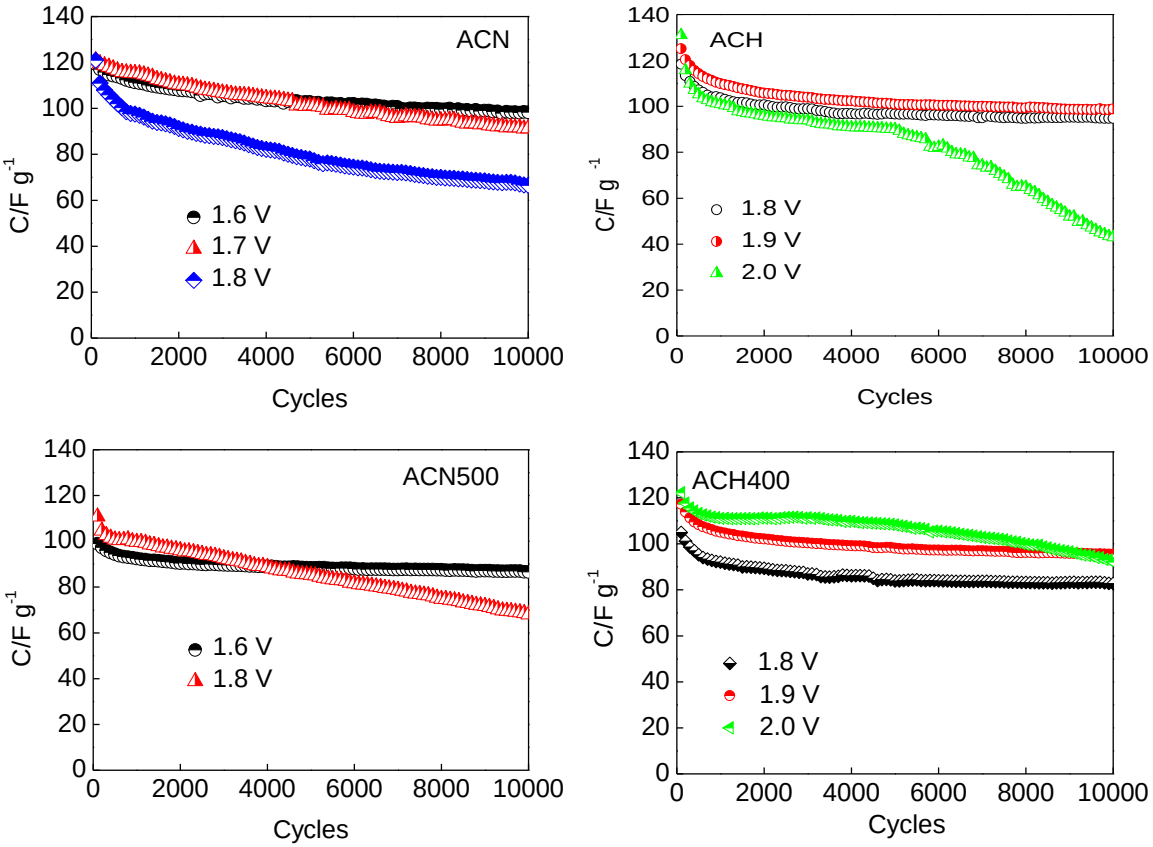

Figure 48 Evolution of discharge capacitance during galvanostatic (1 A g^{-1}) charge/discharge cycling of symmetric carbon/carbon capacitors in 2 mol L^{-1} Li_2SO_4.

The worst performance of the ACN based supercapacitors in comparison to the AC ones can be explained by recording the real working potential range of each electrode during the charge/discharge of the supercapacitor, introducing a reference electrode into the systems. By comparison with the pristine AC, figure 49a shows that the maximum potential of the positive electrode shifts to higher values for all the ACN based systems. Therefore, as it has been discussed previously, a serious electrochemical oxidation can be predicted on the positive ACN-type electrodes during a long-term cycling.

By contrast, in the previous section, it has been shown that a moderate chemical oxidation by hydrogen peroxide could sidestep the destructive oxidation of the carbon AC, leading to an enhanced voltage from 1.8 to 1.9 V with symmetric systems in 2 mol L^{-1} Li_2SO_4. For this reason, ACH has been subjected to thermal treatment at 400°C under nitrogen

(sample named ACH400), in order to evaluate the possibilities of further expanding the voltage range by decreasing the concentration of surface functional groups which can participate in irreversible redox reactions, e.g., the carboxylic ones. Figure 48 confirms that the cycling stability could be slightly improved by removing the CO_2-type groups (see the quantification in Table 11). However, the maximum cell voltage is still not higher than 1.9 V. The reasons why higher cell voltages cannot be reached with the ACH based systems can be extracted from Figure 49b, which shows the operational potential range of the electrodes during the charge/discharge of the supercapacitor at different cell voltages. Although being lower than for the ACN-type carbons, the maximum potential of the positive ACH-type electrodes is still too high for expanding the cell voltage up to the total stability potential window of the carbon material, i.e., 2.0 V. However, the negative electrode still operates at negative potentials higher than the H_2 evolution limit, i.e., -1.0 V vs. NHE (as extracted from the blue loop in Figure 46), even at cell voltage of 2.0 V. Therefore, further breakthrough on increasing the operating cell voltage can be expected by using asymmetric configurations allowing the negative electrode potential to be pushed towards smaller values.

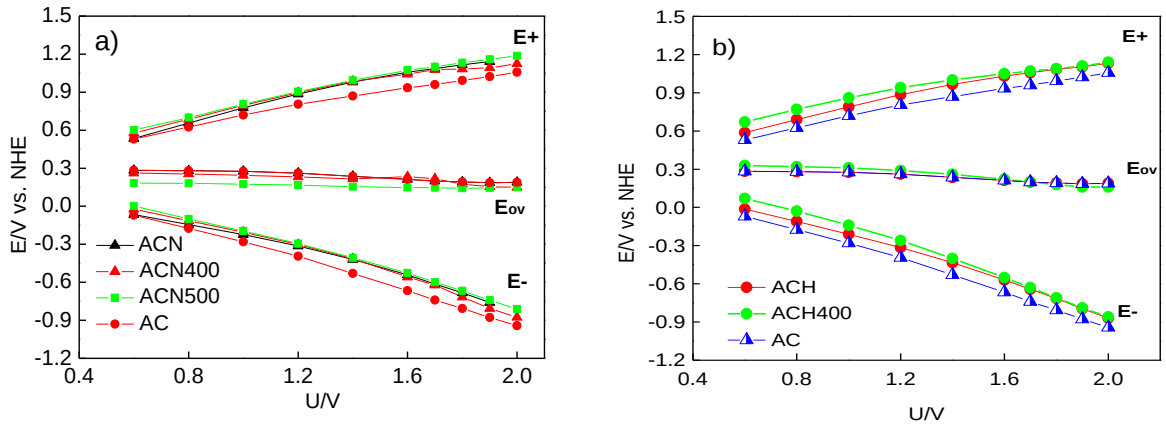

Figure 49 Potential limits of positive (E+) and negative (E-) electrodes during the galvanostatic (200 mA g^{-1}) cycling of symmetric carbon/carbon capacitors up to different values of maximum voltage. An Hg/Hg_2SO_4 reference electrode has been introduced to express the potential values. The E_{0V} values correspond to the electrodes potential when the working voltage is shifted to 0 V before each change of maximum voltage. Electrolyte: 2 mol L^{-1} Li_2SO_4.

4.5 Asymmetric carbon/carbon configurations in 2 mol L^{-1} Li_2SO_4

As mentioned above, in order to adjust the electrodes potential and to explore the possibility to expand the voltage range up to 2.0 V, an asymmetric configuration by balancing

the electrode mass ratio (positive/negative) could be an effective way. Actually, the charge stored (***Q***) at the positive and negative electrodes is equivalent (Equation 26):

$$Q+ = Q- \quad (26)$$

It depends on the specific capacitance (***C***), the potential range (***ΔE***) of the charge-discharge process and the mass (***m***) of electrode (Equation 27):

$$m+ * C+ * \Delta E+ = m- * C- * \Delta E- \quad (27)$$

where ***m+*** and ***m-*** are the mass, ***C+*** and ***C-*** the specific capacitance, and ***ΔE+*** and ***ΔE-*** the potential range for the positive and negative electrode, respectively.

Then, it becomes feasible to obtain the optimal voltage by adjusting the potential range of each electrode to its maximum value through balancing the mass ratio (***R***) between the positive and the negative electrodes according to formula (28) [133] [134].

$$R = \frac{m_+}{m_-} = \frac{C_- \times \Delta E_-}{C_+ \times \Delta E_+} \quad (28)$$

Figures 50 compares the extreme potentials vs voltage during charge-discharge cycling of symmetric and asymmetric (mass positive/mass negative = 1.2) ACH400/ACH400 cells, including a reference electrode. As expected, in the asymmetric cell, the potential range of the negative electrode is extended to lower values, while the maximum potential of the positive one does not increase in comparison with the symmetric cell.

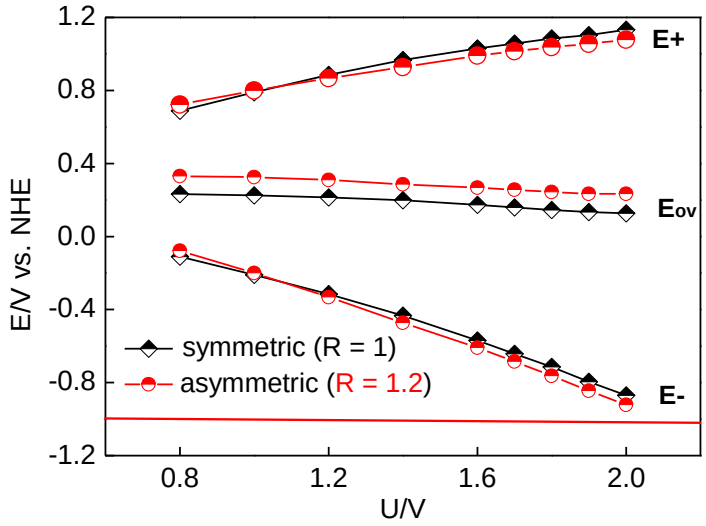

Figure 50 Potential limits of positive (E+) and negative (E-) electrodes during the galvanostatic (200 mA g^{-1}) cycling of symmetric and asymmetric ACH400/ACH400 capacitors up to different values of maximum voltage.

An Hg/Hg_2SO_4 reference electrode has been introduced to express the potential values. The E_{0V} values correspond to the electrodes potential when the working voltage is shifted to 0 V before each change of maximum voltage. Electrolyte: 2 mol L^{-1} Li_2SO_4.

In order to verify if such potential adjustment could have a positive effect, long-term galvanostatic charge/discharge cycling has been further performed at 2.0 V. After a slight decrease during the initial 1,000 cycles, Figure 51 shows that the capacitance keeps almost constant during 10,000 charge/discharge cycles. By comparison to figure 48 where a drop of capacitance was observed after 3,500 cycles with the same carbon, it is now clear that the slight asymmetry in mass allows to demonstrating that carbon based capacitors are able to operate up to 2 V in aqueous lithium sulfate electrolyte.

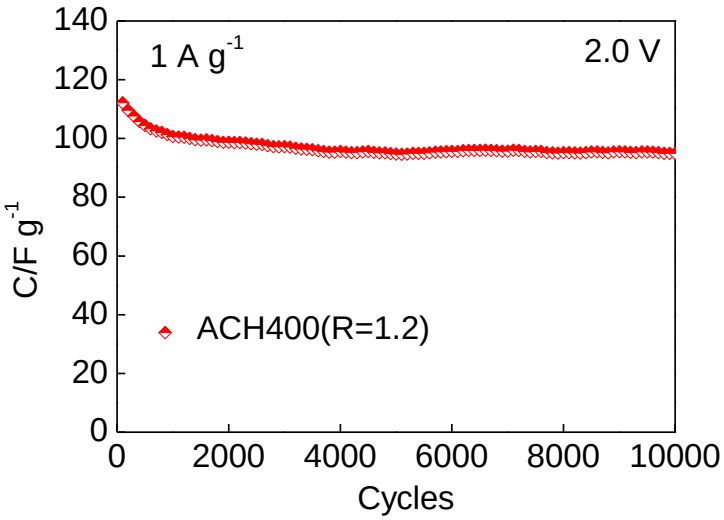

Figure 51 Evolution of discharge capacitance during galvanostatic (1 A g^{-1}) cycling of an asymmetric (Mass ratio ***R*** = positive/negative = 1.2) ACH400/ACH400 supercapacitor in 2 mol L^{-1} Li_2SO_4 electrolyte.

5 Symmetric carbon/carbon pouch cells in aqueous lithium sulfate electrolyte

Encouraged by the above result, the next step in our strategy was to demonstrate the feasibility of such system in conditions closer to industrial requirements. For that, we have first to remind that all the previously presented data were obtained in laboratory Swagelok® cells with electrodes of 0.8 cm^2 and gold current collectors. Considering the cost criterion, we want now to investigate a cost-competitive construction based on laboratory-type pouch cells made with carbon electrodes coated on stainless steel current collectors (20 cm^2). These

electrodes were kindly manufactured by Batscap, France, in the frame of the ABHYS project supported by the French Agency for Research (ANR). Carbons ACX and ACY optimized for organic electrolyte were used to manufacture the electrodes.

5.1 Textural characteristics of the ACX and ACY carbons

Table 12 summarizes the textural properties of the two carbons ACX and ACY used for preparing the coatings. Both of them are highly micro-porous carbons with a relatively high specific surface area above 1500 $m^2\ g^{-1}$ and a reasonable amount of mesopores. For ACY the ultramicropore volume is higher than the micropore one; it indicates that most of the microporosity for this carbon is in the range below 0.7-0.8 nm.

Table 12 Porosity parameters of the ACX and ACY carbons

Carbon	$S_{BET}(N_2)$ $m^2\ g^{-1}$	$V_{ultramicro}$ [a] $cm^3\ g^{-1}$	V_{micro} [b] $cm^3\ g^{-1}$	V_{meso} [c] $cm^3\ g^{-1}$
ACX	1560	0.58	0.62	0.21
ACY	1770	0.67	0.58	0.41

(a) DR equation applied to the CO_2 adsorption data; (b) DR equation applied to the N_2 adsorption data; (c) NLDFT method applied to the N_2 adsorption data

5.2 Electrochemical characterizations of ACX and ACY-based symmetric capacitor

The first electrochemical tests were performed in laboratory Swagelok® cells, using the coated electrodes cut into 0.8 cm^2 disks. Figure 52 presents the discharge capacitance evolution of the two carbons determined by galvanostatic (1 A g^{-1}) charge-discharge cycling at different cell voltages. For comparison purpose, pressed electrodes (pellets) of 0.8 cm^2 have been prepared from the ACX carbon.

Firstly, Figure 52 shows higher capacitance values for the ACY carbon than the ACX one. Therefore, we have tried to explain the different capacitance values of the two carbons by determining their accessible surface area for electrolyte ions. For this purpose, we must remind that, due to the larger diameter of the hydrated lithium ion (0.76 nm) [159] in comparison to the hydrated sulfate one (0.533 nm) [160][161], and according to equation (3), the capacitance of the symmetric system is only controlled by the negative electrode. Hence,

the cumulated specific surface area (calculated by applying the QSDFT method to the N_2 adsorption data) has been plotted vs average pore width (Figure 53), and the accessible surface area for the electrolyte ions could be obtained by taking the cumulated value corresponding to an average pore size higher than the diameter of hydrated lithium. The values of accessible surface area were found to be 708 and 870 m^2/g for ACX and ACY, respectively, explaining clearly that the larger specific capacitance obtained for ACY is due to a higher accessible specific surface area.

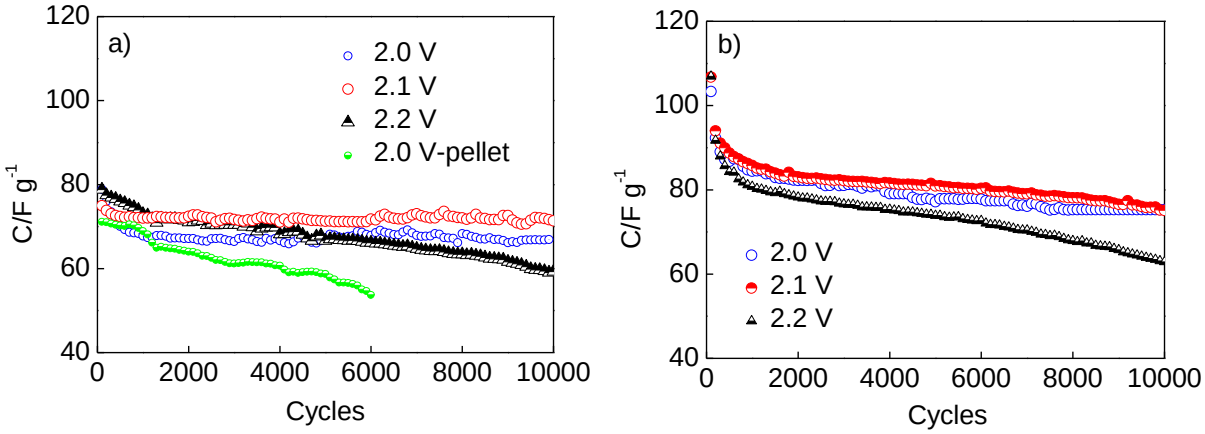

Figure 52 Evolution of discharge capacitance during galvanostatic (1 A g^{-1}) cycling of symmetric carbon/carbon capacitors in 2 mol L^{-1} Li_2SO_4 electrolyte based on: a) ACX electrodes, b) ACY electrodes.

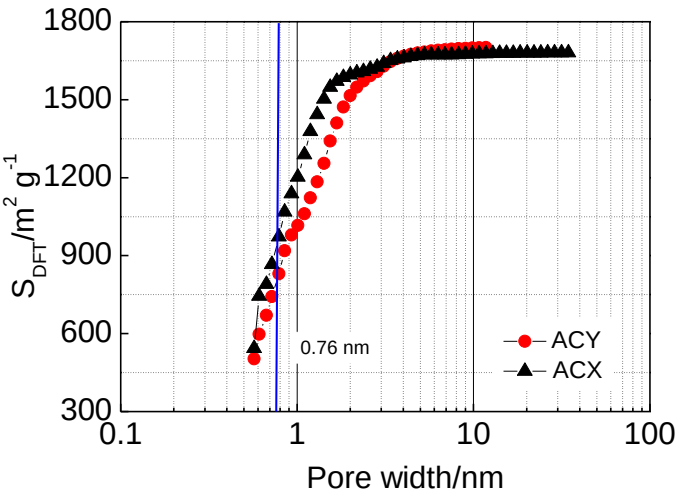

Figure 53 Cumulated QSDFT specific surface area of the carbons ACX and ACY vs their pore width. The vertical line at 0.76 nm represents the diameter of hydrated lithium.

As far as the cycle life is concerned, figure 52 shows that the systems using coated electrodes operate satisfactorily up to 2.1 V. After an initial loss of capacitance during the first 2,000 cycles, which is probably related to the potential evolution of the electrodes as demonstrated previously, the system does not show remarkable loss after 10,000 charge-discharge cycles. By contrast, with pellet type electrodes the capacitance loss already reaches 25 % after only 6,000 cycles at a lower voltage of 2.0 V (Figure 52a). In section 3, it has been shown that symmetric cells using pellets electrodes in Li_2SO_4 electrolyte are limited to a voltage of 1.8 V. Hence, one key parameter for the performance of supercapacitors is the contact between the active electrode mass and the current collector, which is obviously optimal in the case of coated electrodes and not for pellet ones.

The differences in capacitance between the ACX and the ACY systems with coated electrodes were further evaluated by electrochemical impedance spectroscopy, which allows a simultaneous determination of capacitance and resistance [162]. Nyquist plots of the ACX and ACY-based symmetric capacitors are shown in Figure 54. Since the only difference between the two systems is the nature of the carbon electrodes, it is likely to attribute the different signature of the Nyquist plots to the differences in porous texture, although some other parameters as surface functionality may influence the adhesion on the current collector. From the point of view of equivalent series resistance (ESR) values at 10 kHz, 1.83 and 1.55 Ω for ACX and ACY system, respectively, the two systems are comparable. By contrast, the ion diffusion resistance (EDR), which reflects the ion transportation into the pores of carbons, is 25 and 8.9 Ω for the ACX and ACY-based system, respectively, meaning that the diffusion of ions is more difficult in ACX than in the ACY, being another reason for the lower capacitance of ACX. The better diffusion in the case of ACY might be attributed to its larger mesoporous character, with twice more mesopore volume than for ACX, and possibly also to a better interconnection of micropores with the mesoporous network. The larger ultramicropore volume of ACY compared to ACX is the main explanation for the largest capacitance of the former, confirming the statement that pores in the range of 0.7-0.8 nm are optimal and that ions penetrates at least partially desolvated in these pores [52][55].

Figure 55 presents the cyclic voltammograms of symmetric ACX/ACX and ACY/ACY pouch cells in 2 mol L^{-1} Li_2SO_4. The supercapacitors show a typical capacitive behavior with rectangular shaped curves at voltage ranges up to 1.6 V; afterwards redox contributions appear at higher cell voltages. The capacitance obtained for the pouch cells using ACX and

ACY electrodes are in the same range than those obtained for the small laboratory cells. Thus, higher values of specific capacitance are obtained when using ACY based electrodes. The less resistive character of ACY is also confirmed.

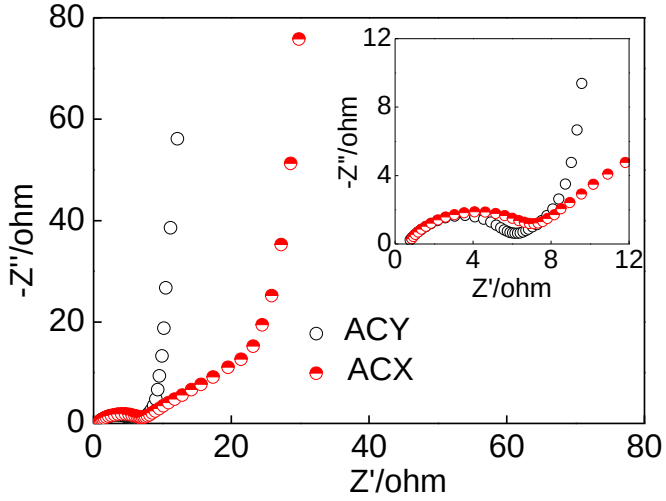

Figure 54 Nyquist plots of the symmetric ACX/ACX and ACY/ACY Swagelok capacitors in 2 mol L^{-1} Li_2SO_4.

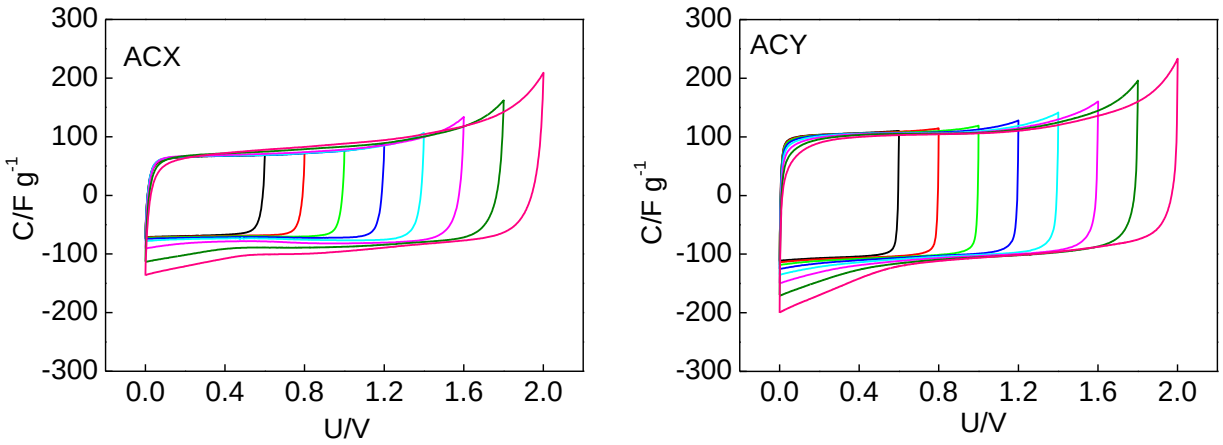

Figure 55 Cyclic voltammograms (CVs, 2 mV s^{-1}) of symmetric two-electrode pouch cells assembled with ACX and ACY coated electrodes in 2 mol L^{-1} Li_2SO_4 as electrolyte.

Long term galvanostatic (1 A g^{-1}) cycling stability has been further investigated for assessing the reliability of a system to be further implemented in a prototype device. In this sense, Figure 56 shows that a symmetric pouch cell using ACX as electrode active material presents an excellent cycling stability at 2.1 V in aqueous Li_2SO_4. The capacitance retention

ratio is as high as 92 % after 10,000 cycles, while 88 % was obtained in the small laboratory Swagelok cells (included in Figure 56 for comparison purpose).

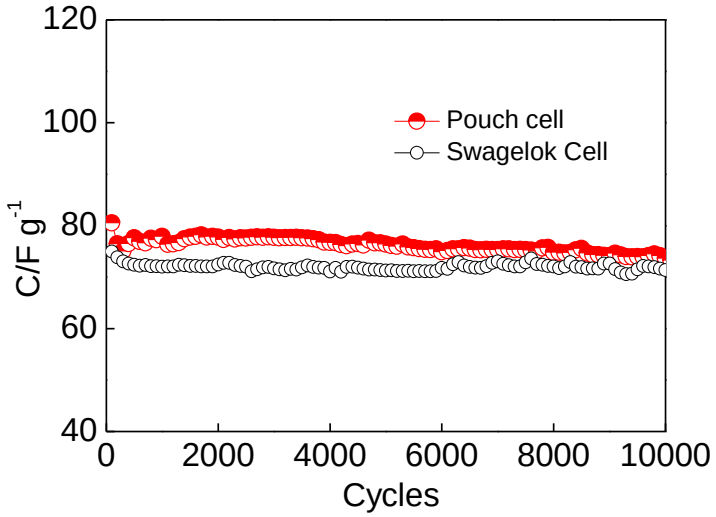

Figure 56 Evolution of discharge capacitance during galvanostatic (1 A g^{-1}) cycling of symmetric ACX/ACX Swagelok and pouch cells operating at 2.1 V in 2 mol L^{-1} Li_2SO_4 electrolyte.

Another important parameter to take into account for evaluating the reliability of a system is the self-discharge. In stand-alone or standby applications, supercapacitors are not connected to an electrical network, and actually the self-discharge corresponds to the natural decay of the supercapacitor voltage over time, i.e., the decay in available energy, after it is fully charged to a given voltage [164]. For carbon based supercapacitors, the self-discharge is related to the charge redistribution in the carbon pores and to the kinetics of the Faradaic self-discharge [164][165].

Figure 57 presents self-discharge measurements on symmetric ACX pouch cell in 2 mol L^{-1} Li_2SO_4 electrolyte after charging up to different cell voltages at 20°C and -10°C. As expected, the higher the charging voltage, the faster the self-discharge after 24 hours at open circuit, independently of temperature [166][167]. The voltage retention ratio after 24 hours is 74 % and 66 % for 1.0 and 1.8 V at 20°C, respectively, and 75 % and 72.5 % for 1.8 V and 2.0 V at -10°C, indicating that self-discharge is faster at higher temperatures. Considering that pseudo-capacitance related with hydrogen contributes to the large voltage of these systems, the values found for the self-discharge are relatively reasonable. Moreover, for some specific applications as start-stop systems, which automatically shut down and restart the internal

combustion engine to minimize the amount of time idling, such long times as 24 hours are not elapsed between the charge and the discharge. Therefore, the inset of Figure 57 represents the self-discharge during the first 12 minutes, showing a voltage retention ratio as high as 94 % and 91% for 1.0 V and 1.8 V, respectively; at -10°C, it even reaches 95 % and 94.5 %, respectively. Hence, it is clearly demonstrated that the AC/AC system is highly promising for applications which do not require recovering the charged energy after a long period.

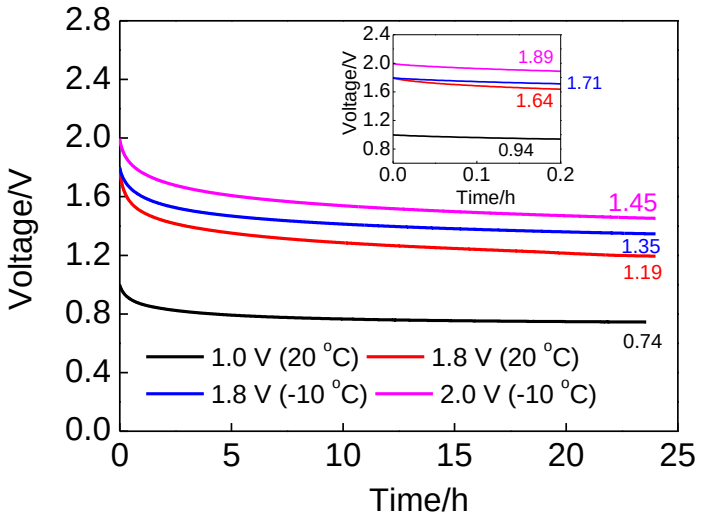

Figure 57 Self-discharge (open-circuit) profiles of symmetric ACX/ACX pouch cells in 2 mol L^{-1} Li_2SO_4 after charging at a current density of 0.2 A g^{-1} up to 0.0 to 1.0, 1.8, and 2.0 V and held at the given voltage for 0.5 h. The values on the right of the curves indicate the voltage reached after the considered period of time.

6 Conclusions

Promising voltage values up to ca. 2 V have been obtained with AC/AC supercapacitors using aqueous alkali sulfate solutions, in particular lithium sulfate, allowing forecasting the production of low cost and environmentally friendly systems based on this concept.

After comparing different alkali sulfates at room temperature, the largest power and energy density was obtained for symmetric AC/AC capacitors operating in aqueous K_2SO_4 electrolyte. The reasons of such results are the smallest cation size and highest electrical conductivity among the alkali sulfates tested. However, when taking into account the low temperature requirements, Li_2SO_4 is a better option, because of its higher solubility, allowing the AC/AC supercapacitors to operate down to -10°C at a concentration of 2 mol L^{-1}.

We have found that the operating voltage is limited by the destructive oxidation of the positive carbon electrode when its potential becomes too high. Due to this carbon degradation, the system exhibits continuous capacitance decay during cycling. By controlled chemical oxidation of carbon before its implementation in the positive electrode, we could successfully reduce its maximum operation potential to relatively lower values and consequently sidestep its irreversible electro-oxidation during long term cycling. Using such modified electrodes in a symmetric cell, an operating voltage of 1.9 V has been reached; by a small mass asymmetry of 1.2 between the positive and negative electrodes, the voltage could be even extended up to 2.0 V.

Prototype pouch cells realized with coated electrodes presented an exceptional stability at 2.1 V during 10,000 charge/discharge cycles. This better performance compared to Swagelok cells with pellet electrodes is attributed to a better contact between the active mass and the current collectors. Therefore, it is extremely important to mention that an excellent engineering of electrodes is more important than the development of complicated and expensive nanostructured carbon materials.

In summary, the results presented in this chapter confirm that the usage of alkali sulfate solutions is a very promising strategy to produce environment friendly carbon/carbon supercapacitors, able to reach in the future the target energy and power density of organic electrolyte based commercial systems with acceptable temperature performance.

Chapter III

Optimizing carbons for supercapacitors in organic medium by a novel high pressure/low temperature activation protocole

Résumé

La densité d'énergie des condensateurs à double couche (EDLC) peut en particulier être renforcée en améliorant la capacité spécifique des électrodes à base de carbone.

Durant cette étude, nous avons développé une méthode d'activation efficace pour ajuster la taille moyenne des pores à celle des ions de l'électrolyte 1 mol L^{-1} $TEABF_4$ dans l'acetonitrile. Cette méthode consiste à oxyder à basse température (200-250 °C) un carbone non poreux par le peroxyde d'hydrogène comme source de dioxygène actif dans la plage de pression 89-135 bars, suivie de la désorption des groupes fonctionnels de surface à 900 °C sous flux de N_2. Il a été constaté que le développement de la porosité est essentiellement contrôlé par l'étape d'oxydation. Dans des conditions d'oxydation douces (PO_2 = 89 bar, 200 °C pendant 4 heures), la porosité est développée en exécutant quelques cycles d'oxydation/désorption thermique. Ainsi, cette méthode permet de finement ajuster la taille des pores à celle des ions TEA^+, ce qui entraine l'optimisation de la capacité spécifique. Par ailleurs, si la procédure d'oxydation est conduite dans des conditions un plus agressives (PO_2 = 135 bars, 200 ° C pendant 12 heures), des pores de taille requise pour l'ion TEA^+ peuvent être obtenus en un seul cycle d'oxydation/désorption thermique, tel que confirmé par les voltammogrammes cycliques obtenus pour les 2 carbones.

1 Introduction

Energy density of electrical double-layer capacitors (EDLCs) operating in organic electrolytes can in particular be enhanced by improving the capacitance of carbon based electrodes. It has been extensively reported that such objective can be reached when the carbon nanopore size fits the dimensions of desolvated ions [58][53][168]. The most common view supported by several relevant studies (e.g., [53][58]) is that the optimum capacitance can be expected from highly micro-porous carbons with essentially sub-nanometric pores. However, even if pores are exclusively in the sub-nanometric range and porosity is insufficiently developed, saturation of porosity may occur during charging, leading to a decrease of the capacitive current for the highest voltage values [63]. Therefore, it is necessary to produce carbons with well-developed porosity while maintaining a narrow pore size distribution.

Most of the conventional production methods of nano-porous carbons are based on the partial gasification of a precursor (carbon or carbide) in oxidative conditions at 800-900°C. The most common oxidizing agents are CO_2, steam, chlorine, KOH and NaOH [1][43][169][170][171] and, in all cases, the development of porosity leads to an uncontrolled pore widening, lowering the capacitance and density of the materials. As a consequence the volumetric capacitance and the volumetric energy density generally do not reach the expectations of industry. Therefore, to eliminate the negative influence from the wide pores in traditionally-made activated carbons and provide the required ion/pore size compatibility, novel activation methods for developing micropores can be of great interest.

Di-oxygen has been suggested as activating agent for decreasing the reaction temperature [172]. However, as it is a very fast and exothermic process, the carbon-oxygen reaction is very difficult to control. Other activation strategies based on a milder use of di-oxygen are also described in the literature. Highly micro-porous carbons can be prepared by the repeated low-temperature oxidation of carbonaceous materials. Thus, Quinn *et al.* [173] patented an activation method that minimizes the formation of macropores by heating a carbon sample between 150 and 250^{o}C for 45 to 75 minutes in the presence of di-oxygen (carbon oxidation) with subsequent thermal treatment (between 750 and 950^{o}C) under nitrogen for 15 to 45 minutes (pore formation by decomposition of oxygenated functionalities). However, the weight loss is about 1 % in each cycle, and many oxidation/desorption cycles are required for developing the porosity. This feature presents a

serious obstacle to large-scale manufacturing, although the above two-step process is highly controllable. In another related work, Py *et al.* [174] used KOH-activated molecular-sieve carbon and steam-activated coconut carbon as precursor materials subjected to air oxidation at 200^{o}C followed by pyrolysis (900 ^{o}C under nitrogen flow). The procedure allows a substantial decrease in the number of oxidation/desorption cycles in comparison to Ref. [173], but the need for pre-activated material presents the inconvenience of the method.

By contrast, Conesa *et al.* [175] worked out a procedure, in which one single step is necessary for activating carbonized macadamia nut shell charcoal by using di-oxygen derived from the decomposition of hydrogen peroxide dissolved in flowing hot liquid water at high pressure. The idea was to better manage the carbon-O_2 reaction by controlling its exothermicity in the presence of water. Following a single-step treatment, an activated carbon with a relatively small BET surface area of 620 m^2 g^{-1} was produced, consisting essentially of micropores with a narrow pore size distribution centered at 1 nm. The same group tried to improve the experimental method by increasing the di-oxygen pressure, but several cycles were needed to achieve a BET specific surface area of about 1000 m^2 g^{-1} with a low carbon yield [176].

Taking into account the literature cited above, in the present chapter, we describe effective routes for obtaining high density microporous carbons with a pore size perfectly fitting the diameter of the electrolyte ions. The chapter is divided into two sections:

- In the first section, we show that it is possible to obtain dense microporous carbons with a finely tuned porosity by cyclic oxidation/thermal desorption without any additional pre-activation. The porosity-forming procedure involves 3-4 cycles to perfectly adapt the pore entrances to the electrolyte ions.
- In the second section, a more detailed study on the reaction mechanisms during the oxidation/thermal desorption, will allow to adjust the reaction parameters to obtain the targeted porosity in only one cycle.

2 Cyclic oxidation/thermal desorption as an effective process to tailor the pore size of EDLC carbons

2.1 Starting materials

Sucrose or microcrystalline cellulose was used as raw materials. Before carbonization, sucrose was dehydrated using concentrated sulfuric acid. The dehydrated sucrose-derived

material or microcrystalline cellulose were carbonized by heating up to 1050°C under nitrogen flow to get the carbons further used in this study for the high pressure activation.

2.2 Effect of the activation parameters on the physicochemical characteristics of carbons

For the optimization of the activation parameters, the carbon:H_2O_2 ratio has been fixed to be 3:5 to provide a di-oxygen (P[O_2]) pressure lower than 100 bar inside the autoclave at 200°C. In the different trials, parameters were varied such as the oxidation temperature, the number of oxidation/thermal desorption cycles or the carbon precursor.

Table 13 presents the results of the TPD analysis for the sucrose char after oxidation at 20°C, 100°C and 200°C. The amount of oxygen fixed to the carbon surface and evolving as CO_2 or CO in the thermal treatment is identical for the products oxidized at 20 and 100°C, but it increases if the oxidation temperature is further shifted up to 200 °C. These results indicate that the carbon is poorly oxidized under P[O_2] = 70 bar at 100°C, whereas the P[O_2] pressure of 89 bar at 200°C seems to be sufficiently high to enhance the amount of dissolved O_2 [177], which is brought in contact with the carbon, favoring the carbon-O_2 reaction.

Table 13 TPD analysis of sucrose-based carbons after H_2O_2 oxidation at different temperatures and after the 1st and 4th oxidation at 200°C.

T/°C – nth oxidation	**CO_2** **µmol g^{-1}**	**CO** **µmol g^{-1}**	**O** **wt.%**
20 °C – 1st oxidation	348	634	2.9
100 °C - 1st oxidation	342	724	2.7
200 °C - 1st oxidation	711	1716	5.9
200 °C – 4th oxidation	1435	3351	10.7

Table 13 also shows that the extent of carbon oxidation depends on the number of oxidation/thermal desorption cycles realized prior to oxidation. For example, if the carbon material is further oxidized beyond 3 activation cycles, the amount of oxygen fixed on the surface nearly doubles compared to the first oxidation. Actually, the N_2 adsorption/desorption isotherms (Figure 58a) demonstrate an important porosity development during the consecutive oxidation/thermal treatment cycles. Hence, the growth of specific surface area

connected with the number of activation cycles causes higher carbon reactivity towards di-oxygen, subsequently enriching the material in surface oxygen.

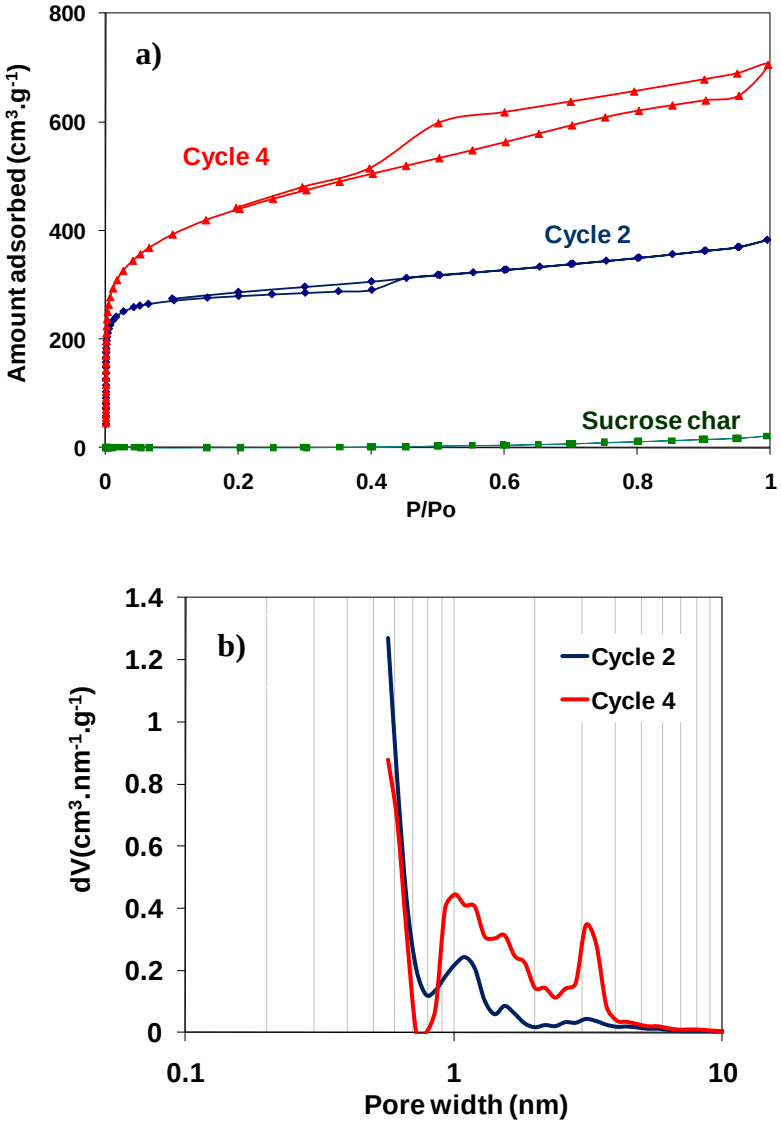

Figure 58 Nanoporous texture of sucrose-based carbons after 2 and 4 oxidation/thermal treatment cycles; a) N_2 adsorption/desorption isotherm at 77 K; b) QSDFT pore size distribution.

Following two activation cycles only, the sucrose-based carbon already exhibits a specific surface area of 1176 m^2 g^{-1}, whereas the later reaches 1592 m^2 g^{-1} after 4 cycles (Table 14). However, Figure 58b shows that the pore size distribution was considerably widened following 4 activation cycles, leading to a three-time increase in the mesopore

volume in addition to the development of micropores. As a consequence, the average pore size increases from 0.86 nm to 1.34 nm in only two additional activation cycles.

Table 14 Porous texture of sucrose-based carbons after various numbers of oxidation/thermal treatment cycles

	$S_{DR}(N_2)$ $m^2\ g^{-1}$	$V_{DR\ ultramicro}$ $cm^3\ g^{-1}$	$V_{DFT\ micro}$ $cm^3\ g^{-1}$	$V_{DFT\ meso}$ $cm^3\ g^{-1}$	L_0 nm
Cycle 2	1176	0.51	0.39	0.15	0.86
Cycle 4	1592	0.57	0.56	0.45	1.34

Since four oxidation/thermal treatment cycles give rise to an important pore widening on the sucrose-based carbon, we decided to investigate in detail the intermediate materials applying the pre-selected oxidation conditions, e.g., 200 °C during 4 hours, but this time using the cellulose-based carbon as precursor. Additionally, the experimental work is simplified as the cellulose carbon is directly obtained by carbonization at 1050°C, while a de-hydration step is required before pyrolysis for the sucrose one.

The TPD results on the cellulose-derived materials prepared by oxidation after consecutive oxidation/thermal desorption cycles are presented in Figure 59 and Table 15. From the 1st to the 5th oxidation treatment, there is an increase of the amount of gases evolved as CO_2 (Figure 59a) or CO (Figure 59b), confirming that the extent of the oxidation reaction in each cycle exceeds that of the preceding one. The comparison of tables 13 and 15 also shows that the oxygen wt. % fixed on the surface is lower for the cellulose-based carbon than for the sucrose-based one oxidized in the same conditions (compare the 3rd line in Table 13 and the 1st line in Table 15 or the 4th line in Table 13 and the 4th line in Table 15), which indicates a better controllability of the carbon-O_2 reaction arising because of the lower reactivity of the cellulose-based carbon precursor. However, the reactivity of the carbon material is greatly enhanced between the 4th and the 5th oxidation treatment, as evidenced by an abrupt increase in the amount of evolved gases (Table 15) and by a considerably higher amount of oxygen chemisorbed on the surface. The carbon yields obtained after each oxidation/thermal treatment cycle are in good agreement with these results, being 82 wt. %, 80 wt. %, 75 wt. %, 73 wt. % and 61 wt. % for the 1st to the 5th cycle materials, correspondingly.

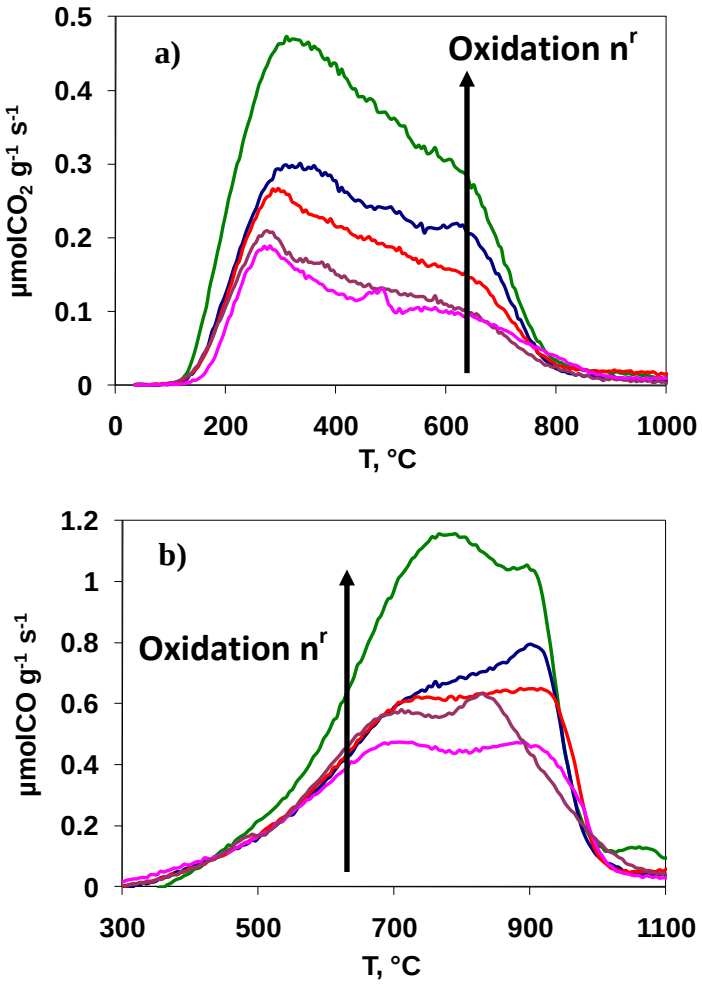

Figure 59 Gases evolved during the TPD analysis of cellulose-based carbons oxidized by H_2O_2 after different numbers of oxidation/thermal treatment cycles a) CO_2; b) CO.

Table 15 TPD analysis of cellulose-based carbons obtained after various numbers of H_2O_2 oxidation treatments at 200°C. n^{th} oxidation means that the sample has been subjected to n-1 cycles and finally to a n^{th} oxidation at 200°C.

n^{th} oxidation	CO_2 µmol g^{-1}	CO µmol g^{-1}	O wt.%
1^{st}	444	1444	4.0
2^{nd}	483	1289	4.0
3^{rd}	669	1594	5.0
4^{th}	792	1645	5.7
5^{th}	1218	2402	8.4

The data on the porous texture of the materials produced after the consecutive oxidation/decomposition cycles are given in Table 16. They particularly show a strong increase in S_{DR} (N_2) after the first cycle, taking into account that the carbonized cellulose has a specific surface area (S_{DR} (N_2)) of only $5 m^2 g^{-1}$. This fact together with the high carbon yield of the first cycle could indicate that existing closed porosity is opened in the first oxidation/thermal treatment cycle. The S_{DR} (N_2) increase during the subsequent cycles is much weaker, although it is strengthened as the cycle number becomes higher. The mesopore volume does not change from the starting material up to the 3rd oxidation cycle, meaning that only micropores are opened/formed in cycles 1 to 3. On the other hand, the ultramicropore surface, $S_{DR}(CO_2)$, and volume, $V_{ultramicro}$, both increase sharply in the first cycle and then experience slower growth up to the 3rd cycle (Table 16 and Figure 60), pointing out a preferential opening/development of small micropores in the initial cycles. Further oxidation (cycles 3 to 5) is associated with a decrease in the amount of ultramicropores (smaller values of $S_{DR}(CO_2)$ and $V_{ultramicro}$) as well as the formation of larger micropores and mesopores (larger values of V_{micro}, V_{meso} and $S_{DR}(N_2)$), indicating a widening of porosity. In this sense, Table 16 and Figure 60 demonstrate a stepwise increase in average pore size L_0, underlying the controllability of the pore enlargement procedure. This conclusion is supported by the DFT analysis (Figure 61), demonstrating narrow pore size dispersion for cycles 1 to 3 and a slight broadening for cycles 4 and 5. Using all the porosity data collectively, we can therefore conclude that the build-up of pore volume in cycles 1 to 3 proceeds essentially through the opening/formation and deepening of narrow micropores, whereas pore widening appears to be the main outcome of cycles 4 and 5.

Table 16 Porous texture of cellulose-based carbons after different numbers of oxidation/thermal treatment cycles

Cycle	$S_{DR}(N_2)$ $m^2 g^{-1}$	$V_{DR\ ultramicro}$ $cm^3 g^{-1}$	$V_{DFT\ micro}$ $cm^3 g^{-1}$	$V_{DFT\ meso}$ $cm^3 g^{-1}$	L_0 nm
Cycle 1	955	0.41	0.31	0.09	0.72
Cycle 2	1042	0.46	0.34	0.08	0.80
Cycle 3	1089	0.60	0.34	0.10	0.86
Cycle 4	1221	0.57	0.40	0.23	1.02
Cycle 5	1493	0.54	0.48	0.33	1.39

To summarize, porosity analysis demonstrates clearly that the presented activation method is well suited for tailoring carbon pore size - in particular when using cellulose as carbon precursor - and can supposedly be employed for producing carbon electrode materials perfectly adapted to ion size of the supercapacitor electrolyte.

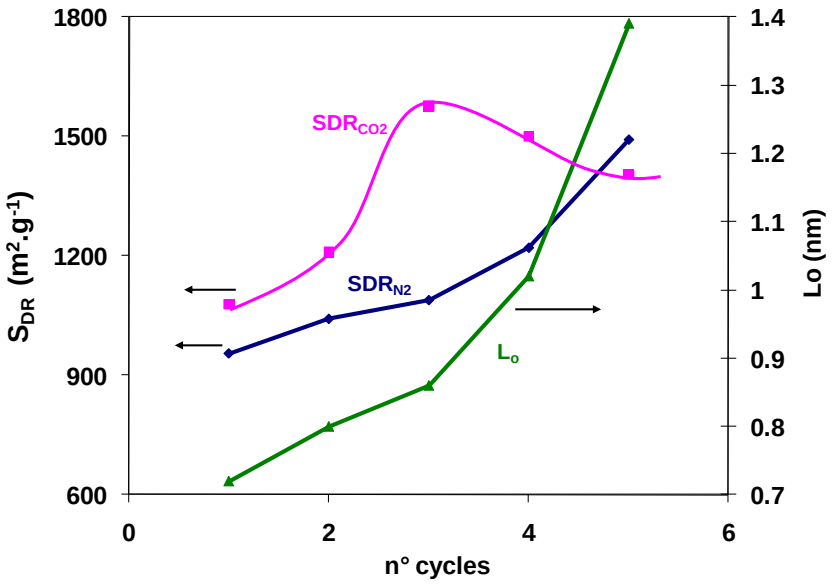

Figure 60 Evolution of the porous texture parameters ($S_{DR}(N_2)$, $S_{DR}(CO_2)$ and L_0) of cellulose-based carbons after different numbers of oxidation/thermal treatment cycles.

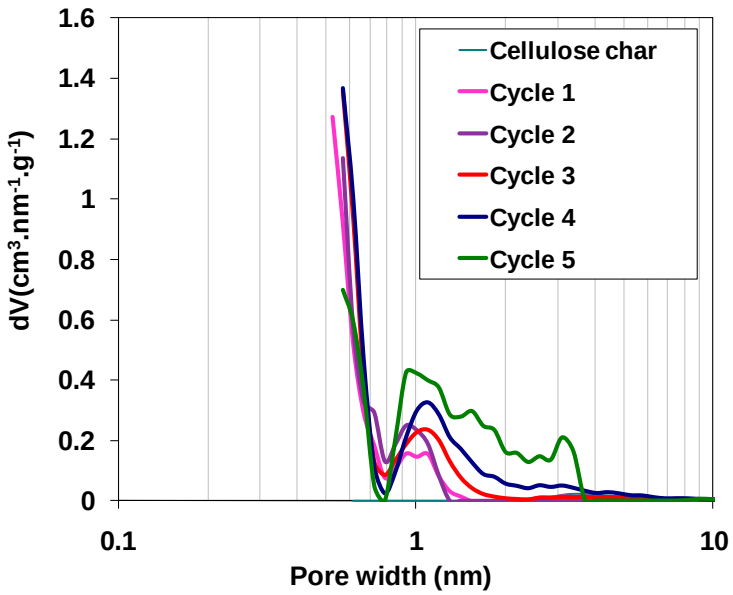

Figure 61 QSDFT pore size distribution of cellulose-based carbons after different numbers of oxidation/thermal treatment cycles.

2.3 Electrochemical characterization of the porous carbons in 1 mol L^{-1} $TEABF_4$/Acetonitrile electrolyte

Figure 62 shows the cyclic voltammograms (CVs, 5 mV s^{-1}) of two-electrode cells built with the series of cellulose-based carbons prepared after 1 to 5 activation cycles. The CVs of consecutive cycles are apparently different, revealing a cycle-by-cycle increase in the ion storage capacity of the materials (see the capacitance values in Table 17). Moreover, one can note that the capacitive current at higher voltage for the materials prepared in 1 to 3 activation cycles (especially for the 1st-cycle material). To explain the lower current at higher voltage, the concept of accessible specific surface area (S_{DFT}>0.68 nm in Table 17), described in references [63][65], is of a great help. To a reasonable approximation, the surface area accessible to both ions, TEA^+ and BF_4^-, can be evaluated from a cumulative DFT curve as the DFT surface area of the pores whose entrances are wider than the size of the largest ion (0.68 nm for desolvated TEA^+ vs. 0.44 nm for desolvated BF_4^- [53][178]). Table 17 shows that the gradual increase in specific surface area and average pore size in consecutive cycles goes together with the growth of accessible surface area (see Table 16). By using these values, the charge accumulated on the basis of the full occupancy of cation-accessible pore surface (Q_{max}) can be calculated from the number of ions filling the accessible surface area (see [63][65] for details), and be compared to the experimental charge (Q_{exp}) measured from the CVs presented in Figure 62. The estimated values of Q_{max} and Q_{exp} for the materials of cycles 1 to 5 are presented in Table 17. We note quite a close match between the values of Q_{max} and Q_{exp} for the materials of cycles 2 and 3, which may in fact indicate that the porosity of those carbons is almost saturated. The slightly higher Q_{exp} than Q_{max} for these materials may be caused by some Faradic contribution to the current and errors involved in geometry-based estimations. On the other hand, the fact that the material of cycle 1 displays $Q_{exp} < Q_{max}$, though showing a decreasing current, may point to cation accessibility issues due to the very narrow pores (L_0 = 0.72 nm), which slow down the diffusion of the TEA^+ cation. Additionally, the accessible surface area was calculated to be 187 m^2 g^{-1} only, being close to the error of surface area determination (usually about 100 m^2 g^{-1}). Thus, it appears difficult at this stage to distinguish between porosity saturation and ion sieving for the material of cycle 1, whereas there are strong reasons for considering the behaviour of materials 2 and 3 as porosity saturation.

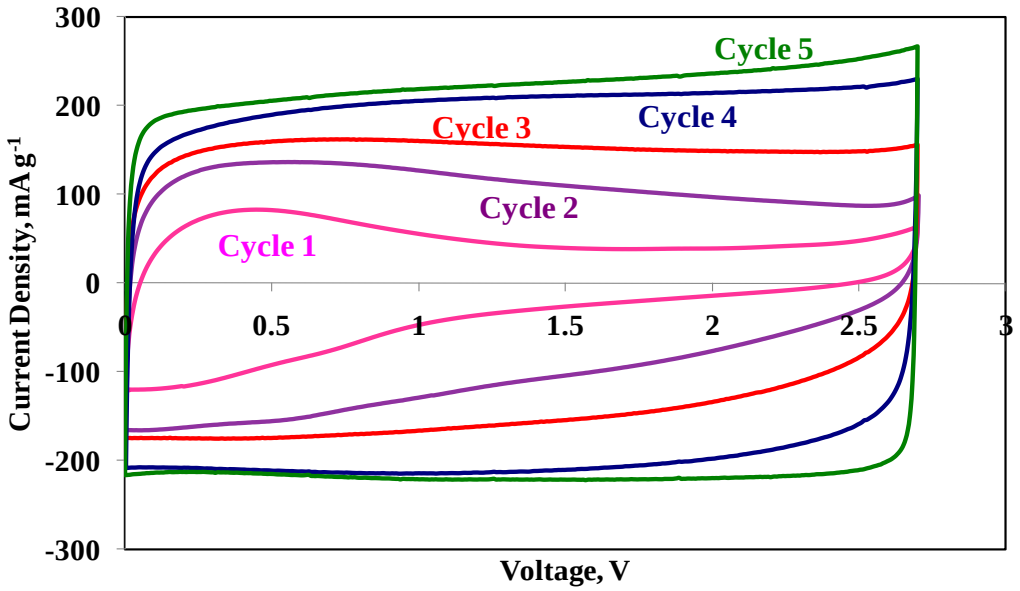

Figure 62 Cyclic voltammograms (5 mV s^{-1}) of supercapacitors in 1 mol L^{-1} $TEABF_4$ using the cellulose based carbons obtained after 1 to 5 activation cycles.

Finally, the CVs for the materials of cycles 4 and 5 do not show any current decay, in concordance with the fact that $Q_{max} > Q_{exp}$, indicating that the surface of those carbons can perfectly accommodate the ions on charging, even at a cell voltage of 2.7 V.

Table 17 Electrochemical characteristics of the supercapacitors built with the cellulose-based carbons obtained after different numbers of oxidation/thermal treatment cycles. The capacitance at 2.7 V was determined from galvanostatic charge/discharge cycling at a current density of 0.2 A g^{-1}.

Cycle	C F g^{-1}	$S_{DFT>0.68}$ m^2 g^{-1}	Q_{max} C g^{-1}	Q_{exp} C g^{-1}	C_s µF cm^{-2}
Cycle 1	17	191	50	28	8.9
Cycle 2	44	217	58	59	20.3
Cycle 3	60	275	74	81	21.8
Cycle 4	77	429	137	93	17.9
Cycle 5	80	712	244	120	11.2

Cyclic voltammetry on three-electrode cells was used to characterize the materials of cycles 1, 2 and 4 separately under negative and positive polarization (Figure 63). Comparing the negative and positive portions of the CV, one can note a much lower current for negative potentials for the 1st and 2nd materials, confirming that the porosity saturation occurs for the

TEA^+ ion. This effect is much stronger for the material of cycle 1 because of its lower accessible specific surface area, and it is not visible for the material of cycle 4, presenting a typical capacitive CV for a porous carbon [47]. In summary, since the capacitance of a supercapacitor is controlled by the electrode with the smallest capacitance, according to the relationship (29):

$$1/C = 1/C_{positive} + 1/C_{negative} \quad (29)$$

the data obtained with the two-electrode cells mainly reflect the behaviour of the negative electrode, i.e., the one where the largest ions are electrosorbed.

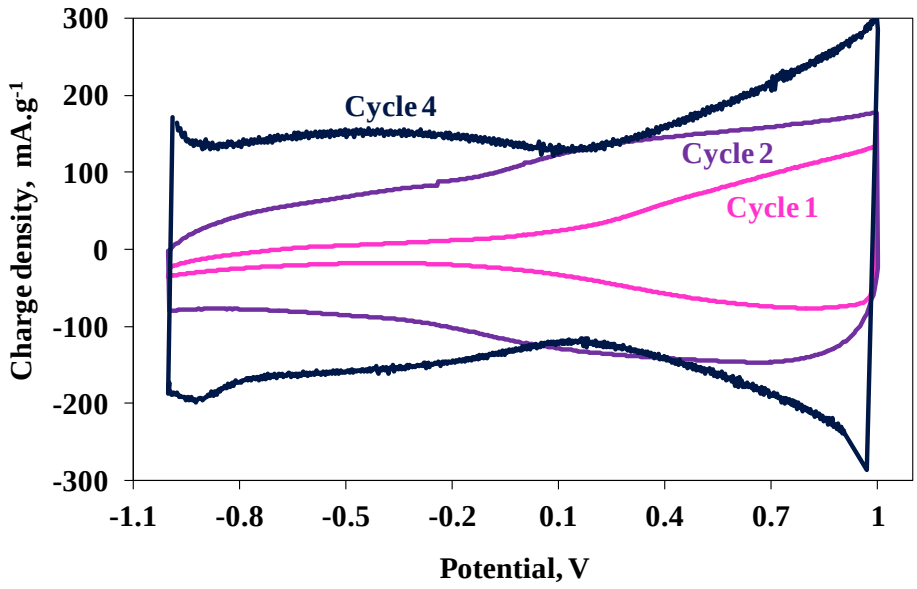

Figure 63 Three-electrode cyclic voltammograms (2.5 mV s^{-1}) in 1 mol L^{-1} $TEABF_4$ of the cellulose based carbons obtained after 1, 2 or 4 activation cycles.

The effect of average pore size on the electrochemical performance can be also analyzed through capacitance normalization, e.g., the capacitance per unit of accessible surface area (Figure 64 and Table 17). If the 1st cycle material is excluded for the reasons exposed above, the normalized capacitance follows the expected trend: the lower the pore size, the higher the normalized capacitance [53][55]. For explaining such a behaviour, we recall the theoretical treatment suggesting an electric wire-in-cylinder capacitor to be the most accurate model for describing an experimental capacitance C in micropores [79][80] as expressed by the relation (7). Under ion confinement inside the pores, the pore size approaches the ion size with b/a_0 nearing unity, which should abruptly increase the capacitance. However, establishing the

optimum pore size/ion size relation presents several precision issues. First, there are uncertainties in ion size determination due to effects such as partial desolvation [53][76] and distortion of confined non-rigid electrolyte ions [63][65][179]. Second, the reported values of average pore size are often calculated by different methods, e.g., by the DFT treatment of adsorption data [57] or by the Dubinin–Radushkevich equation [55], in addition to the errors inherent in adsorption measurements. Third, the compatibility of pore/ion sizes in microporous carbons, while generally desired, is closely connected with performance-deteriorating phenomena such as ion trapping [180] and porosity saturation [63][65]. Nevertheless, the clear result is that our activation method allows the average pore size to be finely adjusted, cycle-by-cycle, to that of ions of the standard organic electrolyte. In these experimental conditions, the pore size optimized with regard to capacitance is obtained in 3-4 activation cycles for the cellulose carbon.

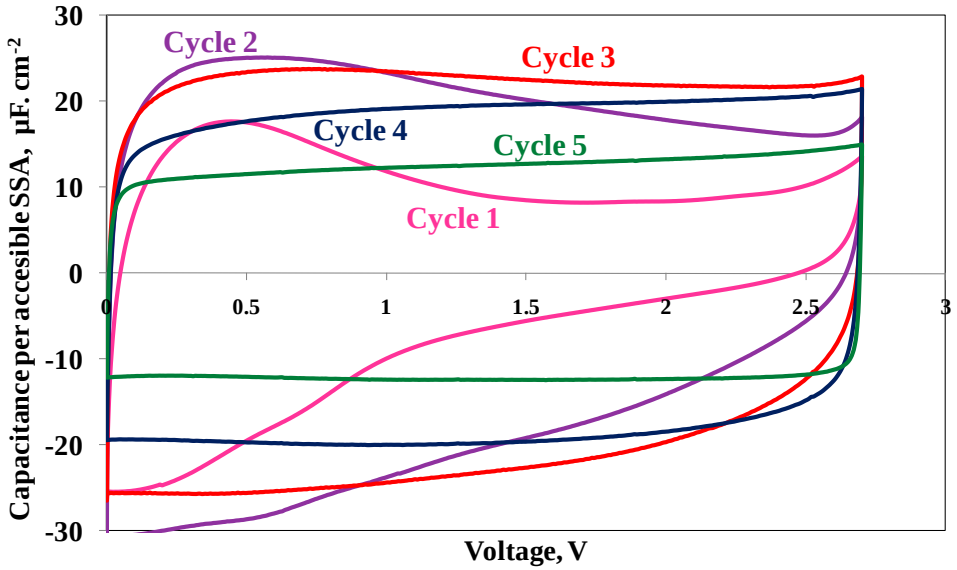

Figure 64 Cyclic voltammograms (5 mV s^{-1}) of supercapacitors in 1 mol L^{-1} $TEABF_4$ using the cellulose based carbons obtained after 1 to 5 activation cycles. The y-axis represents the capacitance normalized per accessible specific surface area.

Another important advantage of this novel activation method is related to the density enhancement of the active coatings prepared on aluminum current collectors. Thus, the coatings from the 4^{th}-cycle cellulose-based carbon exhibit a high density of 0.71 g cm^{-3}. For comparison purposes, with an activated carbon optimized for the supercapacitor industry

(AC; $S_{DR}(N_2)$ = 1820 m^2 g^{-1}; $V_{ultramicro}$ = 0.58 cm^3 g^{-1}; V_{micro} = 0.62 cm^3 g^{-1}; V_{meso} = 0.21 cm^3 g^{-1}), the coating density is only 0.52 g cm^{-3}. Undoubtedly, the important difference between the two values is related to the very low burn-off of the herein developed cyclic activation method in comparison to the classical physical activation by steam. Even though the gravimetric capacitance of the cellulose-based carbon - 78 F g^{-1} - is smaller than for AC - 111 F g^{-1} – due to the larger micropore volume of the later, the higher density of the cellulose carbon coating allows a volumetric capacitance of 56 F cm^{-3} comparable to that of AC (58 F cm^{-3}). As far as supercapacitor applications are considered, these results demonstrate that this new type of carbons holds a high promise in term of volumetric energy density, which can further be improved by optimizing various activation parameters.

3 Carbons for supercapacitors obtained in only one step of pressure induced oxidation at low temperature

3.1 Introduction

In the previous section, we have shown that it is possible to obtain dense microporous carbons with a finely tuned porosity by cyclic oxidation/thermal desorption. The porosity-forming procedure involves 4 to 5 cycles to perfectly adapt the pore entrances to the size of ions of the standard organic electrolyte – 1 mol L^{-1} $TEABF_4$ in acetonitrile. This section, aims at reducing the activation procedure to one oxidation/thermal desorption step by playing on the various oxidation parameters.

3.2 Porosity and surface chemistry characterizations

We have found that the oxidation, and consequently the activation, can be easily controlled by the di-oxygen pressure, temperature and oxidation time. In particular, at 200°C and 4 hours oxidation time, a di-oxygen ($P[O_2]$) pressure increase from 89 to 135 bar (by increasing the H_2O_2 to carbon mass ratio from 5:3 to 7:1) results in a different development of nanoporous texture after oxidation and desorption of the generated oxygenated surface functionalities. Starting from the cellulose char (S_{BET} = 5 m^2 g^{-1}), the specific surface area of the thereof activated carbons reaches 768 m^2 g^{-1} and 927 m^2 g^{-1} at 89 and 135 bar, respectively. Although the specific surface area values are relatively comparable, the material prepared at 135 bar presents a broader pore size distribution with a noticeable amount of

pores larger than 0.7 nm (Figure 65). Actually, the average pore size of this material is centred at 0.80 nm against only 0.56 nm for the material prepared after oxidation at 89 bar.

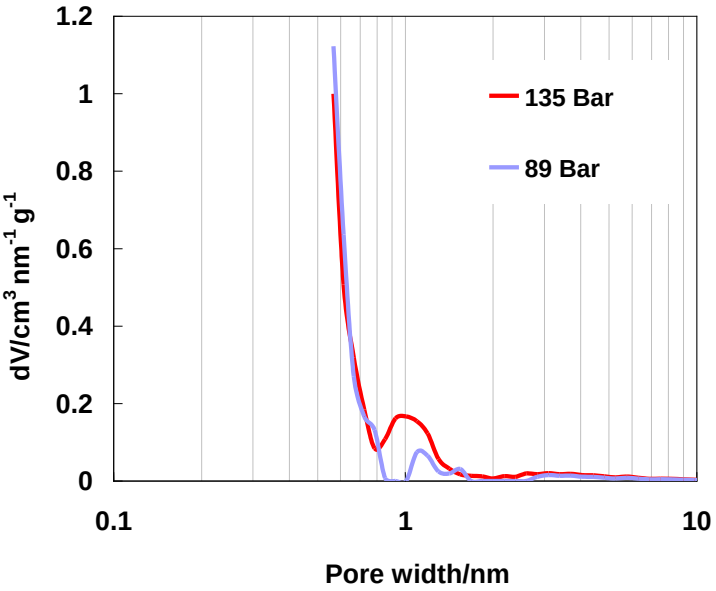

Figure 65 QSDFT pore size distribution of cellulose-based carbons oxidized under di-oxygen pressure of 89 bar or 135 bar at 200 °C during 4 hours and further submitted to thermal desorption.

The porosity data may be easily explained by considering all the possible processes able to take place during the contact of carbon and H_2O_2. Carbon is a well-known catalyst for H_2O_2 decomposition into H_2O and O_2. Even if the mechanism is still far for being completely understood, it has been postulated that the decomposition goes through an electron transfer reaction generating free radicals intermediates [181][182]:

$$AC + H_2O_2 \rightarrow AC^+ + OH^- + \cdot OH \quad (30)$$

$$AC^+ + H_2O_2 \rightarrow AC + H^+ + \cdot OOH \quad (31)$$

Such free radicals could be recombined in the liquid phase and/or onto the carbon surface for giving H_2O and O_2. Moreover, it can be also postulated that the free radicals could interact with the free edge sites or the unpaired electrons on the basal planes carbon for generating oxygenated surface functionalities [114]. Most likely, the oxygen produced during H_2O_2 decomposition will react with carbon following two different processes: oxygen chemisorption (Equation 32) and carbon gasification (Equation 33):

$$2\ C + O_2 \rightarrow 2\ C(O) \quad (32)$$

$C + O_2 \rightarrow CO_2$ (33)

Since the contact between carbon and the oxidizing phase increases with the solubility of di-oxygen in water [15], the di-oxygen pressure influences the extent of both reactions. On the one hand, the burn-off linked to the oxidation reaction (Equation 33) increases from 6 to 17 wt. % when P [O_2] increases from 89 to 135 bar. On the other hand, the amount of oxygen chemisorbed on the carbon surface (Equation 32), determined by thermal programmed desorption (Figure 66), increases from 4.0 wt. % to 8.4 wt. % when increasing P [O_2] from 89 to 135 bar.

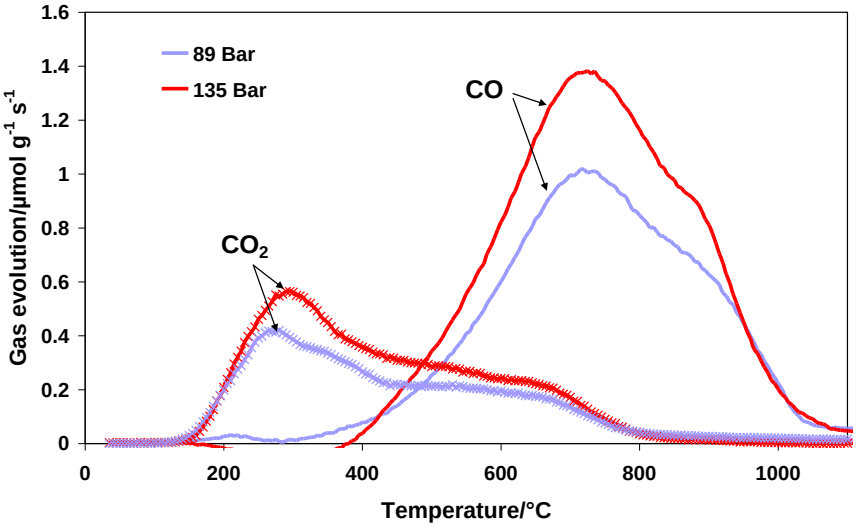

Figure 66 Gas evolution during thermal programmed desorption on cellulose-based carbons oxidized under P [O_2] of 89 bar or 135 bar at 200 °C during 4 hours.

In order to determine whether porosity is mainly developed during carbon oxidation or during desorption of the oxygenated functionalities generated by oxidation, the porous texture of the cellulose carbon has been measured after each step of the process during two oxidation/desorption cycles under P [O_2] = 135 bar. Table 17 shows that the most important development of porosity occurs during the first oxidation with the drilling/opening of micropores (see $S_{DR}N_2$), and particularly ultramicropores (see $S_{DR}CO_2$). Afterwards, during the desorption step; the specific surface area increases more moderately because of unblocking pores entrances. The second oxidation gives rise to an additional burn-off of 19 wt. %, and 9.6 wt. % of oxygen is chemisorbed on the carbon surface. After desorbing the oxygenated surface functionalities generated during oxidation, the specific surface area

finally reaches 1200 m^2 g^{-1}. Overall, from the first oxidation to the second desorption, both ultramicropores and micropores are developed (Table 18), and mesopores start to develop from the second oxidation (Figure 67), resulting in an increase of the average pore size L_0 and a decrease of the $S_{DR}CO_2/S_{DR}N_2$ ratio (Table 18).

Table 18 Textural characteristics of cellulose-based carbons after oxidation (ox) under P [O_2] = 135 bar at 200°C during 4 hours and after a further thermal desorption (des). Results of two consecutive oxidation/desorption cycles are shown. The cellulose carbon precursor has a BET specific surface area of 5 m^2 g^{-1}.

Sample	$S_{DR}(N_2)$ m^2 g^{-1}	$S_{DR}(CO_2)$ m^2 g^{-1}	Lo nm
Cycle 1-ox	750	921	0.65
Cycle 1-des	927	1113	0.80
Cycle 2-ox	1061	1190	1.00
Cycle 2-des	1202	1247	1.18

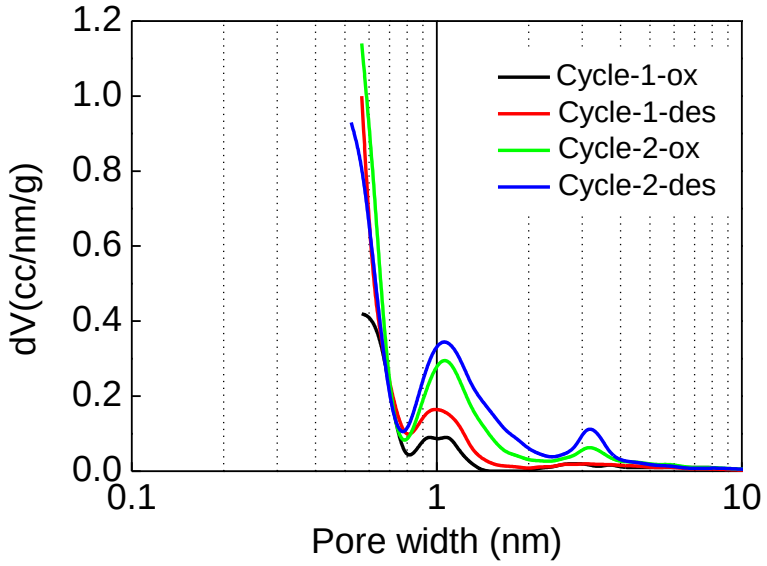

Figure 67 QSDFT pore size distribution of cellulose-based carbons after oxidation (ox) under P [O_2] = 135 bar at 200 °C during 4 hours and after a further thermal desorption (des). Results of two consecutive oxidation/desorption cycles are shown.

From the foreword, it can be concluded that the porosity is mainly generated during the first oxidation and that the desorption step is necessary for the elimination of surface groups

and pores unblocking. Consequently, the oxidation conditions, in particular P [O_2], may control the nanotextural parameters which crucially influence the performance of carbons in supercapacitors.

3.3 Electrochemical performance of the resulting carbons

Figure 68a presents the cyclic voltammograms (CVs) of supercapacitors built with the carbons obtained after either one oxidation (P [O_2] = 89 or 135 bar) /desorption cycle or two oxidation (P [O_2] = 135 bar)/desorption cycles. Whatever the di-oxygen pressure, one cycle is not sufficient for a good development of porosity. Indeed, the capacitive current dramatically decreases at high voltage, being the signature of porosity saturation of one or both electrodes during the polarization [63]. A typical capacitive behaviour, with a rectangular CV, is found after two oxidation/desorption cycles using a high di-oxygen pressure. Figure 68b shows the evolution of specific capacitance vs. specific surface area for the above presented carbons. The capacitance sharply increases from 26 to 84 F g^{-1} while the specific surface area increases only from 768 to 1202 m^2 g^{-1}. At this step, remembering that the average pore size increases together with the specific surface area, it is better to consider the evolution of accessible surface area for the unsolvated electrolyte ions – in particular TEA^+ (diameter 0.67 nm) which is larger than BF_4^- (diameter 0.48 nm). Figure 68b shows parallel dependences of accessible surface area (defined as the surface area corresponding to pores larger than 0.67 nm) and specific capacitance vs. specific surface area, and confirms that the capacitance is essentially controlled by the volume of pores accessible to TEA^+. However, the fact that two oxidation/desorption cycles – with a cumulated carbon yield of only 42 wt.% - are needed for obtaining a porous texture adapted to the electrolyte ions size, reveals that the activation process is not yet optimized for the targeted supercapacitor application.

Since the development of porosity can be influenced by the oxidation conditions, such adapted porous texture has been sought by using more harsh reaction conditions in order to realize only one oxidation/desorption cycle. Therefore, the temperature or the oxidation time has been increased for a given H_2O_2 to carbon ratio of 7:1.

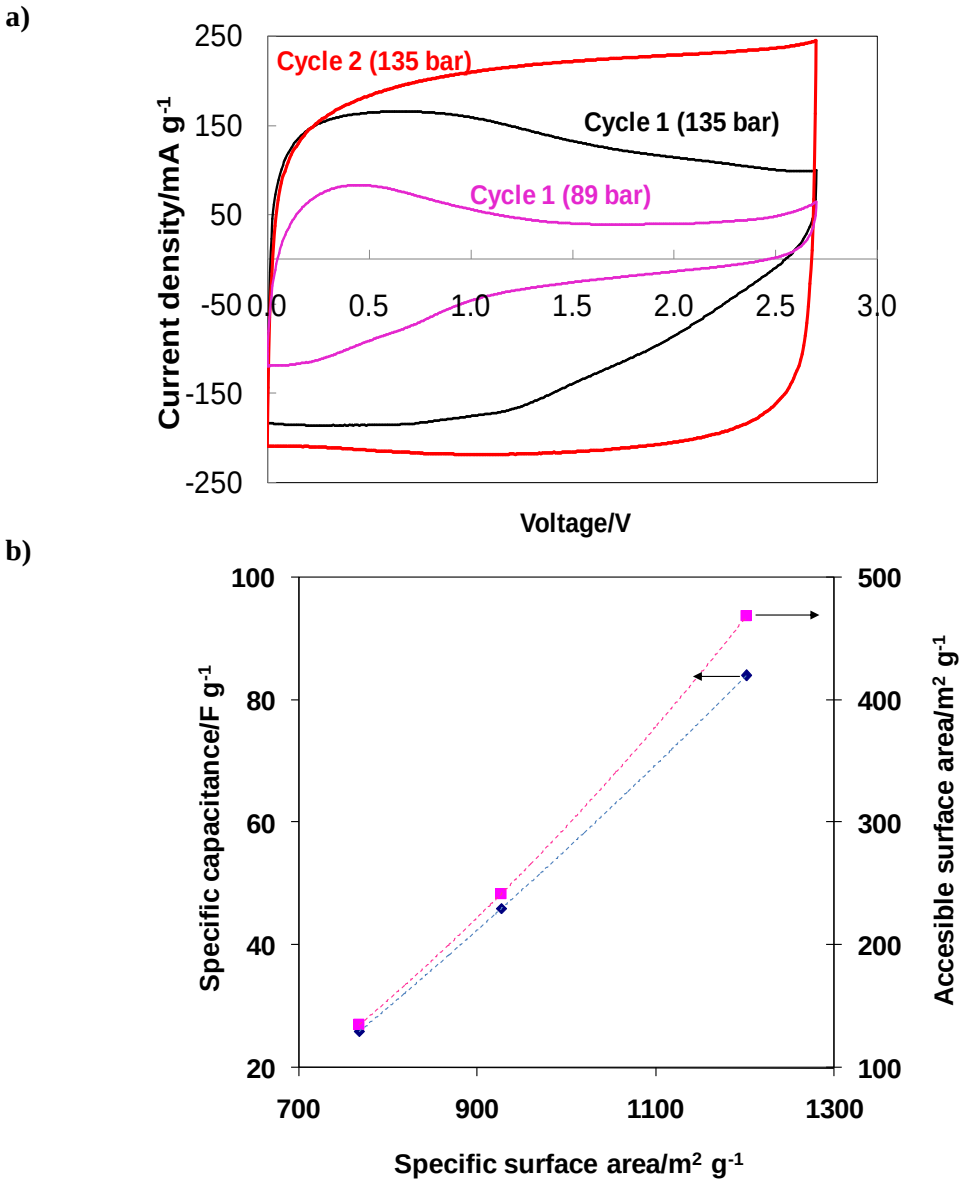

Figure 68 Capacitance and textural characteristics of cellulose based porous carbons prepared either after one oxidation/desorption cycle under PO_2 = 89 bar or after one and two cycles under PO_2 = 135bar. a) cyclic voltammograms 5 mV s^{-1}) using 1 mol L^{-1} $TEABF_4$ in acetonitrile; b) specific capacitance and accessible surface area vs specific surface area.

Raising the reaction temperature from 200 °C to 250 °C is a way to increase the di-oxygen pressure (P [O_2]) because O_2 solubility in water decreases [177]. Moreover, increasing the temperature favours the oxygen chemisorption (Equation 32), the carbon gasification reaction (Equation 33) and the possible reactions between carbon and the intermediate radicals produced during H_2O_2 decomposition. Additionally, at 250 °C, in

parallel to the oxidation reaction there is a continuous desorption of oxygen fixed on the surface of the carbon material as CO_2 (see Figure 66), what generates new active sites for the reactions (32) and (33). For all these reasons, the carbon burn-off after oxidation at 250°C (P $[O_2]$ = 149 bar) and subsequent desorption is twice higher than at 200°C, while keeping the same reaction time of 4 hours (see Table 19). Although the specific surface area is only slightly higher after oxidation at 250°C than at 200°C, the average pore size notably increases from 0.8 nm to 1.05 nm. This pore size variation appears in Table 19 as a decrease of ultramicropore volume and an increase of mesopore volume.

Table 19 Experimental conditions applied for obtaining cellulose-based porous carbons, porous texture characterization and electrochemical characterization. The normalized capacitance (C/S_{DFT} > 0.68 nm) is expressed as the gravimetric capacitance divided by the accessible specific surface area (DFT specific surface area corresponding to pores larger than 0.68 nm)

T °C	t h	PO_2 bar	Burn-off %	$S_{DR}(N_2)$ $m^2\ g^{-1}$	$V_{ultramicro}$[a] $cm^3\ g^{-1}$	V_{micro}[b] $cm^3\ g^{-1}$	V_{meso}[c] $cm^3\ g^{-1}$	L_0 nm	C $F\ g^{-1}$	$C/S_{DFT > 0.68nm}$ $\mu F\ cm^{-2}$
200	4	135	27	927	0.42	0.30	0.10	0.80	46	19.0
250	4	149	59	1029	0.35	0.32	0.23	1.05	68	17.4
200	12	135	30	1138	0.36	0.38	0.11	0.90	74	21.0

[a] Pore diameter < 0.7 nm; [b] Pore diameter < 2.0 nm; [c] 2.0 nm<Pore diameter < 50 nm

The CVs presented in Figure 69 demonstrate that the material obtained after oxidation at 250 °C during 4 hours posses enough accessible surface area for accumulating the TEA^+ ions during the charge of the supercapacitor up to 2.7 V, while narrowing of CV related with porosity saturation starts to appear at 1.0 V for the carbon resulting of oxidation at 200°C. Nevertheless, Table 19 shows that the normalized capacitance (expressed as the gravimetric capacitance divided by the accessible specific surface area) is smaller for the material with the higher L_0, confirming that the ions interact less efficiently in the larger pores. Consequently, even if Figure 69 shows that it is possible to get a material with enough developed surface area after only one oxidation (250°C)/desorption cycle, the porosity is not yet optimal for an usage as active electrode material for supercapacitors.

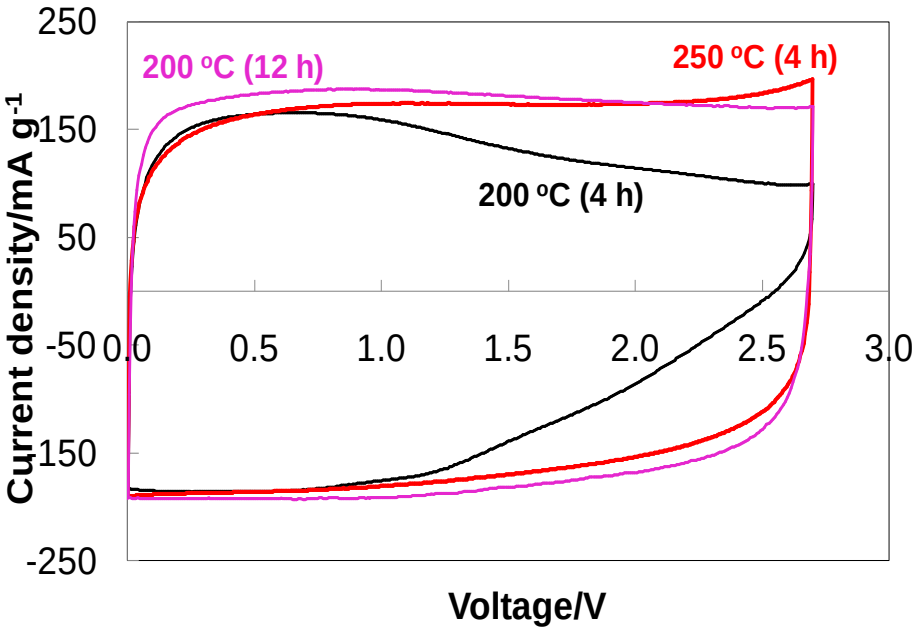

Figure 69 Cyclic voltammograms (5 mV s^{-1}) of supercapacitors using carbons prepared by oxidation/desorption at different oxidation temperatures or times. Electrolyte: 1 mol L^{-1} $TEABF_4$ in acetonitrile.

The time is another parameter which can influence the extent of the oxidation reaction. By keeping the temperature at 200°C, but increasing the time from 4 to 12 hours, the oxygen amount chemisorbed on the carbon surface slightly increases from 8.4 wt. % to 9.2 wt. %, and consequently the carbon burn-off after the oxidation/desorption process increases from 27 wt.% to 30 wt.%. Increasing the reaction time up to 24 hours, did not bring any further modification, indicating that all the active surface sites for reactions (32) and (33) are saturated after 12 hours.

After 12 hours oxidation at 200 °C and surface groups desorption at 900 °C, the small increase of specific surface area is associated to a slight enlargement of micropores (the ultramicropore volume slightly decreases) without generating mesopores (Table 19); the average pore size thereby increases from 0.8 nm to 0.9 nm. Whereas saturation of porosity was observed on the cyclic voltammogram of the carbon obtained after 4 hours oxidation, the slight pore widening after prolonging the oxidation time to 12 hours suppresses the narrowing of the CV curve when the capacitor is charged up to 2.7 V (Figure 69). The average pore size of 0.9 nm seems to be perfectly adapted for an optimal access of the TEA^+ cations when the cell is charged up to 2.7 V. This conclusion is confirmed by the highest value of normalized capacitance for this material, 21 µF cm^{-2} (Table 19).

In summary, it is possible to obtain carbons with a porous texture perfectly tuned for being used in supercapacitors in only one cycle of oxidation/thermal desorption just by adjusting the oxidation conditions.

4 Conclusions

We have demonstrated that highly microporous carbons, with porosity characteristics targeted to the organic electrolyte for supercapacitors, can be produced through high-pressure cyclic oxidation of nonporous carbons by using hydrogen peroxide as an active di-oxygen source. The activation process is perfectly controlled with respect to pore size distribution, average pore size and pore volume, by playing with the oxidation parameters (temperature, pressure, time),

Actually, the proposed activation method has notable differences compared to the previously reported works: (i) the number of activation cycles is dramatically reduced (only 4-5 cycles versus tens cycles in Ref.[173]); (ii) there is no need for pre-activated materials as in Ref.[174]. The porosity is mainly generated during the oxidation step, while the desorption one is necessary to eliminate the surface groups and unblock the pore entrances. When using a relatively low oxidation pressure and a short oxidation time, the targeted pore size for supercapacitors is achieved after 3 to 4 activation cycles, whereas the number of activation cycles is remarkably reduced to only one by increasing the pressure and oxidation time.

Another advantage of the method is a low burn-off and consequently a high carbon yield. The main mechanism associated with this low burn-off seems to be a drilling of the narrow pores existing initially in the chars. In other words, the inhomogeneities in non-activated materials may serve as reactive sites for initiating reaction with di-oxygen, further leading to porosity formation. Thus, the activation appears to occur mostly at definite sites and is thus less chaotic than traditional activation methods. This can also be the reason for getting denser carbons than with the traditional activation method.

Due to the high density of the coated electrodes, the resultant carbons demonstrate high volumetric capacitance in organic electrolyte reaching a competitive value compared to commercial carbons, with the advantages of a more environment friendly, cost-effective, high yield and less energy consumption process. A higher volumetric energy can be expected with this new family of carbons in the near future through further optimization, by varying the synthesis parameters and the nature of the carbonaceous precursors.

General conclusion

General conclusion

The most important challenge in carbon/carbon supercapacitor development is to improve the energy density while keeping a high power density and a long cycle life. For achieving this objective, in this work, we have followed two different strategies depending on the electrolyte used: i) in aqueous electrolytes, our efforts were focused on extending the operating cell voltage by using alkali sulfate salts; and ii) in organic electrolyte, our target was to improve the volumetric capacitance by setting an activation method able to produce a porous carbon with pore size matching the ions size, without broadening the pores when the porosity is developed.

For the aqueous electrolyte, the electrochemical performance has been first systematically screened by using aqueous Li_2SO_4, Na_2SO_4, and K_2SO_4. At room temperature, the highest power and energy density was obtained when operating in aqueous K_2SO_4 due to the smallest size of the hydrated potassium cation. Actually, the capacitance values were in the sequence 0.5 mol L^{-1} Li_2SO_4 < 0.5 mol L^{-1} Na_2SO_4 < 0.5 mol L^{-1} K_2SO_4 as for the hydrated cation size (K^+ < Na^+ < Li^+). At low temperature (-10°C), the K_2SO_4 and Na_2SO_4 based electrolytes were not appropriate because their solubility is below 0.5 mol L^{-1} leading to a resistive behavior of the systems, probably because of the salt precipitation in the pores of carbon. By contrast, Li_2SO_4 keeps advantageously a great solubility which enables highly concentrated solutions. Hence, we demonstrated a good power performance and long cycle life for an AC/AC system operating at -10°C and at voltage as high as 1.8 V in 2 mol L^{-1} Li_2SO_4. Taking into account that extending the operating temperature range to negative values is mandatory for most of the applications, the AC/AC supercapacitor in 2 mol L^{-1} Li_2SO_4 is very promising; therefore it has been further investigated in order to understand the parameters limiting the maximum voltage and in final to get recipes for optimizing this voltage.

We have found that the voltage range is limited by the destructive oxidation of the positive carbon electrode when its potential becomes too high. Due to the positive electrode degradation, the system exhibits continuous capacitance loss during cycling. By mild chemical oxidation of the carbon before its implementation in the positive electrode, we could successfully push its maximum operation potential to relatively lower values and consequently sidestep its irreversible electro-oxidation during long term cycling. Consequently, a slightly enhanced operating voltage from 1.8 to 1.9 V could be verified after 10,000 charge/discharge cycles at 1 A g^{-1}. It was proved that CO-type groups are favorable

for an increase of voltage range, while CO_2-type groups induce a negative effect and are precluded for this application.

In symmetric AC/AC cells, at voltage higher than 1.9 V, the potential of the positive electrode starts to be beyond the thermodynamic limit for water oxidation, while the potential of the negative electrode is still far higher than the limit related to di-hydrogen evolution. In these conditions, we demonstrated that there is some room available for another extension of the voltage range up to 2.0 V, simply by balancing the masses of the two electrodes (mass positive = 1.2 x mass negative). In such configuration, the extreme positive and negative electrode potentials are pushed towards smaller values, enabling to take advantage of the whole stability potential window for both electrodes.

Finally, pouch cells have been realized in lithium sulfate electrolyte using carbon coatings on stainless steel. The pouch cells demonstrated good capacitance retention after 10,000 galvanostatic cycles up to 2.1 V. This enhanced performance compared to pressed electrodes in Swagelok® cells is related to a much better contact between the active material and the current collectors in the case of coated electrodes.

In summary, our strategy of using aqueous alkali sulfate solutions as electrolytes has been shown to be very effective for producing low cost and environment friendly carbon/carbon supercapacitors able to deliver a high energy density.

For improving the volumetric capacitance and energy density of carbon/carbon supercapacitors operating in organic electrolytes, we have shown that highly microporous and dense carbons, with a finely controlled porosity, can be produced through pressure-induced cyclic oxidation of nonporous carbons by using H_2O_2 as an active di-oxygen source at low temperature.

By moderate oxidation (P [O_2] = 89 bar at 200 °C during 4 hours) of the cellulose-based carbon, the optimal pore size for the organic electrolyte is achieved after 3 to 4 activation cycles. The increase of pore volume during the first 3 cycles proceeds essentially through the opening/formation and deepening of narrow micropores, whereas pore widening appears to be the main outcome of the subsequent cycles. The coated electrodes made from the carbon obtained after four oxidation/desorption cycles are much denser (0.71 g cm^{-3}) than the steam-activated carbon based ones (0.52 g cm^{-3}), being the origin of a high volumetric energy for this new family of carbons.

General conclusion

Under high di-oxygen pressure at low temperature, the main mechanism associated with the low burn-off values seems to be a drilling of the narrow pores existing initially in the chars. In other words, the in-homogeneities in non-activated materials may serve as reactive sites for initiating the reaction with di-oxygen, further leading to porosity formation.

Gas adsorption experiments done after oxidation or after the oxidation/thermal desorption cycle confirm that the porosity is mainly generated during the oxidation, while the desorption step is necessary for the elimination of surface groups and pores unblocking. Therefore, the nanotextural parameters can be controlled by the oxidation parameters. In this sense, we showed that it is possible to adapt the average pore size to the expected value in a single oxidation/thermal desorption by a control of the oxidation conditions (pressure, temperature, time). In particular, for a cellulose char, the oxidation conditions bringing the desired porous texture consist in using a H_2O_2 to carbon ratio of 7:1 at 200°C, with an oxygen pressure of 135 bar, during 12 hours.

To sum up, the process shows notable advantages when compared with the traditional activation techniques consisting in higher yield and the production of denser carbons, being definitively more environmentally friendly and cost-effective.

In conclusion, this thesis demonstrated that it is possible to reach an adapted solution for increasing the energy density of carbon/carbon supercapacitors depending on the electrode/electrolyte couple used.

As perspectives, for systems in neutral salt aqueous solutions, *in situ* characterization of the surface functionality of the electrodes during cycling of the AC/AC supercapacitors would be quite useful to better elucidate the ageing mechanism of the electrode materials and to suggest strategies to enhance the voltage range. In this sense, the asymmetric systems should be more extensively investigated especially by using different carbons for both electrodes. In such a way, one could also explore the effects of porosity of the electrode materials on voltage expansion and further enhance the voltage range by an adapted carbon nanotexture. As it has been done for the organic systems, *ex-situ* NMR experiments after charging up to different voltage values could provide information on the hydration degree of ions in the aqueous electrolyte and on the ways to better adapt the porosity of carbons.

One-step oxidation at high pressure and low temperature appears as a promising eco-process to produce nanoporous carbons with a well-controlled porosity. Preliminary

investigations conducted during this thesis demonstrated that dense electrodes could be realized using carbon precursors obtained by hydrothermal carbonization (HTC) of biomass wastes. The screening of a broad range of resources, by combining HTC and high pressure oxidation, should be investigated in detail in order to determine if it exists a relationship between the final physico-chemical characteristics of the obtained porous carbons and the nature of the inorganic resources initial carbonized. In the objective of reducing the environmental impact of the process and the cost, it could be also of interest to determine if the thermal desorption step could be avoided by measuring the electrochemical properties of carbons obtained just after the oxidation step.

Conclusions Générale

General conclusion

L'objectif de notre travail est l'augmentation de la densité d'énergie stockée dans les supercondensateurs de type carbone/carbone fonctionnant dans un électrolyte aqueux neutre ou organique. Pour réaliser ces objectifs, il est indispensable d'augmenter la tension de fonctionnement du système et/ou la capacité spécifique de stockage de charges des carbones activés.

La première partie se concentre sur l'exploration de la plage de tension de condensateurs symétriques carbone/carbone utilisant les électrolytes aqueux neutres. Les sulfates alcalins aqueux montrent une plus grande fenêtre de stabilité en tension et des propriétés non corrosives par rapport à un milieu acide ou basique.

Les plus grandes puissances et densités d'énergie ont été obtenues en utilisant un électrolyte aqueux K_2SO_4 en raison de la plus petite taille des cations et de la conductivité ionique plus élevée dans ce milieu à température ambiante. A basse température (-10 ^oC), les performances de supercondensateurs symétriques à base de Li_2SO_4 sont les meilleures. La stabilité exceptionnelle jusqu'à une tension de 1.8 V a été mise en évidence, avec un taux de rétention de la capacité atteignant 92 % après 10, 000 cycles de charge/décharge dans Li_2SO_4 á 2 mol L^{-1}. Cette tension est deux fois plus élevée que les valeurs généralement atteintes pour des condensateurs symétriques carbone/carbone conventionnels opérant en milieu aqueux acide ou basique. Ces bonnes performances sont attribuées à la surtension vis-à-vis de la formation de dihydrogène, liée au mécanisme de stockage d'hydrogène naissant à la surface des carbones activés. Les variations de capacité avec la température pourraient être attribuées essentiellement à la barrière de diffusion cinétique, aux changements de dimensions d'ions et à moins de pseudo-capacité liée à la contribution du stockage de l'hydrogène.

La tension maximale de fonctionnement des condensateurs opérant en milieu aqueux neutre est limitée essentiellement par une électro-oxydation irréversible du carbone activé de l'électrode positive. Si le potentiel de l'électrode positive va au-delà d'une valeur donnée pendant le fonctionnement du système, une électro-oxydation trop importante du carbone entraîne une augmentation néfaste du potentiel maximal de fonctionnement de l'électrode positive et une augmentation de la résistance du système conduisant à une diminution de la capacité spécifique. Ces phénomènes peuvent être évités en procédant à une oxydation chimique contrôlée de la surface du carbone activé par le peroxyde d'hydrogène. En

conséquence, le potentiel maximum de l'électrode reste stable pendant le fonctionnement de la cellule jusqu'à une tension atteignant alors 1.9 V et le système peut être chargé/déchargé pendant 10, 000 cycles avec une perte très modérée de la capacité et une faible augmentation de la résistance.

Comme il a été montré, un carbone oxydé pourrait être utile à l'amélioration de la gamme de tension dans un condensateur asymétrique. C'est pourquoi un carbone activé a été modifié par l'acide nitrique puis traité thermiquement. Par conséquent, une série de carbones a été obtenue, montrant différentes concentrations de fonctionnalités de surface. Cependant, l'augmentation de la quantité de groupes de surface ne contribue pas de manière notable à l'amélioration les tensions de fonctionnement, même pour des condensateurs symétriques dans Li_2SO_4. D'autre part, en diminuant la teneur en groupes de surface, il a également été possible d'évaluer le rôle de la chimie de surface. Dans un électrolyte aqueux neutre tel Li_2SO_4, un carbone activé présentant des groupes oxygénés de surface se décomposant par TPD en groupes CO plutôt que CO_2 donnerait de meilleures performances. Une quantité relativement faible de groupes de surface pourrait être favorable à l'amélioration de la tension de fonctionnement d'un condensateur carbone/carbone à l'électrolyte aqueux Li_2SO_4. Enfin, la tension de fonctionnement peut être étendue jusqu'à 2.0 V en réalisant une configuration asymétrique avec un rapport massique entre les électrodes (R = m + / m-) de 1.2.

Ainsi, il devient réaliste de prévoir la production de supercondensateurs à haute densité d'énergie en utilisant des matériaux d'électrode et un électrolyte respectueux de l'environnement, peu onéreux et sûrs. Un système de supercondensateurs réel de type pouch-cell a été développé en utilisant des électrodes préparées par l'enduction de carbone dans l'électrolyte aqueux préparé à partir de sel de sulfate de lithium. Une stabilité exceptionnelle de 2.1 V a été obtenue avec un tel système durant 10, 000 cycles de charge-décharge. Cette tension plus élevée est évidemment due à un meilleur contact entre les matières actives et les collecteurs de courant. En outre, la capacité peut être améliorée grâce à l'utilisation d'électrodes du type revêtement au lieu d'électrodes de type granulé, en raison du meilleur contact entre les matériaux et les collecteurs de courant.

La deuxième partie met en évidence l'amélioration de la capacité volumique des condensateurs symétriques carbone / carbone à électrolyte organique grâce à la préparation de

carbone via une nouvelle méthode. Une meilleure compréhension du comportement des ions dans les petits micropores met en évidence que des carbones microporeux avec une taille moyenne des pores contrôlée (en dessous de 1 nm), une surface relativement grande et distributions de taille de pores étroite sont une priorité afin d'augmenter la densité d'énergie des supercondensateurs.

Un carbone hautement microporeux, avec des pores ciblée pour l'électro-sorption des ions dans un électrolyte organique, peuvent être produits par une haute pression induite dioxygène forage à basse température. À l'aide de peroxyde d'hydrogène comme source d'oxygène, l'oxydation est réalisée d'une manière très contrôlée par rapport à la distribution de taille des pores, la taille moyenne des pores et le volume des pores souhaités. Sous haute pression de dioxygène à des températures basses, le mécanisme principal associé aux faibles combustions des valeurs semble être un forage des pores étroits existant initialement dans les chars. La contrôlabilité du processus est bien illustré à la fois par les caractéristiques d'adsorption et la réponse électrochimique des matériaux produits. En outre, des électrodes préparées à partie de ces carbones par l'enduction ont permis d'atteindre des densités supérieure à celle-ci électrodes de préparées avec du charbon activé à la vapeur optimisés pour l'industrie supercondensateurs.

Dans l'ensemble, le faible coût et la haute densité d'énergie sont devenus les paramètres les plus importants pour les supercondensateurs à base de carbone. Acquérir une meilleure compréhension des effets fondamentaux sur l'élargissement de la gamme de tension dans les milieux aqueux neutres de sulfates alcalins ouvrirait une porte au développement de ce type de supercondensateurs. D'autre part, l'amélioration de l'énergie volumique nécessite des matériaux carbonés microporeux denses et peu coûteux.

Comme perspectives, pour les systèmes dans les solutions aqueuses de sels neutres, la caractérisation in situ de la fonctionnalité de surface des électrodes au cours du cyclage des supercondensateurs carbone/carbone serait très utile pour mieux élucider le mécanisme de vieillissement des matériaux d'électrode et de proposer des stratégies pour améliorer la gamme de tension. En ce sens, les systèmes asymétriques devraient être plus largement étudiés notamment par l'utilisation de différents carbones pour les deux électrodes. De cette

façon, on pourrait aussi explorer les effets de la porosité des matériaux d'électrode sur l'expansion de tension et de renforcer la gamme de tension d'un nano texturé carbone adapté. Comme cela a été fait pour les systèmes organiques, les ex-situ des expériences de RMN après le chargement jusqu'à des valeurs de tension peuvent fournir des informations sur le degré d'hydratation des ions dans l'électrolyte aqueux et sur les moyens de mieux adapter la porosité de carbones.

Une étape d'oxydation à haute pression et à basse température apparaît comme un éco-procédé prometteur pour produire carbones nanoporeux à porosité bien contrôlée. Les enquêtes préliminaires menées durant cette thèse ont démontré que les électrodes denses pourraient être réalisées en utilisant des précurseurs de carbone obtenus par carbonisation hydrothermale (HTC) de déchets de la biomasse. La projection d'un large éventail de ressources, en combinant oxydation sous pression HTC et élevé, devrait être étudiée en détail afin de déterminer s'il existe une relation entre les caractéristiques physico-chimiques finales des carbones poreux obtenus et la nature des ressources minérales initiales carbonisées. Dans l'objectif de réduire l'impact environnemental du processus et le coût, il pourrait être également intéressant de déterminer si l'étape de désorption thermique pourrait être évité en mesurant les propriétés électrochimiques de carbones obtenus juste après l'étape d'oxydation.

Experimental annex

1 Synthesis of porous carbon and surface modification

1.1 Modification of surface functionality for the applications in Li_2SO_4 electrolyte

The activated carbon AC for the study was a commercial sample (MeadWestvaco, USA - 2.5 at.% O determined by XPS, S_{BET} = 2250 m^2 g^{-1}).

A carbon ACN was obtained by chemical oxidation of AC (10 g) with 200 mL of 30 wt. % HNO_3 at 80^{o}C during 2 h. In order to prepare carbons containing different type and amount of surface oxygenated functionalities, ACN was subjected to heat treatment under N_2 flow of 100 mL min^{-1} during 2 h. ACN 400 and ACN 500 represent the samples thermally treated at 400^{o}C and 500^{o}C, respectively.

A carbon ACH was prepared through oxidation of AC (1 g) with 40 mL of 35 wt. % H_2O_2 solution under stirring during 1h at room temperature. In order to prepare carbons containing different type and amount of surface functional groups, ACH was subjected to heat treatment under N_2 flow of 100 mL min^{-1} during 2 h. ACH400 represents the sample thermally treated at 400^{o}C.

1.2 Nanoporous carbons for organic electrolyte prepared by cyclic oxidation/thermal desorption

Sucrose and microcrystalline cellulose (FMC Corporation, USA) were used as raw materials. Before carbonization, sucrose was dehydrated using concentrated sulfuric acid (H_2SO_4 96%) and the resulting carbon was washed off and dried at 120^{o}C. Microcrystalline cellulose was used as received. Dehydrated sucrose-derived carbon or microcrystalline cellulose were carbonized by heating up to 1050^{o}C under nitrogen flow (100 ml min^{-1}) in a tubular furnace (d = 35 mm) at a ramp rate of 5^{o}C/min with subsequent holding for 3 h.

The following procedure refers to the adjusted synthesis conditions, but the optimization parameters will separately be considered in connection with either gas adsorption or electrochemical data used as control in the experiments. The carbonized material (3 g) was put in an autoclave (inner volume: 46.6 mL), 15 g of hydrogen peroxide solution (35 wt.%) were poured over the carbonized material, and the closed autoclave was placed into a muffle furnace and then heated at 10^{o}C/min with a subsequent isothermal step for 4 h at the final temperature. To investigate the influence of experimental parameters, carbonized cellulose (1

g) was oxidized by 20 g of hydrogen peroxide (35 wt. %) in the same autoclave at temperatures between 200°C and 250°C during 4 to 24 hours.

The solid reaction product was washed with water and dried at 120°C for 3 h. The material was then subjected to high temperature treatment (900°C) during 2 h in a tubular furnace under nitrogen flow (100 mL min^{-1}, a heating ramp rate of 10°C/min), allowing the surface groups to be eliminated. The oxidation/desorption procedure was repeated 4 to 5 times and the samples of intermediate cycles were kept for gas adsorption and electrochemical analysis.

2 Physico-chemical characterizations of the porous carbons

2.1 Textural properties

To characterize the porous texture of the activated products, nitrogen and CO_2 adsorption isotherms were recorded at 77 K and 273 K, respectively, using a Quantachrome Autosorb-1 instrument. The samples were preliminarily outgassed for 12 h at 300°C.

For AC and the chemically modified ACH and ACN series, the specific surface area was evaluated from the N_2 adsorption isotherm using the Brunauer-Emmett-Teller equation (BET)[183]. The micropore and ultra-micropore (pores in the range of 0.4-0.8 nm) volumes were obtained by application of the Dubinin-Radushkevich equation to N_2 and CO_2 adsorption data[46], respectively. The mesopore volume was determined by applying the non-linear differential functional theory equation (NL-DFT) to N_2 adsorption data [46].

For the nanoporous carbons obtained from cyclic activation, the N_2 adsorption data were used to calculate the specific surface area ($S_{DR(N_2)}$), the micropore volume (V_{micro}) and the average micropore width (L_0) from the application of the Dubinin–Radushkevich and Stoeckli equations [46], respectively, to the adsorption data up to $P/P_0 \leq 0.015$. The pore size distribution was calculated according to the quenched solid density functional theory approach (QSDFT)[184][185], from which the mesopore volume (V_{meso}) has been extracted. The CO_2 adsorption isotherms at low relative pressure $P/P_0 < 0.1$ were used for calculating the ultramicropore volume ($V_{ultramicro}$) and surface ($S_{DR(CO_2)}$) according to the Dubinin–Radushkevich equation, as they correspond to adsorption into ultramicropores.

2.2 Surface oxygenated functionality analysis

The surface functionality of carbons was analyzed by temperature-programmed desorption (TPD) under an inert atmosphere (He). The sample (20 mg) was placed in a STA 449C Thermo-balance (Netzch, Germany) and kept at room temperature for 1 h under helium flow of 150 mL min^{-1}. Then, the temperature was increased to 1100°C at a rate of 10°C min^{-1}. The decomposition products were detected by on-line mass spectrometry (QMS 403C, Aeolos, Netzch, Germany). To investigate the evolution of surface chemistry during charge-discharge cycling, positive electrodes were taken out from supercapacitors after 5,000 galvanostatic charge-discharge cycles and washed carefully with distillated water to remove the electrolyte ions. Fresh electrodes were also subjected to the same treatment for a comparison with the cycled ones.

X-ray photo-electron spectra (XPS) on carbon powder were recorded with a VG ESCALAB 250 spectrometer using an Al Kα monochromatic source (15 kV, 15 mA) and a multi-detection analyzer, under 10^{-8} Pa residual pressure.

3 Electrochemical characterizations

3.1 Electrodes preparation

3.1.1 Pellet type electrodes

For aqueous medium, the pellet-type electrodes (1 cm diameter, thickness 300 μm ± 50 μm, and mass 8-10 mg) were pressed at 5 tons from a mixture of carbon active materials (80 wt. %), acetylene black (10 wt. %, pure black, Superior Graphite Co., USA), and PTFE (10 wt. %, Aldrich) as binder.

In the case of organic electrolyte, electrodes were prepared by mixing the carbon material (80 wt. %) with a conductivity additive (10 wt. %, carbon black-Pureblack®, Superior Graphite Co., USA) and PVDF (10 wt. %, polyvinylidene fluoride). The electrode mass was pressed at 5 tons into 10-15 mg pellets.

3.1.2 Coated electrodes

For assessing the volumetric energy density of supercapacitors in organic electrolyte, electrodes have been prepared by coating an Al foil current collector with a slurry containing the active material. The slurry was a mixture of nanoporous carbon (82 wt. %),

carboxymethyl cellulose (4 wt. %), Styrene-Butadiene-Rubber (SBR, 4 wt. %) and carbon black (10 wt %) in water. The slurry was spread with uniform thickness over the current collector using a precision "doctor blade", then dried under atmospheric pressure and vacuum at 120 ^{o}C, and finally the electrodes (4 x 5 cm^2) for pouch cells were cut out. The pouch cells were assembled in the glove box under argon atmosphere providing for O_2 and H_2O content less than 1 ppm.

All the electrochemical data in figures and tables regarding the carbons for organic medium refer to the pelletized electrodes because the necessary amount of material for the coated electrodes was difficult to produce in each cycle on a laboratory scale. The coated electrodes for the cycle 4 material did not show a sensible difference in capacitance from the pelletized ones, but exhibited lower ESR values. For that reason, the coatings will solely be discussed with regard to the electrode density as they can directly be compared with industrial electrodes.

3.2 Electrochemical cell configurations

3.2.1 Three electrode cell

For aqueous electrolytes, the three-electrode cell consists of a pellet-type electrode as working electrode, Hg/Hg_2SO_4 as a reference electrode and a graphite rod (3 mm diameter) as counter electrode. The working electrode was stuck onto the gold current collector with a graphite conductive adhesive 502 (13 wt. %, Electron Microscopy Sciences Company, UK).

A special two-electrode cell equipped with two identical carbon electrodes and Hg/Hg_2SO_4 reference electrode has been utilized to study separately the positive and negative electrodes during the charge/discharge of the capacitor.

In organic medium, three-electrode Swagelok cells were assembled with a silver wire as pseudo-reference electrode, an active material pellet as working electrode and a high-surface area activated carbon (Meadwestvaco, S_{BET} = 2500 m^2g^{-1}) pellet as counter electrode.

3.2.2 Two electrode cell

For aqueous medium, two-electrode cells were built using a Teflon Swagelok® construction with a glass fiber separator (Fisher Scientific, 173 μm thickness) and gold current collectors. The electrolytes were 0.5 and 2 mol L^{-1} Li_2SO_4, 0.5 mol L^{-1} Na_2SO_4 and 0.5 mol L^{-1} K_2SO_4 during the electrochemical analysis.

In organic electrolyte, two-electrode cells were assembled in a Teflon Swagelok® airtight system using two identical carbon pellets (electrodes), two titanium current collectors, a porous cellulose membrane separator (32 μm), 1 mol L^{-1} $TEABF_4$ in acetonitrile as electrolyte. The cells were assembled under argon atmosphere in a glove box under argon atmosphere providing for O_2 and H_2O content less than 1 ppm.

3.3 Electrochemical tests

All the electrochemical investigations were performed with a VMP2 multichannel potentiostat/galvanostat (Biologic, France). For aqueous electrolytes, cyclic voltammetry (CV) was performed at 2 mV s^{-1} and galvanostatic charge/discharge cycling (GA) at 0.2 to 10 A g^{-1}). All potential values are expressed vs. normal hydrogen electrode (NHE). Electrochemical impedance spectra (EIS) were recorded at 0 V with applying amplitude of 10 mV in the frequency range of 100 kHz to 0.01 Hz. Before starting the frequency scan, the capacitors were subjected to soaking at the applied potential of 0 V to stabilize the current. The gravimetric capacitance in farads per gram (F g^{-1}) of electrode materials was obtained by galvanostatic charge/discharge cycling at a current density of 200 mA g^{-1}.

In organic medium, electrochemical investigations were performed by cyclic voltammetry (CV, 5 mV s^{-1}) and galvanostatic (GA, 200 mA g^{-1}) charge-discharge cycling.

In all cases, the gravimetric capacitance *C* was calculated from galvanostatic discharge and expressed per electrode (F g^{-1}) from two-electrode cell data using the formula (1):

$$C = (2)I/[(dV/dt)\, m_{am}] \qquad (1)$$

where *I* is the current (A), *dV/dt* is the slope of the discharge curve (V s^{-1}), m_{am} is the mass of carbon in each electrode for symmetric capacitors while considering the average mass of carbon active materials for asymmetric capacitors (g) .

Bibliographical References

[1] F. Béguin, E. Frackowiak. Carbons for Electrochemical Energy Storage and Conversion Systems. CRC Press, Boca Raton, 2010, pp 329-373 & 454-463.

[2] E. Frackowiak. Carbon materials for supercapacitor application. Phys. Chem. Chem. Phys., 9 (2007) 1774-1785.

[3] E. Frackowiak, F. Béguin. Carbon materials for the electrochemical storage of energy in capacitors. Carbon 39 (2001) 937-950.

[4] H. I. Becker. Low voltage electrolytic capacitor. United States Patent 2800616, 1957.

[5] M. Endo, T. Takeda, Y. J. Kim, K. Koshiba, K. Ishii. High power electric double layer capacitor (EDLC's): from operating principle to pore size control in advanced activated carbons. Carbon Sci. 1 (2001) 117-128.

[6] A. G. Pandolfo, A.F.Hollenkamp. Carbon properties and their role in supercapacitors. J Power Sources 157 (2006) 11-27.

[7] P. Sharma, T. S. Bhatti. A review on electrochemical double-layer capacitors. Energy Convers. Manage. 51 (2010) 2901-2912.

[8] G. P. Wang, L. Zhang, J. J. Zhang. A review of electrode materials for electrochemical supercapacitors. Chem. Soc. Rev., 41 (2012) 797-828.

[9] P. Simon, Y. Gogotsi. Materials for electrochemical capacitors. Nature Materials 7 (2008) 845-854.

[10] L. L. Zhang, X. S. Zhao. Carbon-based materials as supercapacitor electrodes. Chem. Soc. Rev., 38 (2009) 2520-2531.

[11] Y. Zhang, H. Feng, X. B. Wu, L. Z. Wang, A. Q. Zhang, T. C. Xia, H. C. Dong, X. F. Li, L. S. Zhang. Progress of electrochemical capacitor electrode materials: a review. Int J Hydrogen Energy 34 (2009) 2467-2470.

[12] J. T. Zhang, X. S. Zhao. On the configuration of supercapacitors for maximizing electrochemical performance. ChemSusChem 5 (2012) 818-841.

[13] C. Portet, P. L. Taberna, P. Simon, E. Flahaut, C. Laberty-Robert. High power density electrodes for carbon supercapacitor applications. Electrochim. Acta 50 (2005) 4174-4181.

[14] C. Portet, P .L. Taberna, P. Simon, E. Flahaut. Influence of carbon nanotubes addition on carbon-carbon supercapacitor performances in organic electrolyte. J Power Sources 139 (2005) 371-378.

[15] N. L. Wu, S. Y. Wang. Conductivity percolation in carbon-carbon supercapacitor electrodes. J. Power Sources 110 (2002) 233-236.

[16] A. Burke. R&D considerations for the performance and application of electrochemical capacitors. Electrochim. Acta 52 (2007) 1083-1091.

[17] M. Toupin, D. Bélanger, I. R. Hill, D. Quinn. Performance of experimental carbon blacks in aqueous supercapacitors. J Power Sources 140 (2005) 203-210.

[18] P. J. Hall, M. Mirzaeian, S. I. Fletcher, F. B. Sillars, A. R. Rennie, G. O. Shitta-Bey, G. Wilson, A. Cruden, R. Carter. Energy storage in electrochemical capacitors: designing functional materials to improve performance. Energy Environ. Sci. 3 (2010) 1238-1251.

[19] L. Demarconnay, E. Raymundo-Piňero, F. Béguin. A symmetric carbon/carbon supercapacitor operating at 1.6 V by using a neutral aqueous solution. Electrochem. Commun. 12 (2010) 1275-1278.

[20] M. P. Bichat, E. Raymundo-Piňero, F. Béguin. High voltage supercapacitor built with seaweed carbons in neutral aqueous electrolyte. Carbon 48 (2010) 4351-4361.

[21] Q. T. Qu, B. Wang, L. C. Yang, Y. Shi, S. Tian, Y. P. Wu. Study on electrochemical performance of activated carbon in aqueous Li_2SO_4, Na_2SO_4 and K_2SO_4 electrolytes. ELectrochem. Commun. 10 (2008) 1652-1655.

[22] K. Fic, G. Lota, M. Meller, E. Frackowiak. Novel insight into neutral medium as electrolyte for high-voltage supercapacitors. Energy Environ. Sci., 5 (2012) 5842-5850.

[23] E. Frackowiak, K. Fic, M. Meller, G. Lota. Electrochemistry serving people and nature: high-energy ecocapacitors based on redox-active electrolytes. ChemSusChem 5 (2012) 1181-1185.

[24] P. Azaïs, L. Duclaux, P. Florian, D. Massiot, M. Lillo-Rodenas, A. Linares-Solano, J. Peres, C. Jehoulet, F. Béguin. Causes of supercapacitors ageing in organic electrolyte. J Power Sources 171 (2007) 1046-1053.

[25] M. Ue, K. Ido, S. Mori. Electrochemical properties of organic liquid electrolytes based on quaternary onium salts for electrical double-layer capacitors. J Electrochem. Soc. 141 (1994) 2989-2996.

[26] P. Kurzweil, M. Chwistek. Electrochemical stability of organic electrolytes in supercapacitors: Spectroscopy and gas analysis of decomposition products. J Power Sources 176 (2008) 555-567.

[27] R. Y. Lin, P-L. Taberna, S. Fantini, V. Presser, C. R. Pérez, F. Malbosc, N. L. Rupesinghe, K. K, Teo, Y. Gogotsi, P.Simon. Capacitive energy storage from -50 to 100 ^{o}C using an ionic liquid electrolyte. J. Phys. Chem. Lett. 2 (2011) 2396-2401.

[28] E. Lust, A. Jänes, M. Arulepp. Influence of solvent nature on the electrochemical parameters of electrical double layer capacitors. J. Electroanal. Chem. 562 (2004) 33-42.

[29] P. Liu, M. Verbrugge, S. Soukiazian. Influence of temperature and electrolyte on the performance of activated-carbon supercapacitors. J. Power Sources 156 (2006) 712-718.

[30] R. Kötz, M. Hahn, R. Gallay. Temperature behavior and impedance fundamentals of supercapacitors. J. Power Sources 154 (2006) 550-555.

[31] K. Hung, C. Masarapu, T. Ko, B. Q. Wei. Wide-temperature range operation supercapacitors from nanostructured activated carbon fabric. J. Power Sources 193 (2009) 944-949.

[32] A. Brandt, A. Lex-Balducci, A. Balducci. Adiponitrile-based electrochemical double layer capacitor. J Power Sources 204 (2012) 213-219.

[33] A. Balducci, R. Dugas, P. L. Taberna, P. Simon, D. Plée, M. Mastragostino, S. Passerini. High temperature carbon-carbon supercapacitor using ionic liquid as electrolyte. J Power Sources 165 (2007) 922-927.

[34] M. Galiński, A. Lewandowski, I. Stępniak. Ionic liquids as electrolytes. Electrochim. Acta 51 (2006) 5567-5580.

[35] S. Bose, T. Kuila, A. K. Mishra, R. Rajasekar, N. H. Kim, J. H. Lee. Carbon-based nanostructured materials and their composites as supercapacitor electrodes. J. Mater. Chem. 22 (2012) 767-784.

[36] C. Liu, F. Li, L-P. Ma, H-M. Cheng. Advanced materials for energy storage. Adv. Mater. 22 (2010) E28-E62.

[37] F. Rodríguez-Reinoso. The role of carbon materials in heterogeneous catalysis. Carbon 36 (1998) 159-175.

[38] D. Pech, M. Brunet, H. Durou, P. H. Huang, V. Mochalin, Y. Gogotsi, P-L. Taberna, P. Simon. Ultrahigh-power micrometer-sized supercapacitors based on onion-like carbon. Nature Nanotechnol. 5 (2010) 651-654.

[39] E. Frackowiak, F. Béguin. Electrochemical storage of energy in carbon nanotubes and nanostructured carbons. Carbon 40 (2002) 1775-1787.

[40] G. Lota, K. Fic, E. Frackowiak. Carbon nanotubes and their composites in electrochemical applications. Energy Environ. Sci. 4 (2011) 1592-1605.

[41] Y. W. Zhu, S. Murali, M. D. Stoller, K. J. Ganesh, W. W. Cai, P. J. Ferreira, A. Pirkle, R. M. Wallace, K. A. Cychosz, M. Thommes, D. Su, E. A. Stach, R. S. Ruoff. Carbon-based supercapacitors produced by activation of graphene. Science 332 (2011) 1537-1541.

[42] Y. Huang, J. Liang, Y. Chen. An overview of the applications of graphene-based materials in supercapacitors. Small 8 (2012) 1805-1834.

[43] V. Presser, M. Heon, Y. Gogotsi. Carbide-derived carbons-from porous networks to nanotubes and graphene. Adv. Funct. Mater. 21 (2011) 810-833.

[44] P. Simon, Y. Gogotsi. Capacitive energy storage in nanostructured carbon-electrolyte systems. Acc. Chem. Res. 46 (2013) 1094-1103.

[45] H. Shi. Activated carbons and double layer capacitance. Electrochim. Acta 41 (1996) 1633-1639.

[46] T. A. Centeno, F. Stoeckli. The assessment of surface areas in porous carbons by two model-independent techniques, the DR equation and DFT. Carbon 48 (2010) 2478-2486.

[47] O. Barbieri, M. Hahn, A. Herzog, R. Kötz. Capacitance limits of high surface area activated carbons for double layer capacitors. Carbon 43 (2005) 1303-1310.

[48] G. Gryglewicz, J. Machnikowski, E. Lorenc-Grabowska, G. Lota, E. Frackowiak. Effect of pore size distribution of coal-based activated carbons on double layer capacitance. Electrochim. Acta 50 (2005) 1197-1206.

[49] G. Salitra, A. Soffer, L. Eliad, Y. Cohen, D. Aurbach. Carbon electrodes for double-layer capacitors: I. Relations between ion and pore dimensions. J. Electrochem. Soc. 147 (2000) 2486-2493.

[50] L. Eliad, G. Salitra, A. Soffer, D. Aurbach. Ion sieving effects in the electrical double layer of porous carbon electrodes: estimating effective ion size in electrolytic solutions. J. Phys. Chem. B 105 (2001) 6880-6887.

[51] L. Eliad, E. Pollak, N. Levy, G. Salitra, A. Soffer, D. Aurbach. Assessing optimal pore-to-ion size relations in the design of porous poly (vinylidene chloride) carbons for EDL capacitors. Appl. Phys. A82 (2006) 607-613.

[52] C. Vix-Guterl, E. Frackowiak, K. Jurewicz, M. Friebe, J. Parmentier, F. Béguin. Electrochemical energy storage in ordered porous carbon materials. Carbon 43 (2005) 1293-1302.

[53] J. Chmiola, C. Largeot, P-L. Taberna, P. Simon, Y. Gogotsi. Desolvation of ions in subnanometer pores and its effect on capacitance and double-layer theory. Angew. Chem. Int. Ed. 47 (2008) 3392-3395.

[54] M. Deschamps, E. Gilbert, P. Azais, E. Raymundo-Piñero, M. R. Ammar, P. Simon, D. Massiot, F. Béguin. Exploring electrolyte organization in supercapacitor electrodes with solid-state NMR. Nature Mater. 12 (2013) 351-358.

[55] E. Raymundo-Piñero, K. Kierzek, J. Machnikowski, F. Béguin. Relationship between the nanoporous texture of activated carbons and their capacitance properties in different electrolytes. Carbon 44 (2006) 2498-2507.

[56] H. Nishihara, H. Itoi, T. Kogure, P-X. Hou, H. Touhara, F. Okino, T. Kyotani. Investigation of the ion storage/transfer behavior in an electrical double-layer capacitor by using ordered microporous carbons as model materials. Chem. Eur. J 15 (2009) 5355-5363.

[57] J. Chmiola, G. Yushin, R. Dash, Y. Gogotsi. Effect of pore size and surface area of carbide derived carbons on specific capacitance. J Power Source 158 (2006) 765-772.

[58] J. Chmiola, G. Yushin, Y. Gogotsi, C. Portet, P. Simon, P. L. Taberna. Anomalous increase in carbon capacitance at pore sizes less than 1 nanometer. Science 313 (2006) 1760-1763.

[59] C. Largeot, C. Portet, J. Chmiola, P. Taberna, Y. Gogotsi, P. Simon. Relation between the ion size and pore size for an Electric double-layer capacitor. J. Am. Chem. Soc. 130 (2008) 2730-2731.

[60] G. Feng, R. Qiao, J. S. Huang, B. G. Sumpter, V. Meunier. Ion distribution in electrified micropores and its role in the anomalous enhancement of capacitance. ACS Nano 4 (2010) 2382-2390.

[61] C. Merlet, B. Rotenberg, P. A. Madden, P-L. Taberna, P. Simon, Y. Gogotsi, M. Salanne. On the molecular origin of supercapacitance in nanoporous carbon electrodes. Nature Mater. 11 (2012) 306-310.

[62] Y. Shim, H. J. Kim. Nanoporous carbon supercapacitors in an ionic liquid: a computer simulation study. ACS Nano 4 (2010) 2345-2355.

[63] R. Mysyk, E. Raymundo-Pinňero, F. Béguin. Saturation of subnanometer pores in an electric double-layer capacitor. Electrochem. Commun. 11 (2009) 554-556.

[64] W. G. Pell, B. E. Conway, N. Marincic. Analysis of non-uniform charge/discharge and rate effects in porous carbon capacitors containing sub-optimal electrolyte concentrations. J. Electroanal. Chem. 491 (2000) 9-21.

[65] R. Mysyk, E. Raymundo-Pinňero, J. Pernak, F. Béguin. Confinement of symmetric tetraalkylammonium ions in nanoporous carbon electrodes of electric double-layer capacitors. J. Phys. Chem. C 113 (2009) 13443-13449.

[66] H. Nishihara, T. Kyotani. Templated nanocarbons for energy storage. Adv. Mater. 24 (2012) 4473-4498.

[67] J. Rodriguez-Mirasol, T. Cordero, L. R. Radovic, J. J. Rodriguez. Structural and textural properties of pyrolytic carbon formed within a microporous zeolite template. Chem. Mater. 10 (1998) 550-558.

[68] Z. Ma, T. Kyotani, Z. Liu, O. Teraski, A. Tomita. Very high surface area microporous carbon with a three-dimensional nano-array structure: synthesis and its molecular structures. Chem. Mater. 13 (2001) 4413-4415.

[69] H. Nishihara, Q-H. Yang, P-X. Hou, M. Unno, S. Yamauchi, R. Saito, J. I. Paredes, A. Martínez-Alonso, J. M. D. Tascón, Y. Sato, M. Terauchi, T. Kyotani. A possible buckbowl-like structure of zeolite template carbon. Carbon 47 (2009) 1220-1230.

[70] T. Kyotani, Z. Ma, A. Tomia. Template synthesis of novel porous carbons using various types of zeolites. Carbon 41 (2003) 1451-1459.

[71] H. Itoi, H. Nishihara, T. Kogure, T. Kyotani. Three-dimensionally arrayed and mutually connected 1.2-nm nanopores for high-performance electric double layer capacitor. J. Am. Chem. Soc. 133 (2011) 1165-1167.

[72] A. Kajdos, A. Kvit, F. Jones, J. Jagiello, G. Yushin. Tailoring the pore alignment for rapid ion transport in microporous carbons. J. Am. Chem. Soc. 132 (2010) 3252-3253.

[73] Y. Gogotsi, A. Nikitin, H. Ye, W. Zhou, J. E. Fischer, B. Yi, H. C. Foley, M. W. Barsoum. Nanoporous carbide-derived carbon with tunable pore size. Nature Mater. 2 (2003) 591-594.

[74] A. Jänes, T. Thomberg, E. Lust. Synthesis and characterization of nanoporous carbide-derived carbon by chlorination of vanadium carbide. Carbon 45 (2007) 2717-2722.

[75] A. Jänes, T. Thomberg, H. Kurig, E. Lust. Nanoscale fine-tuning of porosity of carbide-derived carbon prepared from molybdenum carbide. Carbon 47 (2009) 23-29.

[76] R. Lin, P. L. Taberna, J. Chmiola, D. Guay, Y. Gogotsi, P. Simon. Microelectrode study of pore size, ion size, and solvent effects on the charge/discharge behavior of microporous carbons for electrical double layer capacitors. J Electrochem. Soc. 156 (2009) A7-A12.

[77] M. Rose, Y. Korenblit, E. Kockrick, L. Borchardt, M. Oschatz, S. Kaskel, G. Yushin. Hierarchical micro- and mesoporous carbide-derived carbon as a high-performance electrode material in supercapacitors. Small 7 (2011) 1108-1117.

[78] M. Arulepp, J. Leis, M. Lätt, F. Miller, K. Rumma, E. Lust, A. F. Burke. The advanced carbide-derived carbon based supercapacitor. J Power Sources 162 (2006) 1460-1466.

[79] J. Huang, B. G. Sumpter, V. Meunier. Theoretical model for nanopores carbon supercapacitors. Angew. Chem. Int. Ed. 47 (2008) 520-524.

[80] J. Huang, B. G. Sumpter, V. Meunier. A universal model for nanoporous carbon supercapacitors applicable to diverse pore regimes, carbon materials, and electrolytes. Chem. A Eur. J. 14 (2008) 6614-6626.

[81] B. E. Conway, V. Birss, J. Wojtowicz. The role and utilization of pseudocapacitance for energy storage by supercapacitors. J Power Sources 66 (1997) 1-14.

[82] B. E. Conway, W. G. Pell. Double-layer and pseudocapacitance types of electrochemical capacitors and their applications to the development of hybrid devices. J Solid State Electrochem. 7 (2003) 637-644.

[83] N. L. Wu. Nanocrystalline oxide supercapacitors. Mater. Chem. Phys. 75 (2002) 6-11

[84] H. Xia, Y. S. Meng, G. L. Yuan, C. Cui, L. Lu. A symmetric RuO_2/RuO_2 supercapacitor operating at 1.6 V by using a neutral aqueous electrolyte. Electrochem. Solid-State. Lett. 15 (2012) A60-A63.

[85] M. Toupin, T. Brousse, D. Bélanger. Charge storage mechanism of MnO_2 electrode used in aqueous electrochemical capacitor. Chem. Mater. 16 (2004) 3184-3190.

[86] W. F. Wei, X. W. Cui, W. X. Chen, D. G. Ivey. Manganese oxide-based materials as electrochemical supercapacitor electrodes. Chem. Soc. Rev. 40 (2011) 1697-1721.

[87] Q. Lu, M. W. Lattanzi, Y. P. Chen, X. M. Kou, W. F. Li, X. Fan, K. M. Unruh, J. G. Chen, J. Q. Xiao. Supercapacitor electrodes with high-energy and power densities

prepared from monolithic NiO/Ni nanocomposites. Angew. Chem. Int. Ed. 50 (2011) 6847-6850.

[88] M. P. Yeager, D. Su, N. S. Marinkovic, X. W. Teng. Pseudocapacitive NiO fine nanoparticles for supercapacitor reactions. J Electrochem Soc. 159 (2012) A 1598-A1603.

[89] G. A. Snook, P. Kao, A. Best. Conducting-polymer-based supercapacitor devices and electrodes. J. Power Sources 196 (2011) 1-12.

[90] T. A. Centeno, F. Stoeckli. The role of textural characteristics and oxygen-containing surface groups in the supercapacitor performances of activated carbons. Electrochim. Acta 52 (2006) 560-566.

[91] E. Frackowiak, G. Lota, J. Machnikowski, C. Vix-Guterl, F. Béguin. Optimisation of supercapacitors using carbons with controlled nanotexture and nitrogen content. Electrochim. Acta 51 (2006) 2209-2214.

[92] K. Jurewicz, E. Frackowiak, F. Béguin. Towards the mechanism of electrochemical hydrogen storage in nanostructured carbon materials. Appl. Phys. A78 (2004) 981-987.

[93] F. Béguin, M. Friebe, K. Jurewicz, C. Vix-Guterl, J. Dentzer, E. Frackowiak. State of hydrogen electrochemically stored using nanoporous carbons as negative electrode materials in an aqueous medium. Carbon 44 (2006) 2392-2398.

[94] K. Fic, E. Frackowiak, F. Béguin. Unusual energy enhancement in carbon-based electrochemical capacitors. J Mater Chem 22 (2012) 24213.

[95] G. Lota, E. Frackowiak. Striking capacitance of carbon/iodide interface. Electrochem. Commun. 11 (2009) 87-90.

[96] G. Lota, K. Fic, E. Frackowiak. Alkali metal iodide/carbon interface as a source of pseudocapacitance. Electrochem. Commnun. 13 (2011) 38-41.

[97] S. Roldán, M. Granda, R. Menédez, R. Santamaría, C. Blanco. Mechanisms of energy storage in carbon-based supercapacitors modified with a quinoid redox-active electrolyte. J. Phys. Chem. C 115 (2011) 17606-17611.

[98] S. Roldán, C. Blanco, M. Granda, R. Menédez, R. Santamaría. Towards a further generation of high-energy carbon-based capacitors by using redox-active electrolytes. Angew. Chem. Int. Ed. 50 (2011) 1699-1701.

[99] S. T. Senthilkumar, R. K. Selvan, Y. S. Lee, J. S. Melo. Electric double layer capacitor and its improved specific capacitance using redox additive electrolyte. J. Mater. Chem. A 1 (2013) 1086-1095.

[100] S. Yamazaki, T. Ito, M. Yamagata, M. Ishikawa. Non-aqueous electrochemical capacitor utilizing electrolytic redox reactions of bromide species in ionic liquid. Electrochim. Acta. 86 (2012) 294-297.

[101] L. Y. Chen, Y. Hou, J. L. Kang, A. Hirata, T. Fujita, M. W. Chen. Toward the theoretical capacitance of RuO_2 reinforced by highly conductive nanoporous gold. Adv. Energy Mater. 2013. Doi: 10.1002/aenm.201300024.

[102] I. H. Kim, J. H. Kim, Y. H. Lee, K. B. Kim. Syhthesis and characterization of electrochemically prepared ruthenium oxide on carbon nanotube film substrate for supercapacitor applications. J Electrochem. Soc. 152 (2005) A2170-A2178.

[103] C-C. Hu, W-C. Chen, K-H. Chang. How to achieve maximum utilization of hydrous ruthenium oxide for supercapacitors. J Electrochem. Soc. 151 (2004) A281-A290.

[104] X. Y. Lang, A. Hirata, T. Fujita, M. W. Chen. Nanoporous metal/oxide hybrid electrodes for electrochemical supercapacitors. Nat. Nanotechnol. 6 (2011) 232-236.

[105] J. L. Kang, L. Y. Chen, Y. Hou, C. Li, T. Fujita, X. Y. Lang, A. Hirata, M. W. Chen. Electroplated thick manganese oxide films with ultrahigh capacitance. Adv. Energy Mater. 2013. Doi: 10.1002/aenm.201201046.

[106] F. Ataherian, K-T. Lee, N-L. Wu. Long-term electrochemical behaviors of manganese oxide aqueous electrochemical capacitor under reducing potentials. Electrochem. Acta 55 (2010) 7429-7435.

[107] F. Ataherian, N-L. Wu. 1.2 volt manganese oxide symmetric supercapacitor. Electrochem. Commun. 13 (2011) 1264-1267.

[108] H. L. Li, J. X. Wang, Q. X. Chu, Z. Wang, F. B. Zhang, S. C. Wang. Theoretical and experimental specific capacitance of polyaniline in sulfuric acid. J Power Sources 190 (2009) 578-586.

[109] S. R. Sivakkumar, W. J. Kim, J-A. Choi, D. R. MacFarlane, M. Forsyth, D-W. Kim. Electrochemical performance of polyaniline nanofibres and polyaniline/multi-walled carbon nanotube composite as an electrode material for aqueous redox supercapacitors. J Power Sources 171 (2007) 1062-1068.

[110] A. Laforgue, P. Simon, C. Sarrazin, J-F. Fauvarque. Polythiophene-based supercapacitors. J Power Sources 80 (1999) 142-148.

[111] L-Z. Fan, J. Maier. High-performance polypyrrole electrode materials for redox supercapacitors. Electrochem. Commun. 8 (2006) 937-940.

[112] V. Khomenko, E. Frackowiak, F. Béguin. Determination of the specific capacitance of conducting polymer/nanotubes composite electrodes using different cell configurations. Electrochim. Acta 50 (2005) 2499-2506.

[113] M. Mastragostino, C. Arbizzani, F. Soavi. Conducting polymers as electrode materials in supercapacitors. Solid State Ionics 148 (2002) 493-498.

[114] L. R. Radovic, B. Bockrath. On the chemical nature of graphene edges: origin of stability and potential for magnetism in carbon materials. J. Am. Chem. Soc. 127 (2005) 5917-5927.

[115] Y-H. Lee, K-H. Chang, C-C. Hu. Differentiate the pseudocapacitance and double-layer capacitance contributions for nitrogen-doped reduced graphene oxide in acidic and alkaline electrolytes. J Power Sources 227 (2013) 300-308.

[116] K. Okajima, K. Ohta, M. Sudoh. Capacitance behavior of activated carbon fibers with oxygen-plasma treatment. Electrochim. Acta 50 (2005) 2227-2231.

[117] H. A. Andreas, B. E. Conway. Examination of the double-layer capacitance of an high specific-area C-cloth electrode as titrated from acidic to alkaline pHs. Electrochim. Acta 51 (2006) 6510-6520.

[118] J. L. Figueiredo, M. F. R. Pereira, M. M. A. Freitas, J. J. M. Órfão. Modification of the surface chemistry of activated carbons. Carbon 37 (1999) 1379-1389.

[119] M. J. Bleda-Martïnez, J. A. Maciá-Agulló, D. Lozano-Castelló, E. Morallón, D. Cazorla-Amorós, A. Linares-Solano. Role of surface chemistry on electric double layer capacitance of carbon materials. Carbon 43 (2005) 2677-2684.

[120] P-Z. Cheng, H. Teng. Electrochemical responses from surface oxides present on HNO_3-treated carbons. Carbon 41 (2003) 2057-2063.

[121] Y. J. Kim, Y. Abe, T. Yanagiura, K. C. Park, M. Shimizu, T. Iwazaki, S. Nakagawa, M. Endo, M. S. Dresselhaus. Easy preparation of nitrogen-enriched carbon materials from peptides of silk fibroins and their use to produce a high volumetric energy density in supercapacitors. Carbon 45 (2007) 2116-2125.

[122] K. Jurewicz, K. Babel, R. Pietrzak, S. Delpeux, H. Wachowska. Capacitance properties of multi-walled carbon nanotubes modified by activation and ammoxidation. Carbon 44 (2006) 2368-2375.

[123] H. M. Jeong, J. W. Lee, W. H. Shin, Y. J. Choi, H. J. Shin, J. K. Kang, J. W. Choi. Nitrogen-doped graphene for high-performance ultracapacitors and the importance of nitrogen-doped sites at basal planes. Nano Lett. 11 (2011) 2472-2477.

[124] M. Seredych, D. Hulicova-Jurcakova, G. Q. Lu, T. J. Bandosz. Surface functional groups of carbons and the effects of their chemical character, density and accessibility to ions on electrochemical performance. Carbon 46 (2008) 1475-1488.

[125] D. Hulicova-Jurcakova, M. Seredych, G. Q. Lu, T. J. Bandosz. Combined effect of nitrogen- and oxygen-containing functional groups of microporous activated carbon on its electrochemical performance in supercapacitors. Adv. Funct. Mater. 19 (2009) 438-447.

[126] G. Lota, K. Fic, K. Jurewicz, E. Frackowiak. Correlation of hydrogen capacity in carbon material with the parameters of electrosorption. Cent. Eur. J. Chem. 9 (2011) 20-24.

[127] S. Haydar, C. Moreno-Castilla, M. A. Ferro-García, F. Carrasco-Marín, J. Rivera-Utrilla, A. Perrard, J. P. Joly. Regularities in the temperature-programmed desorption spectra of CO_2 and CO from activated carbons. Carbon 38 (2000) 1297-1308.

[128] K. Naoi, P. Simon. New materials and new configurations for advanced electrochemical capacitors. Electrochem. Soc. Interf. 17 (2008) 34-37.

[129] K. Naoi. 'Nanohybrid capacitor': The next generation electrochemical capacitors. Fuel Cells 10 (2010) 825-833.

[130] D. Cericola, R. Kötz. Hybridization of rechargeable batteries and electrochemical capacitors: Principles and limits. Electrochem. Acta 72 (2012) 1-17.

[131] L. Demarconnay, E. Raymundo-Piñero, F. Béguin. Adjust of electrodes potential window in an asymmetric carbon/MnO_2 supercapacitor. J Power Sources 196 (2011) 580-586.

[132] V. Khomenko, E. Raymundo-Piñero, F. Béguin. A new type of high energy asymmetric capacitor with nanoporous carbon electrodes in aqueous electrolyte. J Power Sources 195 (2010) 4234-4241.

[133] T. Brousse, P-L. Taberna, O. Crosnier, R. Dugas, P. Guillemet, Y. Scudeller, Y. Zhou, F. Favier, D. Bélanger, P. Simon. Long-term cycling behavior of asymmetric activated carbon/MnO_2 aqueous electrochemical supercapacitor. J Power Sources 173 (2007) 633-641.

[134] V. Khomenko, E. Raymundo-Piñero, F. Béguin. Optimisation of an asymmetric manganese oxide/activated carbon capacitor working at 2 V in aqueous medium. J Power Sources 153 (2006) 183-190.

[135] T. Brousse, M. Toupin, D. Bélanger. A hybrid activated carbon-manganese dioxide capacitor using a mild aqueous electrolyte. J Electrochem Soc. 151 (2004) A614-A622.

[136] G. A. Snook, G. J. Wilson, A. G. Pandolfo. Mathematical functions for optimization of conducting polymer/activated carbon asymmetric supercapacitors. J Power Sources 186 (2009) 216-223.

[137] I. Plitz, A. Dupasquier, F. Badway, J. Gural, N. Pereira, A. Gmitter, G. G. Amatucci. The design of alternative nonaqueous high power chemistries. Appl. phys. A 82 (2006) 615-626.

[138] K. Naoi, S. Ishimoto, J-I. Miyamoto, W. Naoi. Second generation 'nanohybrid supercapacitor': evolution of capacitive energy storage devices. Energy Environ. Sci. 5 (2012) 9363-9373.

[139] V. Khomenko, E. Raymundo-Piñero, F. Béguin. Hign-energy density graphite/AC capacitor in organic electrolyte. J. Power Sources 177 (2008) 643-651.

[140] C. Decaux, G. Lota, E. Raymundo-Piñero, F. Béguin. Electrochemical performance of a hybrid lithium-ion capacitor with a graphite anode preloaded from lithium bis (trifluoromethane) sulfonamide-based electrolyte. Electrochim. Acta 86 (2012) 282-286.

[141] S. R. Sivakkumar, A. G. Pandolfo. Evaluation of lithium-ion capacitors assembled with pre-lithiated graphite anode and activated carbon cathode. Electrochim. Acta 65 (2012) 280-287.

[142] J-H. Kim, J-S. Kim, Y-G. Lim, J-G. Lee, Y-J. Kim. Effect of carbon types on the electrochemical properties of negative electrodes for Li-ion capacitors. J Power Sources 196 (2011) 10490-10495.

[143] F. Béguin, K. Kierzek, M. Fiebe, A. Jankowska, J. Machnikowski, K. Jurewicz, E. Frackowiak, Effect of various porous nanotextures on the reversible electrochemical sorption of hydrogen in activated carbon. Electrochim. Acta 51 (2006) 2161-2167.

[144] K. Jost, C. R. Perez, J. K. McDonough, V. Presser, M. Henon, G. Dion, Y. Gogotsi. Carbon coated textiles for flexible energy storage. Energy Environ. Sci., 4 (2011) 5060-5067.

[145] D. Lide. CRC Handbook of Chemistry and Physics, 88th ed., CRC press, Florida, 2007-2008.

[146] W. F. Linke, A. Seidell. Solubilities: Inorganic and Metal-Organic Compounds, 4th ed., D. van Nostrand, New York, 1965.

[147] A. Cartón, F. Sobrón, S. Bolado, J. L. Gerbolés. Density, viscosity, and electrical conductivity of aqueous solutions of lithium sulfate. J. Chem. Eng. Data 40 (1995) 987-991.

[148] E. Raymundo-Piñero, M. Cadek, F. Béguin, Tuning carbon materials for supercapacitor by direct pyrolysis of seaweeds. Adv. Funct. Mater. 19 (2009) 1032-1039.

[149] M. J. Bleda-Martínez, D. Lozano-Castelló, E. Morallón, D. Cazorla-Amorós, A. Linares-Solano. Chemical and electrochemical characterization of porous carbon materials. Carbon 44 (2006) 2642-2651.

[150] R. Berenguer, J. P. Marco-Lozar, C. Quijada, D. Cazorla-Amorós, E. Morallón. Effect of electrochemical treatments on the surface chemistry of activated carbon. Carbon 47 (2009) 1018-1027.

[151] Y. Yang, Z. G. Lin. In situ FTIR characterization of the electrooxidation of galssy carbon electrodes. J. Appl. Electrochem. 25 (1995) 259-266.

[152] Z. R. Yue, W. Jiang, L. Wang, S. D. Gardner, C. U. Pittman Jr. Surface characterization of electrochemically oxidized carbon fibers. Carbon 37 (1999) 1785-1796.

[153] S. S. Barton, M. J. B. Evans, E. Halliop, J. A. F. MacDonald. Acidic and basic sites on the surface of porous carbon. Carbon 35 (1997) 1361-1366.

[154] J-W. Lang, X- B. Yan, W-W. Liu, R-T. Wang, Q-J. Xue. Influence of nitric acid modification of ordered mesoporous carbon materials on their capacitive performance in different electrolytes. J Power Sources 204 (2012) 220-229.

[155] B. Grzyb, C. Hildenbrand, S. Berthon-Fabry, D. Béguin, N. Job, A. Rigacci, P. Achard. Functionalisation and chemical characterization of cellulose-derived carbon aerogels. Carbon 48 (2010) 2297-2307.

[156] M. J. Bleda-Martínez, J. M. Pérez, A. Linares-Solano, E. Morallón, D. Cazorla-Amorós. Effect of surface chemistry on electrochemical storage of hydrogen in porous carbon materials. Carbon 46 (2008) 1053-1059.

[157] K. Kierzek, E. Frackowiak, G. Lota, G. Gryglewicz, J. Machnikowski. Electrochemical capacitors based on highly porous carbons prepared by KOH activation. Electrochem. Acta 49 (2004) 515-523.

[158] V. Ruiz, C. Blanco, M. Granda, R. Santanaria. Enhanced life-cycle supercapacitors by thermal treatment of mesophase-derived activated carbons. Electrochim. Acta 54 (2008) 305-310.

[159] R. N. Reddy, R. G. Reddy. Sol-gel MnO2 as an electrode material for electrochemical capacitors. J. Power Sources 124 (2003) 330-337.

[160] M. Inagaki, H. Konno, O. Tanaike. Carbon materials for electrochemical capacitors. J. Power Sources 195 (2010) 7880-7903.

[161] M. Endo, T. Maeda, T. Takeda, Y. J. Kim, K. Koshiba, H. Hara, M. S. Dresselhaus. Capacitance and pore-size distribution in aqueous and nonaqueous electrolytes using various activated carbon electrode. J. Electrochem Soc. 148 (2001) A910-A914.

[162] X. Zhang, X. Wang, L. Jiang, H. Wu, C. Wu, J. Su. Effect of aqueous electrolytes on the electrochemical behaviors of supercapacitors based on hierarchically porous carbons. J. Power Sources 216 (2012) 290-296.

[163] J. Niu, B. E. Conway, W. G. Pell. Comparative studies of self-discharge by potential decay and float-current measurements at C double-layer capacitor and battery electrodes. J. Power Sources 135 (2004) 332-343.

[164] J. Black, H. A. Andreas. Prediction of the self-discharge profile of an electrochemical capacitor electrode in the presence of both activation-controlled discharge and charge redistribution. J. Power Sources 195 (2010) 929-935.

[165] J. Black, H. A. Andreas. Effects of charge redistribution on self-discharge of electrochemical capacitors. Electrochem. Acta 54 (2009) 3563-3574.

[166] J. Kowal, E. Avaroglu, F. Chamekh, A. Šenfelds, T. Thien, D. Wijaya, D. U. Sauer. Detailed analysis of the self-discharge of supercapacitors. J. Power Sources 196 (2011) 573-579.

[167] H. Yang, Y. Zhang. Self-discharge analysis and characterization of supercapacitors for environmentally powered wireless sensor network applications. J. Power Sources 196 (2011) 8866-8873.

[168] L. Xing, J. Vatamanu, O. Borodin, D. Bedrov. On the atomistic nature of capacitance enhancement generated by ionic liquid electrolyte confined in subnanometer pores. J. Phys. Chem. Lett. 4 (2013) 132-140.

[169] H. Marsh, F. Rodriguez-Reinoso, *Activated Carbon*, Elsevier Ltd., Oxford, 2006, pp 243-365.

[170] M.A Lillo-Ródenas, D Lozano-Castelló, D Cazorla-Amorós, A Linares-Solano. Preparation of activated carbons from Spanish anthracite II. Activation by NaOH. Carbon 39 (2001) 751-759.

[171] J. A. Maciá-Agulló, B. C. Moore, D. Cazorla-Amorós, A. Linares-Solano. Activation of coal tar pitch carbon fibres : physical activation vs. chemical activation. Carbon 42 (2004) 1367-1370.

[172] P.L. Walker Jr., R.L. Taylor, J.M. Ranish. An update on the carbon-oxygen reaction. Carbon 29 (1991)411-421.

[173] D. F. Quinn, J. A. Holland, Carbonaceous material with high micropore and low macropore volume and process for producing same, US patent 5071820, 1991.

[174] X Py, A. Guillot, B. Cagnon. Activated carbon porosity tailoring by cyclic sorption/decomposition of molecular oxygen. Carbon 41 (2003) 1533-1543.

[175] J. A. Conesa, M. Sakurai, M.J. Jr Antal. Synthesis of a high-yield activated carbon by oxygen gasification of macadamia nut shell charcoal in hot, liquid water. Carbon 38(2000) 839-848.

[176] M. S. Tam, M. J. Jr Antal, E. Jakab, G. Varhegyi. Activated carbon from macadamia nut shell by air oxidation in boiling water. Ind. Eng. Chem. Res. 40 (2001) 578-588.

[177] B. B. Benson, D. Krause, M. A. Peterson. The solubility and isotopic fractionation of gases in diluted aqueous solution. I. Oxygen. J. Solution Chem. 8 (1979) 655–690.

[178] M. Ue, A. Murakami, S. J. Nakamura. A Convenient Method to Estimate Ion Size for Electrolyte Materials Design. J. Electrochem. Soc. 149 (2002) A1385-A1388.

[179] C. O. Ania, J. Pernak, F. Stefaniak, E. Raymundo-Piñero, F. Béguin. Polarization-induced distortion of ions in the pores of carbon electrodes for electrochemical capacitors. Carbon 47 (2009) 3158-3166.

[180] D. Aurbach, M. D. Levi, G. Salitra, N. Levy, E. Pollak, J. Muthu. Cation trapping in highly porous carbon electrodes for EDLC cells. J. Electrochem. Soc. 155 (2008) A745-A753.

[181] L. A. Oliveira, C. Silva, M. Yoshida, R. Lago. The effect of H_2 treatment on the activity of activated carbon for the oxidation of organic contaminants in water and the H_2O_2 decomposition. Carbon 42 (2004) 2279-2284.

[182] A. Rey, J. A. Zazo, J. A. Casas, A. Bahamonde, J. J. Rodriguez. Influence of the structural and surface characteristics of activated carbon on the catalytic decompostion of hydrogen peroxide. Appl. Catal. A-Gen. 402 (2011) 146-155.

[183] K. Sing. The use of nitrogen adsorption for the characterization of porous materials. Colloid Surf A 187-188 (2001) 3-9.

[184] A. V. Neimark, Y. Z. Lin, P. I. Ravikovitch, M. Thommes. Quenched solid density functional theory and pore size analysis of micro-mesoporous carbons. Carbon 47 (2009) 16717-1628.

[185] G. Y. Gor, M. Thommes, K. A. Cychosz, A. V. Neimark. Quenched solid density functional theory method for characterization of mesoporous carbons by nitrogen adsorption. Carbon 50 (2012) 1583-1590.

Résumé

L’enjeu majeur du développement des supercondensateurs reste focalisé sur l’augmentation de la densité d’énergie de ces systèmes tout en adoptant une démarche la plus respectueuse possible de l’environnement. Afin de satisfaire cet objectif, deux stratégies d’optimisation de supercondensateurs carbone/carbone ont été envisagées en fonction du milieu électrolytique utilisé: i) dans le cas du milieu aqueux, des solutions de sulfates alcalins neutres ont été considérées afin d’étendre la tension de fonctionnement du système; ii) dans le cas du milieu organique, une méthode douce d'activation a été mise en œuvre afin d’obtenir des carbones microporeux avec une taille moyenne de pores adaptée à la taille des ions de l’électrolyte.

L’utilisation d’électrolytes aqueux à base de sulfates alcalins dans des supercondensateurs carbone/carbone symétriques a permis d’étendre la fenêtre de tension jusqu’à 1,9 V ; cette dernière a même pu être étendue à 2,0 V par ajustement des masses d’électrodes. Enfin, des électrodes commerciales enduites ont été utilisées dans des cellules type « coffee-bag » offrant une excellente stabilité pendant 10,000 cycles à 2,1 V.

En milieu organique, des carbones nanoporeux denses avec des pores adaptés à la taille des ions de l'électrolyte organique Et_4NBF_4/acetonitrile ont été obtenus par oxydation à haute pression et basse température (environ 200°C) d’un carbone non poreux. Une étape suivante de traitement thermique a ensuite permis d’éliminer les groupements fonctionnels de surface et ainsi d’améliorer l’accessibilité de la porosité. En raison de la faible oxydation, la densité des électrodes est remarquablement élevée permettant d’atteindre des valeurs élevées de capacité volumique.

Abstract

The objective of this work is to improve the energy density of carbon/carbon supercapacitors. For achieving this objective, two different strategies were followed depending on the electrolyte used: i) in aqueous electrolytes, our efforts were focused on extending the operating cell voltage by using neutral alkali sulfate solutions; ii) in organic electrolyte, the target was to improve the volumetric capacitance by setting a mild activation method able to produce a porous carbon with average pore size matching the ion size, while not enlarging the pores upon porosity development.

A practical cell voltage of 1.8 V has been demonstrated by implementing aqueous alkali sulfates in symmetric carbon/carbon capacitors. It has been shown that the voltage is limited by a partial destructive electro-oxidation of the positive electrode. Such irreversible electro-oxidation could be mitigated by mild chemical oxidation of the active carbon material with hydrogen peroxide; consequently, the voltage could be further expanded up to 1.9 V. Even 2.0 V could be attained after mass balancing the electrodes in order to allow them to operate in their stability window. Finally, pouch-cells with carbon coating on stainless steel current collector were realized by using 2 mol L^{-1} Li_2SO_4 as electrolyte. An exceptional cycling stability at cell voltages up to 2.1 V was obtained during 10,000 cycles. Hence, the use of alkali sulfate electrolytes is a cost-effective alternative to organic electrolytes for producing environment friendly and safe carbon/carbon supercapacitors.

Dense nanoporous carbons with pores fitting the dimension of ions of the Et_4NBF_4/acetonitrile organic electrolyte were obtained by high pressure oxidation of non-porous carbon at low temperature, followed by a thermal desorption to remove the surface groups and unblock pore entrances. The activation mechanism consisted in drilling the narrow pores existing initially in the char. Due to the low burn-off, the density of the electrodes was remarkably high allowing high volumetric capacitance values to be reached. This novel production method associates the advantages of environment friendly, cost-effective, high yield and low energy consumption characteristics.